THE UNIVERSITY OF MICHIGAN
FEB 17 1965
PHOENIX LIBRARY

REACTOR MATERIALS

A Quarterly Technical Progress Review

Prepared for DIVISION OF TECHNICAL INFORMATION, USAEC, by
R. W. DAYTON, E. M. SIMONS, and ASSOCIATES, BATTELLE MEMORIAL INSTITUTE

Winter 1964-1965

● VOLUME 7

● NUMBER 4

TECHNICAL PROGRESS REVIEWS

To meet the needs of industry for concise summaries of current atomic developments, the Atomic Energy Commission is publishing this series, Technical Progress Reviews. Issued quarterly, each of the reviews digests and evaluates the latest findings in a specific area of nuclear technology and science.

The five journals published in this series are:

Isotopes and Radiation Technology, P. S. Baker, A. F. Rupp, and associates, Oak Ridge National Laboratory

Nuclear Safety, Wm. B. Cottrell, W. H. Jordan, and associates, Oak Ridge National Laboratory

Power Reactor Technology, W. H. Zinn and J. R. Dietrich, Combustion Engineering, Inc., Nuclear Division

Reactor Fuel Processing, Stephen Lawroski and associates, Chemical Engineering Division, Argonne National Laboratory

Reactor Materials, R. W. Dayton, E. M. Simons, and associates, Battelle Memorial Institute

Each journal may be purchased from the Superintendent of Documents, U. S. Government Printing Office, Washington, D. C., 20402. *Isotopes and Radiation Technology* at $2.00 per year for subscription or $0.55 for individual issues; the other four journals at $2.50 per year and $0.70 per issue. See back cover for remittance instructions and foreign postage requirements.

The views expressed in this publication do not necessarily represent those of the United States Atomic Energy Commission, its divisions or offices, or of any Commission advisory committee or contractor.

Availability of Reports Cited in This Review

Unclassified AEC reports are available for inspection at AEC depository libraries and are sold by the Clearinghouse for Federal Scientific and Technical Information, National Bureau of Standards, U. S. Department of Commerce, 5285 Port Royal Road, Springfield, Va., 22151. Some of the reports cited are not available owing to their preliminary nature; however, the information contained in them will eventually be made available in formal progress or topical reports.

Unclassified reports issued by other Government agencies or private organizations should be requested from the originator.

Unclassified British and Canadian reports may be inspected at AEC depository libraries. British reports are sold by the British Information Service, 45 Rockefeller Plaza, New York, N. Y.; Canadian reports (AECL series) are sold by the Scientific Document Distribution Office, Atomic Energy of Canada, Ltd., Chalk River, Ontario, Canada.

Classified U. S. and foreign reports identified in this journal as Classified may be purchased by properly cleared Access Permit Holders from the Division of Technical Information Extension, U. S. Atomic Energy Commission, P. O. Box 1001, Oak Ridge, Tenn., 37831. Such reports may be inspected at classified AEC depository libraries.

REACTOR MATERIALS

A REVIEW OF RECENT DEVELOPMENTS

Prepared for DIVISION OF TECHNICAL INFORMATION, USAEC,
by R. W. DAYTON, E. M. SIMONS, and ASSOCIATES,
BATTELLE MEMORIAL INSTITUTE

WINTER 1964–1965

VOLUME 7

NUMBER 4

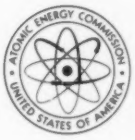

Foreword

Reactor Materials is one of a series of quarterly technical progress reviews broadly covering the field of nuclear science and technology. Under the auspices of the USAEC Division of Technical Information, *Reactor Materials* is prepared by Battelle personnel from worldwide literature. It covers properties, behavior, and fabrication processes of materials applicable to nuclear reactor components and associated equipment.

The reader will recognize that the scope of this Review is too broad to permit detailed coverage of every topic. Rather, the authors and editors attempt to combine the highlights of significant new developments into an information summary of current research for both management and the technical specialist. As a rule, enough of the results are presented to define the research and summarize the findings. For readers desiring more information on any particular topic, a complete set of references is provided at the end of each section.

Each quarter, a number of bibliographies, monographs, and books appear on subjects within the scope of *Reactor Materials*. Although the main purpose of this Review is to call attention to findings that are new and significant, such publications are noted in the text because they often represent excellent compilations of available information on important materials topics.

R. W. DAYTON
E. M. SIMONS
R. W. ENDEBROCK
Battelle Memorial Institute

DEPOSITED BY THE
UNITED STATES OF AMERICA

Contents

I Fuel and Fertile Materials 211
Uranium Metal and Alloys 211
Plutonium 213
Thorium 218
Metal-Ceramic Fuels 218
Coated-Particle Fuel Materials 219
Uranium Oxide Fuel Materials 223
Uranium and Thorium Carbides, Nitrides, and Sulfides 224
Fuel-Water Reactions 225
Basic Studies of Irradiation Effects in Fuel Materials 226
References 227

II Moderator Materials 230
Graphite 230
Beryllium Metal and Alloys 231
Beryllium Oxide 233
Beryllium Intermetallic Compounds . . 233
Solid Hydrides 234
References 234

III Nuclear Poisons 236
Metallic Poison Materials 236
Dispersion Poison Materials 236
References 237

IV Cladding and Structural Materials . 238
Corrosion 238
Metal-Water Reactions 242
Selected Mechanical Properties of Refractory Metals 243
Selected Metallurgical Aspects of Cladding and Structural Materials . . 244
Diffusion Studies 246
Ceramic Technology 247
Radiation Effects in Nonfuel Materials . 249
References 254

V Special Fabrication Techniques . . . 257
Melting, Casting, and Working 257
Cladding 258
Explosive Forming 261
Welding and Brazing 262
Nondestructive Testing 264
References 265

Index, Volume 7 269

Issued quarterly by the U. S. Atomic Energy Commission. Use of funds for printing this publication approved by the Director of the Bureau of the Budget on October 14, 1963.

Section

I

Reactor Materials

Fuel and Fertile Materials

Uranium Metal and Alloys

Unalloyed Uranium

In a comparative study of creep in imperfect single crystals and polycrystals of alpha uranium, the French found[1] that the activation energy during creep of polycrystals remains constant with temperature above 550°C at a value of 42 ± 2 kcal/mole, which is about the same as the value found for self-diffusion. Observation of polygonization during creep suggests that the deformation rate is controlled by climb of dislocations. The activation energy for imperfect single crystals is higher than that for polycrystals.

Deformation mechanisms of beta-uranium single crystals deformed by bending and tension were studied by Rodriguez and Coll.[2] Metallographic observation of the deformation produced allows the recognition of three systems of slip traces. Two of the systems were identified as corresponding to the $\{110\}\langle 001\rangle$ system, reported by Holden, and the third to $\{100\}\langle 001\rangle$. Since the Kronberg zonal dislocation proposed for the $\{110\}\langle 001\rangle$ system cannot be extended to the (100) slip plane, a new model is submitted to explain the $\{100\}\langle 001\rangle$ mechanism. This model, involving an extended dislocation, not only accounts for the difference in morphology observed between the traces corresponding to the two systems, but also explains the stacking faults reported in the iron-chromium sigma phase.

Investigators at Nuclear Metals[3] have attempted to produce fine-grained castings of uranium by the addition of up to 7 wt.% uranium shot to a stream of molten metal. It was concluded that the addition of shot in the −48 +80 range to molten uranium does not noticeably affect the grain size of the resultant casting. More effective grain refinement might be achieved with finer shot and would provide more nucleation sites. Preservation of such fine grains would require rapid cooling through the gamma phase to avoid grain coarsening.

The swelling of uranium on postirradiation annealing has been examined at Argonne.[4] Swelling was investigated by utilizing density measurements in conjunction with the observation of pores in the microstructures of annealed specimens. Specimens were irradiated to about 0.3 at.% burnup in a constrained condition at approximately 275°C and were subsequently pulse annealed. The amount of swelling was less than 1.1% for specimens that were annealed up to 75 hr at temperatures below 550°C; the amount of swelling, however, increased considerably on annealing at temperatures between 550 and 650°C. Specimens annealed up to 75 hr at 618°C decreased in density approximately 18%. The swelling was accompanied by the formation of bubbles on grain boundaries in recrystallized regions. The observations suggest that recrystallization is a prerequisite for pronounced swelling in the alpha phase.

Uranium specimens annealed up to 75 hr at temperatures between 650 and 750°C in the beta phase decreased in density about 5%. Specimens annealed in the beta phase, in contrast to those annealed at 618°C in the alpha phase, were badly cracked and contained smaller diameter pores that were uniformly distributed within the grains. A specimen annealed up to 16 hr at 822°C decreased in density about 20%. This heat-treatment produced large-diameter pores located along grain boundaries, as well as smaller diameter pores distributed uniformly within the grains. (M. S. Farkas)

Alpha-Phase Uranium Alloys

The metastable phases in the uranium-niobium system were studied by French[5] investi-

gators. Uranium alloys containing 0.3 to 17.3 at.% niobium were quenched from the γ-phase field, and the resulting structures were examined by micrography and X-ray diffraction. The α, α'_a, and α'_b phases were successively observed for solute contents below 8.8 at.%. The lattice parameters, as well as hardness values of these orthorhombic phases, were determined as a function of composition. In the range 8.8 to 15.7 at.% niobium, an α''_b phase was formed which is monoclinic, as derived from the orthorhombic system by a variable angle β that increases regularly from 90° as a function of the niobium content. Beyond 15.7 at.% niobium, tetragonal γ^0_d was formed. Comparison of water, oil, and argon quenches showed the pronounced influence of quenching rate. Although the succession of metastable phases observed is qualitatively the same as in the uranium-molybdenum system, composition ranges were systematically displaced toward higher solute contents in the uranium-niobium system. The formation of some of these martensitic phases was satisfactorily explained in terms of a shear of the cubic phase in $\{1\,1\,2\}\,\gamma$ along the $(1\,1\,1)\,\gamma$ directions. The behavior of molybdenum, niobium, and zirconium as solutes was interpreted in terms of the atomic diameters of these elements. However, the origin of the α'_a phase could not be determined.

Mechanical properties of uranium-molybdenum alloys were measured by the English.[6,7] Tensile tests were run on specimens of uranium alloys containing from 1.5 to 30 at.% molybdenum, in the oil-quenched and mercury-quenched condition. The form of the results, in general, was consistent with that suggested by previously obtained hardness values. Two forms of cracking were found at certain ranges of composition. The first type was due to stress corrosion by air; the second was a form of intergranular brittleness. The results of the tensile tests are shown in Figs. I-1 and I-2.

The deformation of compressed specimens of the martensitic alpha structures and the metastable gamma phases of quenched uranium-molybdenum alloys containing 3 to 30 at.% molybdenum has been investigated by metallographic and X-ray means. Knowledge of the deformation characteristics of the alpha phases has helped in the qualitative understanding of the strengths shown by these phases. The true gamma phase has been found to deform by $\{1\,1\,2\}$ twinning, but one metastable gamma phase de-

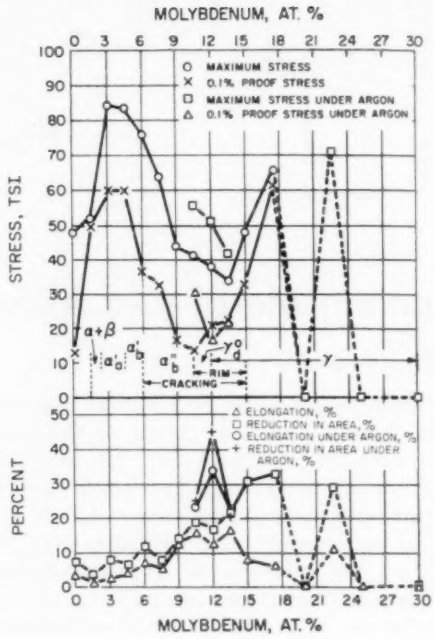

Fig. I-1 Uranium-molybdenum alloys, mercury quenched from 900°C.[7]

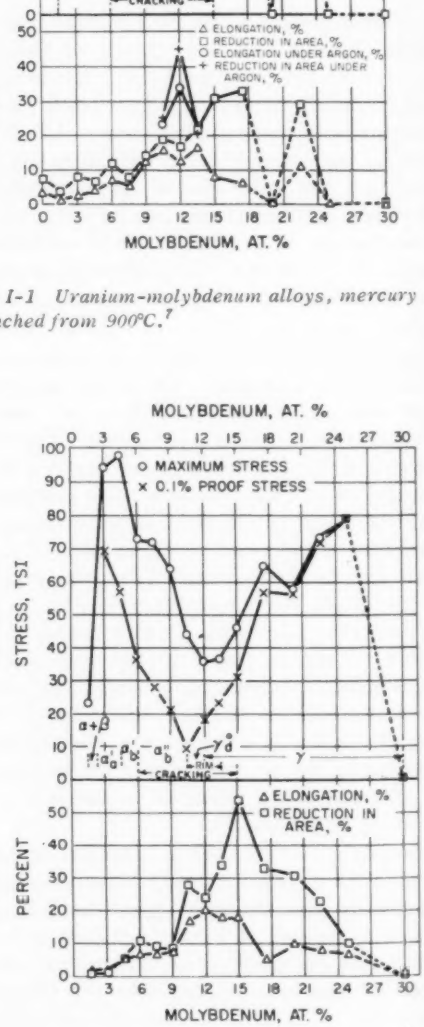

Fig. I-2 Uranium-molybdenum alloys, oil quenched from 900°C.[7]

formed by {1 2 2} twinning, the twins themselves being twinned on {1 2 2} planes. Another metastable gamma phase has been observed to deform by {1 2 2} twinning, but in this case the twins themselves were twinned on {1 1 2} planes. The various twinning phenomena have been discussed in terms of the order thought to exist in the metastable phases.

Uranium-niobium-chromium alloys were examined by the Germans[8] by means of microscopy, thermal analysis, temperature-temperature difference measurements, and X-ray diffraction. The liquidus surfaces and the course of the troughs therein were determined. Isothermal sections at 1050, 850, and 550°C and four vertical sections were presented that give an idea of the shape of the phase region in terms of temperature and concentration. Five four-phase equilibria were observed at 890, 730, 690, 635, and 615°C. Typical of this system were wide, heterogeneous-phase regions, which in most cases contained the intermetallic $NbCr_2$ phase. The addition of chromium did not prevent the liquation of the body-centered cubic uranium-niobium solid solution (gamma) at temperatures lower than 1000°C. In the case of the beta solid solution of the binary uranium-niobium system, the eutectoid decomposition temperature shifted from 640 to around 615°C by the addition of chromium; whereas for the γ_1 solid solution, no shift in the decomposition temperature of 650°C was observed.

A translation of a portion of a Russian book,[9] *Structure and Properties of Uranium, Thorium, and Zirconium Alloys*, is now available. The translated chapters include "Uranium Corner of the Uranium-Aluminum-Iron Phase Diagram," "Effect of Rapid Quenching on Cracking of Uranium Alloys," "Kinetics of Transformation by Sharp Quenching of β-Phase in Alloys of Uranium with Aluminum, Silicon, Iron, Nickel, Molybdenum, and Fissium," and "State of Impurities with Respect to Tempering Temperature of Quenched Uranium Alloys."

(M. S. Farkas)

Dilute Uranium Alloys

The alpha-aluminum solid-solubility limits in the aluminum-uranium system were determined by the Canadians.[10] The maximum solid solubility of uranium in aluminum was found to be 0.06 ± 0.02 wt.% uranium at the eutectic temperature. The alpha-aluminum–UAl_4 eutectic temperature was established by thermal analysis as 646 ± 0.5°C. At 350°C, the solid solubility decreased to less than 0.04 wt.% uranium in the aluminum-uranium system.

(M. S. Farkas)

Plutonium

Plutonium Metal and Alloys

Los Alamos[11] has measured the solubility of tantalum in liquid plutonium over the temperature range 700 to 1000°C. Solubility was found to increase from 45 ppm (by weight) tantalum at 750°C to 1070 ppm tantalum at 1000°C. The data fit the empirical equation

$$\log N_{Ta} = 3.06 - 7.50 \times 10^3 \, T^{-1}$$

where N_{Ta} is the solubility of tantalum expressed as the mole fraction and T is the temperature, °K.

The plutonium-yttrium phase diagram shown in Fig. I-3 has been determined by Mound investigators[12] on the basis of metallographic examination, electron-microprobe analysis, and thermal analysis. Significant features of the diagram were the extensive solid solubility of

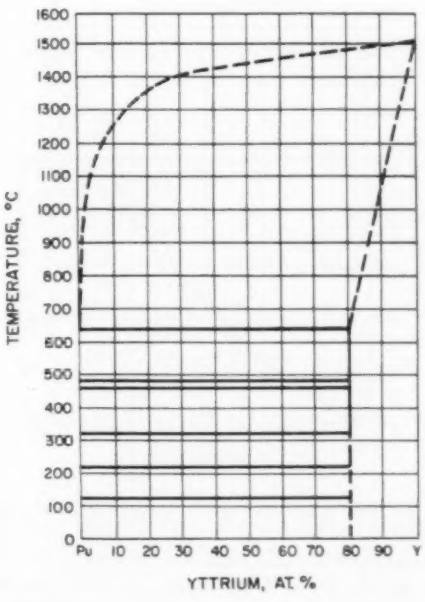

Fig. I-3 The plutonium-yttrium binary system.[12]

plutonium in yttrium and the extremely limited solid solubility of yttrium in plutonium.

The heat capacity of a plutonium–56 at.% cerium–24 at.% cobalt alloy was measured from 100 to 600°C. A plot of the data, Fig. I-4, indicates that the heat capacity of the alloy is comparable to that of pure cerium.

Argonne[13–15] is continuing the investigation of uranium-plutonium base alloys. The heat contents of uranium–10 wt.% plutonium and uranium–10 wt.% plutonium–10 wt.% fizzium alloys which were measured at temperatures up to about 1200°C are plotted in Fig. I-5. In the uranium–10 wt.% plutonium alloy, heats of

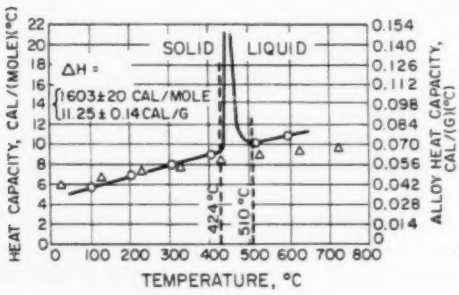

Fig. I-4 Heat capacity of the plutonium-cerium-cobalt eutectic alloy as a function of temperature.[12] ○, plutonium-cerium-cobalt alloy; △, cerium.

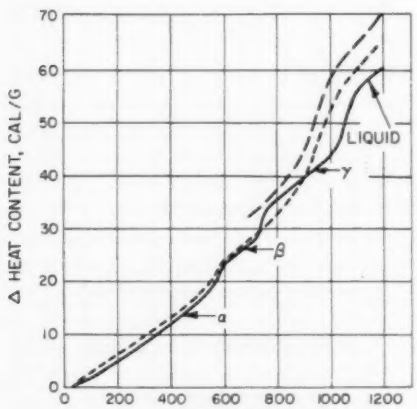

Fig. I-5 Heat contents[13] of uranium–10 wt.% plutonium and uranium–10 wt.% plutonium–10 wt.% fizzium above 25°C. ——, uranium–10 wt.% plutonium; – – –, uranium–10 wt.% plutonium–10 wt.% fizzium; — —, uranium–10 wt.% plutonium–10 wt.% fizzium (calculated).

Table I-1 SOLIDUS, LIQUIDUS, AND SOLID TRANSFORMATION TEMPERATURES OF URANIUM–10 WT.% PLUTONIUM AND URANIUM–10 WT.% PLUTONIUM–10 WT.% FIZZIUM[14]

U–10 wt.% Pu	Temperature by thermal analysis, °C	Temperature from U-Pu phase diagram, °C
$\alpha \rightarrow \alpha + \beta$		580
$\alpha + \beta \rightarrow \beta$		590
$\beta + \gamma \rightarrow \gamma$	735	730
$\beta + \gamma \rightarrow \gamma$		740
Solidus	1025	1030
Liquidus	1060	1080

U–10 wt.% Pu–10 wt.% Fz	Temperature by thermal analysis, °C	Temperature from calorimetry, °C
Solid transformations	535 630	535 600
Solidus	910	900
Liquidus	1010	1030

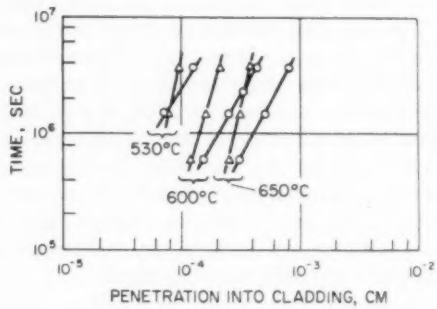

Fig. I-6 Penetration of vanadium–10 wt.% titanium and vanadium–20 wt.% titanium by uranium–10 wt.% plutonium–10 wt.% fizzium.[13] △ and ○, vanadium–20 and 10 wt.% titanium, respectively, vs. uranium–10 wt.% plutonium–10 wt.% fizzium.

transformation from alpha to beta and beta to gamma are 2.9 ± 0.3 and 4.7 ± 0.5 cal/g, respectively. Heat of fusion for the binary alloy is 10.2 ± 1.0 cal/g. For the uranium–10 wt.% plutonium–10 wt.% fizzium alloy, the heat of fusion is 9.5 ± 2.2 cal/g. In Table I-1, thermal-analysis data for solid transformations and melting of the alloys are compared with the uranium-plutonium phase diagram and with calorimetry data.

The results of compatibility tests between uranium-plutonium-fizzium alloys and potential cladding materials at temperatures up to 650°C are summarized in Fig. I-6 and Table I-2.

Table I-2 COMPATIBILITY OF URANIUM-PLUTONIUM-FIZZIUM ALLOYS WITH POTENTIAL CLADDING MATERIALS[13]

Material, wt.%	Temp., °C	Interdiffusion bandwidth, μ 7 days	17 days	42 days	Direction
Nb vs. U–10 Pu–10 Fz	550	3	5	6	Total band width; almost 100% into the cladding
	600	7	10	15	
	650	14	30	80	
Nb–1 Zr vs. U–10 Pu–10 Fz	550	3	6	7	Total band width; almost 100% into the cladding
	600	6	9	15	
	650	12	29	73	
Nb vs. U–20 Pu–10 Fz	550	6	8	12	Total band width; almost 100% into the cladding
	600	10	21	35	
	650	23	75	172	
Nb vs. U–10 Pu	550	Nil	Nil	Nil	No evidence of penetration
	600	Nil	Nil	Nil	
	650	Nil	Nil	Nil	
V vs. U–10 Pu–10 Fz	550		4	5	Total band width; penetration mostly into the fuel
	600		5	6	
	650			11	
V–10 Ti vs. U–10 Pu–10 Fz	550		1	1	Penetration into the cladding; also evidence for some diffusion into the fuel
	600	2	3	4	
	650	3	5	8	
V–20 Ti vs. U–10 Pu–10 Fz	550			1	Penetration into the cladding; also evidence for some diffusion into the fuel
	600	1	2	2	
	650	3	3	4	
Mo vs. U–10 Pu–10 Fz	550	4	6	9	Total band width; about 50% into the cladding
	600	5	8	11	
	650	11	17	24	
304 S.S. vs. U–10 Pu–10 Fz	550	2	3	4	Penetration into the cladding; also evidence for major diffusion into the fuel
	600	5	7	10	
	650	11	16	22	
Hastelloy X vs. U–10 Pu–10 Fz	550				Penetration into the cladding; also evidence for major diffusion into the fuel
	600	5	10	18	
	650	16	29	39	

Penetration rates of vanadium by molten uranium, uranium–10 wt.% plutonium, and uranium–10 wt.% plutonium–10 wt.% fizzium are plotted in Fig. I-7. The rate reversal noted at 1200°C in the curve for the uranium–10 wt.% plutonium–10 wt.% fizzium alloy is believed to be caused by the presence of zirconium-vanadium and ruthenium-vanadium compounds. The sudden increase in penetration rate at 1300°C corresponds to the 1300°C melting temperature of ZrV_2.

Attempts are being made to improve the corrosion resistance of pyrophoric uranium-plutonium alloys by ternary alloying. Results of corrosion tests in air are tabulated in Tables I-3 and I-4.

Results of studies of ignition temperature of plutonium in air and oxygen are listed in Table I-5. In the shielded ignition experiments, the plutonium samples were heated to temperature

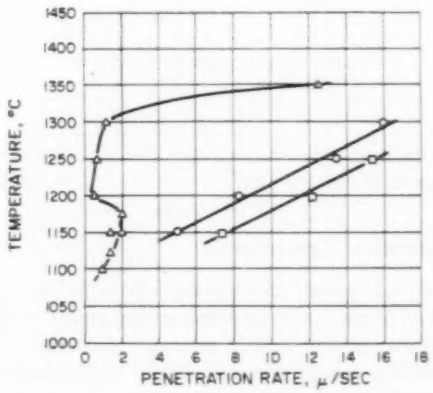

Fig. I-7 Penetration of vanadium by molten uranium, uranium–10 wt.% plutonium and uranium–10 wt.% plutonium–10 wt.% fizzium.[13] *○, vanadium vs. uranium; □, vanadium vs. uranium–10 wt.% plutonium; Δ, vanadium vs. uranium–10 wt.% plutonium–10 wt.% fizzium.*

Table I-3 RESULTS OF CORROSION IN AIR OF URANIUM AND URANIUM-PLUTONIUM BASE ALLOYS[13]

Alloy (balance uranium), at.%	Original weight, g	% weight gain after 1 month	2 months	3 months	4 months	Remarks
27 Pu–6 Al	6.37	13.2	15.1	15.9	16.0	Began gaining weight on 2nd day; completely disintegrated by 6th day
27 Pu–6 C	3.23	12.1	14.8	15.5	15.8	No gain in weight first 5 days; gained 0.03 g by 6th day; completely disintegrated by 6th day
30 Pu	6.85	9.5	13.0	15.2	15.8	Began gaining weight on 2nd day; completely disintegrated by 6th day
27 Pu–6 Cu	4.45	7.6	11.7	14.8	15.7	Showed some signs of swelling and initial disintegration on 6th day; began gaining weight on 7th day; completely disintegrated by 21st day
27 Pu	2.95	0	0	0.7	1.0	Began to disintegrate after 11 weeks, but did not start gaining weight until after 12th week; some powder after 4 months
27 Pu–6 Zr	3.75	0	0	1.3	2.1	Began gaining weight shortly after 2 months, but did not start disintegrating until after 3 months; more powder than Fe alloy
27 Pu–6 Mo	3.49	0	0	0	0	A very thin surface film spalled off after 3 months, but no weight change
20 Pu–10 Fz*	0.10	0	0	0	0	No weight change; surface tarnished
U	3.19	0	0	0	0	No weight change; surface tarnished

*In wt.%.

in helium. At temperature the helium was replaced by the oxidant. (V. W. Storhok)

Plutonium Compounds

A continually increasing effort is being devoted to the understanding of the properties and structures of PuO_2. Mound Laboratory[12] attributes the previously noted voids within the spherical plasma-produced PuO_2 particles to pullout of unmelted areas during metallographic preparation. The same source reports dissolution of 10 wt.% PuO_2 in SiO_2 by melting with the plasma flame; however, no comment on the postmelting composition of the material was offered. More basically, McNeilly[16] of Hanford has measured an activation energy for electronic conduction of 0.52 ev for PuO_{2-x} over a wide range of oxygen content, whereas the activation energy of $PuO_{2.0}$ is 1.8 ev. Another study[17] of the plutonium-oxygen relation is now under way at Argonne. Electrolytic cells and electrical-conductivity measurements are being used, but all data appear quite preliminary. The thermal expansivity[18] of PuO_2 is given as 9.1×10^{-6}/°C to 900°C.

It is reported in a British patent[19] that controlled additions of Fe_2O_3 to PuO_2 greatly increase the sinterability, with values of 95% of theoretical density being attained in the temperature range of 1400 to 1650°C with the use of 0.05 to 2.0 wt.% additive. The dissolution of

Table I-4 CORROSION OF URANIUM-PLUTONIUM BASE ALLOYS IN AIR[14]

Alloy, at.%	Casting method	Length of test, days	Weight gain, %	Remarks
$(U_{0.82}Pu_{0.18})_6Fe$	Injection cast	45	1.9	Very slightly tarnished; weight nearly constant after 14 days
U–27 Pu–6 Mo	Injection cast	35	0.2	Has very thin black film
U–27 Pu–6 Fe	Injection cast	35	7.0	Began disintegrating on 10th day; completely disintegrated by 12th day
$(U_{0.82}Pu_{0.18})_6Fe$	Injection cast	35	0.1	From same casting as specimen No. 10, except cast surface machined off; very slightly tarnished; weight nearly constant after 14 days
$(U_{0.82}Pu_{0.18})_6Fe$	Chill cast as 9.02-cm-thick plate	35	1.1	Very slightly tarnished; weight nearly constant after 14 days
$(U_{0.82}Pu_{0.18})_6Fe$	Chill cast as 2.21-cm-thick plate	31	0.7	Very slightly tarnished; weight constant after 10 days
$(U_{0.82}Pu_{0.18})_6Fe$	Chill cast as 4.57-cm-thick plate	31	0.6	Very slightly tarnished; weight constant after 10 days; developed several cracks after 19 days
U–18 Pu	Injection cast	31	0.4	Blackened, swollen, and cracked 17 days
U–18 Pu	Cast into 270°C mold	18	0.1	Surface blackened in 8 days; began to swell and disintegrate by 18th day
U–18 Pu	Chill cast	14		Surface nearly all black by 14th day

Table I-5 IGNITION TEMPERATURES OF PLUTONIUM IN AIR AND OXYGEN[15]

Foil thickness, mm	Specific area, cm^2/g	Burning-curve ignition temp., °C		Shielded ignition temp.,* °C	
		Air	O_2	Air	O_2
~5 (cube)	0.65	520 508	512 494	442 to 492	
1.0	1.5	492 322	490	378 to 408	327 to 374
0.52	2.5	310 314	468 505	303 to 337	353 to 398
0.22	5.3	518 520 535 519† 521†	524 527	375 to 403	322 to 350
0.17	6.7	282	299		
0.12	11.0	282	305	266 to 280	273 to 284

*Indicated as the highest temperature at which ignition did not occur and the lowest temperature at which ignition did occur.

†Samples were polished with 600-grit SiC paper; all others as received.

PuO_2 in sulfamic acid for 1 hr at 40 and 70°C occurred to the extent of 0.4 and 1.6 mg/liter, respectively,[20] which is less drastic than the attack by 7 *M* to 14 *M* HNO_3.

Hanford[20,21] has indicated that beta-Pu_2O_3 is incompatible with thorium metal above 500°C but that this oxide will not react with tantalum, molybdenum, niobium, or vanadium at 1650°C in helium. No time periods are mentioned.

More details[22] of the self-irradiation damage in PuC showed a saturation effect on lattice-parameter increase after 975 days; self-irradiation damage of Pu_2C_3 continued to increase after 500 days. An irradiation of 20×10^{20} fissions/cm^3 produced numerous cracks and X-ray diffraction indications of severe structural damage in PuO_2, whereas PuN had relatively few cracks, showed some indication of structural damage, and reacted slightly with the aluminum heat-extracting components.[20,22]

The PuN fuels are being more thoroughly studied as their potential is evaluated. Los Alamos[23] reported a refined value for ΔH°_{298} of approximately −69 kcal/mole for the reaction $Pu_{(s)} + \frac{1}{2} N_{2(g)} \rightarrow PuN_{(s)}$. UN–20 wt.% PuN solid solutions prepared in 5 hr at 1800°C under $\frac{2}{3}$ atm of nitrogen[24] exhibited no oxidation under X ray and no densification. The alloy did not react with type 304 stainless steel in $8\frac{1}{2}$ hr at 1000°C. Battelle (unpublished data) did not detect any reactions between PuN and iron-base alloys, Inconel, or the refractory metals below 1300°C.

A brief study[25] of the volatility of PuC and Pu_2C_3 revealed considerable decomposition at 1550°C. Plutonium vaporized preferentially, with the remaining carbon forming Pu_2C_3. The diffusion of plutonium through a surface Pu_2C_3 layer was probably the rate-controlling step.

A method of preparing improved (U,Pu)C solid-solution fuels is reported by Sowden,[26] who reacts the mixed oxides with stoichiometric amounts of carbon at 1500°C at less than 200 μ Hg pressure. A second report[27] indicates solid-solution formation by interdiffusing loose PuC and UC powder at 2000°C for 40 min in vacuum. However, the expected stoichiometry-control problem at a temperature 350°C above the PuC melting point is not detailed.

The previously accepted maximum temperature limit on PuC-tantalum systems may have been extended by a report[24] that the two materials do not react after 11 hr at 1400°C.

(W. M. Pardue)

Thorium

The thorium-ruthenium and thorium-rhodium binary systems were studied by the British[28] over the whole range of compositions at temperatures of 1000 to 1500°C by metallographic and X-ray methods. Four intermetallic compounds were formed between thorium and ruthenium, namely, Th_7Ru_3, Th_5Ru_2, ThRu, and $ThRu_2$, whereas in the thorium-rhodium system, the compounds Th_7Rh_3, ThRh, Th_3Rh_4, Th_3Rh_5, $ThRh_2$, $ThRh_3$, and $ThRh_5$ were detected. The compound $ThRh_2$ undergoes a polymorphic transformation above 1200°C.

Hanford workers report[29] that increasing the uranium content from 2.5 to 5.0 wt.% has little effect on the room-temperature hardness or the 750°C extrusion constant of thorium-base alloys with up to 10.0 wt.% zirconium. Room-temperature hardness curves show a minimum for both uranium levels between 2 and 3 wt.% zirconium.

A pickling solution of 23 g/liter of Alodine deoxidizer (manufactured by Amchem Products, Inc., Ambler, Pa.), 190 ml/liter of nitric acid (70 wt.%), and the balance distilled water has been used to remove surface oxides on thorium at 120°F by investigators at Oak Ridge.[30]

The effect of mechanical work at 700°C on the grain size of thorium, as estimated by Oak Ridge workers,[30] is shown in Fig. I-8.

(R. L. Martin)

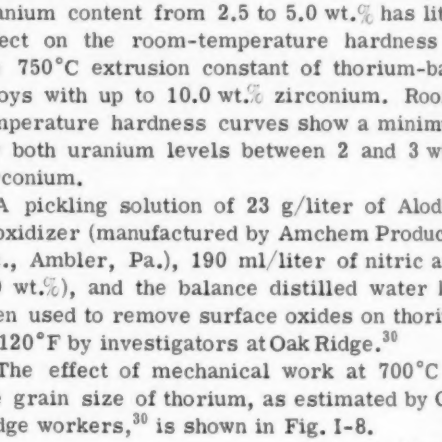

Fig. I-8 The effect of deformation at 700°C on grain size of thorium.[30]

Metal-Ceramic Fuels

Dispersion Fuels

Inhibition of the reaction between UO_2 and aluminum was investigated in Germany.[31] Compressed-powder fuel elements were used, and

these were made with 50-50 vol.% of UO_2 and oxide-free pure aluminum or aluminum-silicon alloys. The green-pressed specimens were heat-treated, examined by metallographic techniques, X-ray diffraction, and chemical analysis, and measured for dimensional changes. The most promising inhibitor appeared to be aluminum nitride, although some inhibition was also attributed to the silicon content of aluminum and to the thermal deactivation of UO_2.

Dispersions containing an enriched-uranium-containing intermetallic phase distributed in both a type 304 stainless steel and an 80 wt.% nickel–chromium alloy matrix have been irradiated in the ETR.[17] Examination of the irradiated specimens indicated that the 80 wt.% nickel–chromium matrix was more resistant to volume changes accompanying the burnup of uranium than the type 304 stainless-steel matrix. The rate of volume change for the 80 wt.% nickel–chromium was about 0.7% $\Delta V/10^{20}$ fissions/cm^3 for temperatures up to 560°C, as compared with 1.6 to 2.6% $\Delta V/10^{20}$ fissions/cm^3 for temperatures up to 560°C for the type 304 stainless steel.

Tubular fuel elements consisting of dispersions of 40 vol.% UO_2 in molybdenum or tungsten have been produced at Los Alamos using the ingenious technique[32] of connecting the powders magnetically. Compaction forces are generated by opposing magnetic fields in a coaxial conductor carrying high pulsed currents. With Los Alamos equipment, dispersion fuel tubes up to 30 in. long with sintered densities over 90% of theoretical have been made. (D. L. Stoltz)

Cermet Fuels

Irradiation specimens containing nominally 58 vol.% UN–tungsten and 65 vol.% UN–molybdenum were irradiated in the ETR at cladding surface temperatures greater than 2000°C for 21 days at approximately 0.2×10^{20} fissions/cm^3. Postirradiation examination of the specimens was conducted at Hanford and revealed no evident reaction zone between the fuel particles and the matrix metals. Preliminary fission-gas release data[24] are tabulated below.

Specimen composition	Fission-product gas released, %	
	Xenon	Krypton
58 vol.% UN–tungsten	61	67
65 vol.% UN–molybdenum	12	15

In addition, three specimens of 64 vol.% UO_2–tungsten were irradiated for 2 to 4 hr at temperatures greater than 2100°C. Extensive post-irradiation measurements and metallography examinations[21] indicated that the specimens were dimensionally and chemically stable.

(D. E. Kizer)

Coated-Particle Fuel Materials

Particle Coating

Work at Oak Ridge[33] includes the development of a means of calculating both stress and strain in pyrolytic carbon (PyC) coatings as functions of geometry, physical and mechanical properties, and operating conditions. The basic mathematical development is reported, and use of the method is illustrated through calculations of stress and strain profiles in coated particles that result from thermal expansion alone. It is planned to apply the method for calculations of stress and strain resulting from combined thermal and radiation-induced changes in typical coated particles. The results of this work should be useful in the optimization of PyC-coated nuclear fuel particles.

Preparation of PyC coatings in a fluidized bed of nuclear fuel particles is often viewed as a relatively simple process in which the quality of the coatings produced is related to the coating temperature, the reactant concentration, and the coating rate. However, the relation of coating quality to coating conditions is complicated by the fact that coating quality can be significantly affected by the geometry of the coating reactor. Battelle[34] reports the results of a series of experiments that provide information on the effect of reactor geometry on the quality of PyC coatings. The results demonstrate that the average rate of deposition, expressed in terms of coating thickness, increases markedly with a decrease in bed inventory as shown in Table I-6. The experiment indicates that the growth rate falls off rapidly as the particles move out of a fairly localized reactant-rich volume of the bed. The localized nature of the reaction is also demonstrated by deposition on carbon threads stretched across a coating reactor at various levels. The variation in coating rate with position is summarized in Table I-7.

Table I-6 VARIATION OF COATING RATE WITH BED SIZE[34]

Coating conditions:
Temperature, 1400°C
Reactant, C_2H_2 (in He)
Reactant concentration, 4.0 mole %
Pressure, ~atmospheric
Total flow (STP), 2500 cm^3/min
Reactor: 1 in. in inside diameter, 37° cone
Bed: 710 to 840-μ PyC-coated spherical coke

Static bed height, in. above cone apex	Static bed volume, cm^3	Average coating rate, μ per hr
0.5	1.1	120
1.5	9.0	33

Table I-7 VARIATION OF COATING RATE WITH LEVEL[34]

Coating conditions:
Temperature, 1400°C
Reactant, C_2H_2 (in He)
Reactant concentration, 5.5 mole %
Pressure, ~atmospheric
Total flow (STP), 1600 cm^3/min
Reactor: 1 in. in inside diameter, 37° cone
Bed: 350 to 420-μ PyC-coated spherical coke

Location, in. above cone apex	Average coating rate, μ per hr
Thread at 0.5	39
Thread at 1.0	89
Thread at 1.5	42
Free particle	23

The suggestion that laminar coatings are formed by periodic accumulation of soot as the particles cycle from a soot-free region at the bottom of the bed to a more-or-less homogeneous sooty region higher up appears to be a valid explanation for the formation of the thin (about 0.1 μ) layers in the structure. It is also suggested that soot particles that are large enough to produce the larger laminations visible at 100× grow by agglomeration as well as by heterogeneous deposition of carbon on individual soot particles. This growth occurs in the voids in the bed, and the degree of growth depends on the ratio of void volume to the area of fuel particles exposed to the void. Thus bubbles in the bed, or a spout through the bed, can lead to the formation of relatively large agglomerates.

Confirmation of the effect of soot particles on the quality of PyC was obtained experimentally. A coating was initiated under conditions yielding visible soot in the product off-gases. A plunger, fitted with a perforated disk, was heated in the hot zone 1 in. above the bed and then forced down on the bed to prevent fluidization. The formation of soot stopped immediately. During about ½ hr, the pressure drop increased as deposition in the interstices restricted flow through the packed bed. Soot formation gradually resumed as the available area for deposition diminished. The material deposited in the static-bed condition was no longer laminar in structure, but was characterized by relatively uninterrupted growth.

The results of a crushing-strength study shown in Fig. I-9 illustrates the complexity involved in relating the properties of PyC-particle coatings to their structure and conditions of preparation. The contrast in data given in Fig. I-9 between acetylene and methane in terms of density vs. reactant concentration and coating rate is thought to be related to dif-

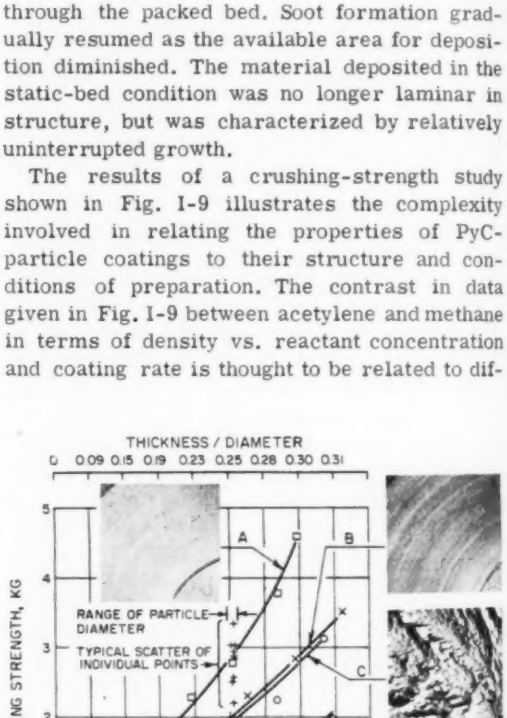

Curve	A	B	C	D
Symbol	□	×	○	△
Reactant	CH_4	C_2H_2	C_2H_2	CH_4
Partial pressure, atm	0.14	0.07	0.017	0.035
Helium flow, liters/min	3.23	3.50	3.50	3.50
Temperature, C	1400	1400	1400	1400
Coating rate, μ/hr	44	52	10	11
Coating density, g/cm^3	1.65	1.45	1.62	1.33
Coating hardness, KHN	123	133	100	83
Appearance of coating, (C = columnar, L = laminar)	L	L	C	C

Fig. I-9 Crushing strength of individual PyC-coated UC_2 particles.[34]

ferences in the size and concentration of soot particles or large-molecule precursors generated with the two reactants. The fact that the thermal decomposition of methane is endothermic, whereas that of acetylene is exothermic, should have a profound effect on the nucleation and growth of soot particles in the void space of the fluidized bed.

Development of BeO coatings applied to UO_2 shot in a fluidized bed is being continued at Battelle.[34,35] High-purity, dense BeO coatings can be prepared routinely by hydrolysis of $BeCl_2$ at temperatures of about 1400°C. Retention of fission gas during irradiation of the coated particles has not been satisfactory, although the coated particles show good integrity in out-of-pile evaluations. It is expected that the improved irradiation performance can be achieved with a randomly oriented submicron grain structure. The present typical product contains 5 to 50 μ preferentially oriented grains. The desired randomly oriented fine-grained structure must be resistant to grain growth for a period of time at the temperature of 1500°C required for incorporation of the coated particles in a BeO matrix or for subsequent use at comparable temperatures.

Neither modification of coating conditions nor codeposition of metal oxides has shown promise of retarding grain growth, as indicated by the results of a heat-treatment of the BeO coatings at 1500°C for 2 hr. However, codeposition of carbon has shown promise. BeO coatings having 8.8 and 15.6 wt.% carbon were fine grained in the as-deposited form and resisted grain growth on heat-treatment at 1500°C for 2 hr. Acid leach tests indicated that both of the carbon-doped coatings were porous. Additional preparations at reduced carbon levels are planned.

Intermittent deposition of 0.5-μ-thick films of tungsten or chromium carbide in the BeO coating has also shown promise as a means of interrupting grain growth in BeO coatings.

(N. D. Veigel)

Irradiation and Evaluation of Coated-Particle Fuels

OXIDE-BASE FUEL

Very little work is now in progress on oxide-coated UO_2 particles, the emphasis being placed on pyrolytic carbon coatings. A graphite-matrix specimen of 200-μ, 80% dense UO_2 particles coated with 60 μ of Al_2O_3 is being irradiated at Battelle.[34–36] Of interest is the fact that no coating failure has occurred after irradiation to an estimated 12 at.% burnup at 900°C. This material is considered to be the optimum Al_2O_3-coated UO_2 fuel, and no irradiation experiments are planned for Al_2O_3 coatings after this one.

The use of porous fuel particles, having been found to be beneficial in the case of Al_2O_3-coated UO_2, is now being tried with PyC coatings. Specimens of 200-μ, 77% dense UO_2 particles coated with 4 μ of laminar PyC to seal the UO_2 pores and overcoated with 69 μ of columnar PyC deposited from acetylene at 1400°C are being irradiated at Battelle.[34–36] No coating failures have been detected after irradiation to 1 at.% burnup at 100°C and to an estimated 2.5 at.% burnup at 815°C. Essentially complete failure has been reported in the past for comparable coatings on dense UC_2 particles irradiated under the same conditions. The porosity in the fuel particles appears to be necessary to accommodate radiation-induced expansion in the interior of the coated particles.

CARBIDE-BASE FUEL

The coatings for which Oak Ridge[37] has observed good performance have all been thicker than 100 μ. This has also been the case at Battelle[34–36] in irradiations at 100°C. With 200-μ dense UC_2 substrates, triplex PyC coatings 80 μ thick have exhibited 80% failure. Ninety-μ coatings have shown 5 to 10% failure, and 100-μ coatings have exhibited approximately 1% failure. In all cases, cracking of the coatings has occurred in less than 0.5 at.% burnup.

Promising results were obtained at Battelle[36] for porous UC_2 particles coated with PyC. A specimen of 127-μ, 80% dense UC_2 particles coated with only 43 μ of columnar PyC exhibited only 1% failure in an irradiation to 0.6 at.% burnup at 100°C, which illustrates the value of using porous fuel particles. In the past, coatings this thin on dense UC_2 particles have failed completely at 100°C.

A recent article by Sayers of Harwell reviews the irradiation behavior of PyC-coated fuel particles.[38] (C. W. Townley)

Compatibility of Coated Particles

A new approach is being considered by workers at General Atomic[39] in a continuing

study of the diffusion of various fuel materials in PyC. In this approach the diffusion matrix is prepared by depositing, under carefully controlled conditions, a thin layer (~100 μ) of PyC on a graphite disk. The resultant coating is then examined for the degree of preferred orientation, density, and crystallite size. Tracer-level diffusion measurements are performed by applying an aqueous salt of uranium (thorium) containing a trace amount of $^{232}U(^{228}Th)$. The objective of the new approach is to study the diffusion of fuel materials into a PyC that has a well-characterized structure so as to subsequently correlate the measured diffusion coefficients with various structural parameters. Initial data obtained for the diffusion of thorium in PyC deposited at 1350°C having a high degree of preferred orientation and a density of 1.95 g/cm^3 are shown in Fig. I-10. Uranium-diffusion experiments are in progress.

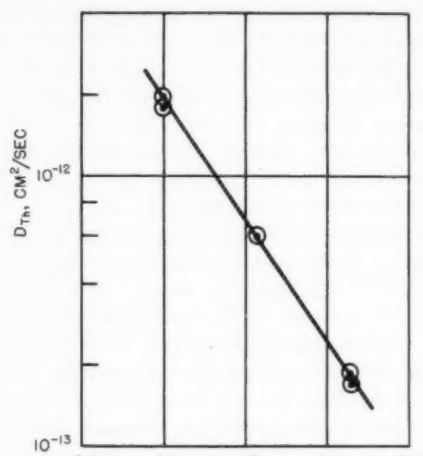

Fig. I-10 Diffusion of thorium in pyrolytic carbon.[39]

In experiments performed at Oak Ridge,[40] the compatibility of PyC-coated UC_2 fuel particles in steam was investigated over the 700 to 1100°C temperature range. Results indicated that the reaction rate at 700°C is extremely slow and that prolonged exposure is required to cause significant damage to the coatings, all of which were laminar. At temperatures greater than 700°C, the reaction rate increases with increasing temperature and water-vapor pressure, as shown in Table I-8.

Two types of attack were observed at temperatures from 800 to 1000°C: (1) uniform (general) attack on the outer edges, resulting in high coating losses but relatively small fuel losses, and (2) localized attack (pitting), resulting in small coating losses but large fuel losses. Tests at 1100°C indicated gross failure by peeling and radial cracking of the PyC.

(W. H. Pfeifer)

Table I-8 REACTIVITY[40] OF COATED PARTICLES FROM BATCHES 3M-113 AND 3M-114 WITH HELIUM CONTAINING H_2O AT PARTIAL PRESSURES OF 55 TO 355 mm Hg (TOTAL PRESSURE, 1 atm) IN THE TEMPERATURE RANGE 700 TO 1000°C

Sample	Weight of sample, g	Time, hr	Temp., °C	Partial pressure of H_2O, mm Hg	Weight loss, g	Amount of coating removed, %	Rate of coating removal, g/(g) hr	Uranium removed by HNO_3 leach	
								Grams	% of total U
3M-113-6	2.16	6	700	355	0.0025	0.2	0.0003	0.0001	0.02
3M-113-5	2.18	4	800	355	0.041	2.6	0.006	0.0232	4.0
3M-113-3	2.47	6	800	355	0.108	6	0.010	0.0021	0.3
3M-113-4	2.56	7	800	355	0.203	11	0.016	0.147	22
3M-113-2	2.51	6	1000	355	0.450	25	0.042	0.654	97
3M-114-4	2.50	6	800	233	0.036	3.2	0.005	0.0031	0.3
3M-114-1	2.45	6	800	355	0.036	3.3	0.006	0.0107	0.9
3M-114-9	1.99	6	900	233	0.127	14	0.024	0.001	0.1
3M-114-10	1.95	6	900	233	0.121	13	0.023	0.001	0.1
3M-114-3	2.41	4	900	355	0.159	15	0.037	0.002	0.2
3M-114-2	2.56	6	900	355	0.211	18	0.030	0.0177	1.4
3M-114-8	2.01	4	1000	55	0.099	11	0.027	0.001	0.1
3M-114-7	2.03	4	1000	92	0.149	16	0.041	0.002	0.2
3M-114-6	2.02	4	1000	149	0.193	21	0.053	0.001	0.1
3M-114-5	2.43	4	1000	355	0.424	39	0.097	0.016	1.3

Uranium Oxide Fuel Materials

Properties and Behavior

Experiments were performed in Norway[41] to measure the number of uranium atoms ejected from UO_2 surfaces by recoiling fission fragments. For fission densities ranging from 5×10^{15} to 7×10^{16} fissions/cm^3, the number of uranium atoms ejected per escaping fission fragment from 95.8% dense sintered UO_2 was about 9. Calculations were made which indicate that knock-ons and not evaporation of material in the thermal spikes are responsible for the ejected uranium atoms under the prevailing experimental conditions.

In-pile studies by Bettis[42] investigators showed that for operating temperatures near 500°C, the effective thermal conductivity of nickel-clad pressure-bonded fuel elements containing UO_2 and $UO_2 + ZrO_2$ remained the same as the unirradiated conductivities for irradiation exposures up to about 10^{19} fissions/cm^3. For UO_2, UO_2 + 34 wt.% ZrO_2, and UO_2 + 46 wt.% ZrO_2, the measured effective thermal conductivities were 0.035, 0.0165, and 0.021 watt/(cm)(°C), respectively. After an exposure of 25×10^{20} fissions/cm^3, these values decreased by 50, 25, and 35%, respectively. Within the temperature range from 100 to 700°C, the in-pile thermal conductivity of the high-density ZrO_2-base fuels was nearly independent of temperature. The effective thermal conductivities for the temperatures and fission densities investigated were consistent with the bulk fuel conductivities expressed by

$$k = \frac{1}{1/k_0 + fz}$$

where k_0 is the thermal conductivity of the unirradiated fuel, f is the fission depletion $\times 10^{-20}$, and z is 1.0 (cm)(°C)/watt/10^{20} fissions/cm^3. The in-pile contact conductances for the fuel-clad interfaces were in good agreement with out-of-pile measurements and calculated values. For interface pressures of about 3000 psi, the contact conductance was about 1 watt/(cm^2)(°C) across a UO_2-Zircaloy interface where the mating surfaces each had an arithmetic mean-surface roughness of less than 1 μ. Contact conductivity was unaffected by either evacuating the interface or filling it with krypton and xenon. There was some indication that contact conductance decreases with UO_2 conductivity; however, further work is necessary to really substantiate such a decrease.

Experiments involving large temperature gradients in UO_2 to simulate the relocation effects observed during high-temperature irradiation were performed by Yunus.[43] These experiments indicated that the columnar grain formation can be attributed to three steps: (1) grain growth by movement of the grain boundaries under the temperature gradient, (2) condensation of a vapor phase, and (3) solidification of a molten phase. No formation of columnar crystals was observed below 1700°C. Volatility of $UO_{2\pm x}$ was investigated at Oak Ridge[44] using thermogravimetric techniques. Between 1100 to 2200°C and oxygen pressures ranging from 10^2 to 10^{-6} torr, the vapor species above UO_{2+x} for x from 0 to 0.2 was UO_4. Above 1700°C, the equilibrium oxygen-to-uranium ratio of $UO_{2\pm x}$ was found to be less than 2.

Existing thermodynamic data for oxygen to UO_{2+x} above 1100°C were correlated by Hagemark.[45] In the range of 0.05 to 0.20 for x, the partial molar entropy of oxygen was found to follow the expression $-6.5 - 115x$ cal/(°C)(mole O_2), and partial molar enthalpy is given as $-6.2 - 54x$ kcal/mole O_2.

Postirradiation examination at Oak Ridge[46] of 96% dense UO_2 irradiated at temperatures above 4000°F to burnups from 87 to 8410 Mwd/metric ton of UO_2 indicated nearly complete release of the fission gas from the fuel. In other fission-product-release studies,[47] Stieglitz measured ^{131}I release from UO_2 during postirradiation heating. Two different diffusion processes were observed. The first process involves diffusion through an outer UO_2 layer containing a small excess of oxygen that follows an activation energy of 30.7 kcal/mole. The second process, which has an activation energy of 62.6 kcal/mole, is diffusion through the UO_2 lattice. A large portion of the ^{131}I that diffused from the UO_2 was found to remain on the sample surface.

Roellig[48] investigated reactions in the aluminum-UO_2 system using powder compacts at temperatures up to about 620°C. The kinetics followed the reaction

$$3UO_2 + 16Al \rightarrow 3UAl_4 + 2Al_2O_3$$

Oxide-free aluminum was found to react faster than aluminum with the normal oxide surface contamination. (R. H. Barnes)

Preparation of Uranium Dioxide Fuel Bodies

By studying the kinetics of reduction of high-density nonstoichiometric UO_2, Canadian investigators[49] have developed a low-temperature sintering process for the production of UO_2 fuel pellets. The oxygen-to-uranium ratio of pellets having a density 95% of theoretical (obtained by argon sintering for 2 hr at 950°C) could be reduced, by heating in hydrogen for 2 hr, from 2.27 to 2.030 at 1050°C without a change in the density.

On the basis of sintering studies in the urania-alumina system, Fiat investigators[50] were able to produce high-density UO_2-Al_2O_3 fuels containing up to 30 wt.% UO_2. Densities were nearly theoretical after sintering for 1 hr at 1600°C.

A recently issued patent[51] deals with the fabrication of a UO_2 fuel exhibiting high strength, density, and thermal conductivity. The process involves mixing the UO_2 starting powder with 0.1 to 1 wt.% of a metallic densifier oxide and 0.5 to 3 wt.% of a plasticizer, compacting the mixture, and sintering the bodies in an atmosphere of either carbon dioxide or carbon monoxide.

A method for the production of dense, coarse-grained UO_2 by reductive precipitation from alkali chloride melts was reported by German workers.[52] Fuel rods having densities of 89% of theoretical were prepared from this material by cold forging in steel tubes.

The production of UO_2 fuel bodies by pneumatic impaction was investigated by workers at Hanford.[53] UO_2 prepared from UF_6 was impacted to 93% of theoretical density at 1180°C and 132,000 psi. Impaction tests on UO_2-PuO_2 fuel mixtures have resulted in densities of 96.3% of theoretical. (T. R. Wright)

Uranium and Thorium Carbides, Nitrides, and Sulfides

Properties

General Atomic[54] reports that after 24 hr at 1800°C slightly hypostoichiometric UC (4.76 to 4.8 wt.% carbon) had reacted with tungsten–2 and 15 wt.% molybdenum alloys to form a grain-boundary liquid throughout the thickness of the tungsten alloys. This liquid was identified by microprobe analysis as a uranium-molybdenum alloy. Liquid present in slightly hypostoichiometric UC at 1800°C did not penetrate pure tungsten.

Crane and Gordon[55] have summarized the results of their irradiations of UC at surface temperatures up to 900°C and burnups up to 5.4 at.% of the uranium. Of several variables examined, the most pronounced effect was noted from variations in carbon content, as illustrated in Figs. I-11 and I-12.

The melting point of ThC_2-UC_2 solid solutions varies from 2640°C for ThC_2 to 2475°C for UC_2, according to data obtained at Oak Ridge.[56] The face-centered cubic solid solution exists down to 1415°C for ThC_2 and down to 1820°C for UC_2. Below 1415°C, ThC_2 becomes monoclinic by a diffusionless transformation. At 1500°C, face-centered cubic ThC_2 has a lattice parameter[57] of a = 5.808 A.

The thermal conductivity of ThS is 0.373 watt/(cm)(°C) at 300°C, according to Oak Ridge.[58]

The thermal conductivity of US is 0.171 watt/(cm)(°C) at 1000°C, according to Argonne.[17] At cladding temperatures of 400 to 790°C and burnups of 3 to 8 × 10^{20} fissions/cm^3, 90% dense US shows volume increases of 0.2 to 0.5% and gas releases of 0.03 to 0.2% of theoretical. Microstructures are unchanged.

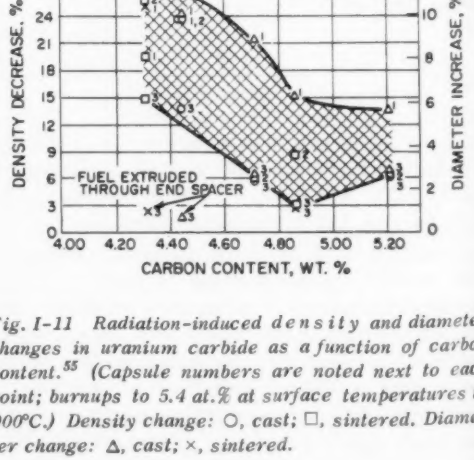

Fig. I-11 Radiation-induced density and diameter changes in uranium carbide as a function of carbon content.[55] (Capsule numbers are noted next to each point; burnups to 5.4 at.% at surface temperatures to 900°C.) Density change: ○, cast; □, sintered. Diameter change: △, cast; ×, sintered.

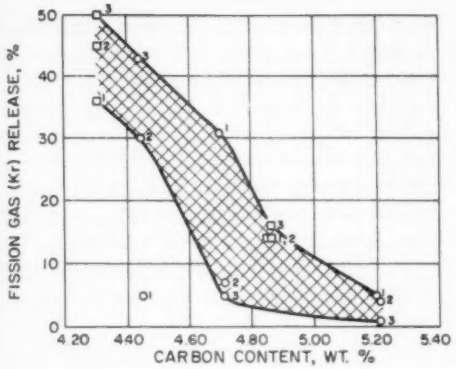

Fig. I-12 Percentage fission-gas release of the total formed in irradiated uranium carbide, as a function of carbon content.[55] (Capsule numbers are noted next to each point; burnups to 5.4 at.% at surface temperatures to 900°C.) ○, *cast;* □, *sintered.*

ThC is found to form a complete series of solid solutions[56] with UC, PuC, and NpC.

(W. Chubb)

Fuel-Water Reactions

Argonne[59] has reported additional results of the reaction of material of the same composition as SL-1 plates (aluminum – 17 wt.% uranium – 2 wt.% nickel). Isothermal data were taken by levitating pellets in an induction coil and exposing them to flowing steam for periods from 5 to 100 min. Agreement of the data with the cubic rate law (slope of $\frac{1}{3}$ on the log-log plot) is shown in Fig. I-13.

The constants of the cubic rate law were obtained by considering not only the aluminum-uranium-nickel alloy data but also previous data for pure aluminum. The following rate law was obtained:

$$w^3 = 4.0 \times 10^9 t \left(\exp -\frac{73{,}500}{RT}\right) \qquad (1)$$

where w = metal reacted, mg aluminum/cm^2
t = time, min
R = gas constant, 1.987 cal/(mole)(°K)
T = temperature, °K

Equation 1 also showed limited agreement with results for the pure aluminum-steam reaction at 1200 and 1300°C, as discussed in Sec. IV.

Argonne studies[60] of the reaction of water with representative aluminum-base fuel materials in TREAT showed the extent of reaction to be considerably greater than that predicted from the isothermal studies. TREAT results indicated that 15% reaction occurs in transient experiments in which the peak temperatures of the specimens submerged in room-temperature water are estimated to be 1200 to 1400°C. In the TREAT experiments, two types of fuel specimens, unclad SL-1 plate material and clad SPERT 1-D plates, were placed in small, high-pressure autoclaves and located at the center of TREAT. Most of the experiments were performed with the specimens immersed in room-temperature water with a 20-psi helium overpressure. One experiment was performed using room-temperature water and a 1000-psi helium overpressure. Residues from high-energy runs indicated the presence of powdery alumina, which is indicative of vapor-phase burning. The results with heated and pressurized water showed that very extensive reaction (75 to 90%) occurred when the estimated peak temperature of the fuel plate exceeded 1200 to 1400°C. The residue from these runs also suggested that burning had occurred. The extent of reaction in room-temperature water that was pressurized to 1000 psi with helium was intermediate (38% reaction); i.e., the extent of reaction was between that found in room-temperature water at 20 psi (10 to 20% reaction) and that found in water that was heated

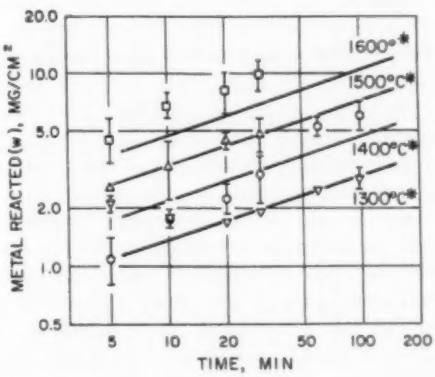

Fig. I-13 Reaction of aluminum – 17 wt.% uranium – 2 wt.% nickel alloy (SL-1 composition) with steam using the levitation melting method.[59] □, *1600°C;* Δ, *1500°C;* ∇, *1400°C;* o, *1300°C. The asterisk indicates that these lines are obtained from the equation:*

$$w^3 = 4.0 \times 10^9 t \left(exp - \frac{73{,}500}{RT}\right)$$

and pressurized (75 to 90% reaction). One experiment was completed with preirradiated SL-1 fuel material. Although 2.2 at.% of the heavy atoms present in the fuel had been fissioned, preirradiation had no apparent effect on the appearance of the residue or the extent of metal-water reaction.

The extreme sensitivity to pressure of the aluminum-water reaction was unexpected because other experiments had shown that the zirconium and stainless-steel–water reactions were relatively unaffected by large pressure changes. The data indicated that steam at high pressure greatly increases the extent of reaction but that inert gas suppresses the reaction.

(A. W. Lemmon, Jr.)

Basic Studies of Irradiation Effects in Fuel Materials

Metals

At Harwell[61] the physical mechanisms deduced from the direct observation in the electron microscope of inert gas bubbles in solids are used to evolve a model or theory for swelling. The model assumes the insolubility of the inert gases and the bodily migration of the bubbles and relies on the equation of state for the inert gas, on the surface energy, the surface self-diffusion coefficient, and the lattice parameter of the solid, and on some internal driving force, which is believed to be related to the line tension of the dislocation lines. With values for these parameters and the irradiation and annealing conditions, the bubble size (r) and number per cubic centimeter (n) are estimated. From these the swelling ($\Delta V/V$) can be calculated, but the effect of grain size, grain-boundary migration, and other structural features of the solid must be considered. The method is tested against several experimental results from a variety of solids, and satisfactory agreement is obtained. The model is thought to be valid for all solids, including nonmetals, and can account for breakaway swelling and gas release. The limitations of the model are discussed.

At Argonne[17] theoretical analyses indicate that random movement of bubbles is insufficient in itself as a mechanism for swelling in solids due to bubble coalescence. Work is in progress to determine more accurately the effect of coalescence by random movement, through consideration of the entire distribution rather than through consideration of an artificial distribution of bubbles of only one radius. The planned approach is to assume an initial distribution of very small bubbles and, with the digital computer, to calculate the distribution of bubble sizes at subsequent times by finite-difference methods.

It is expected that the mechanism of coalescence by random movement of bubbles cannot predict the amount of swelling observed in most postirradiation annealing experiments and that some other mechanism, such as grain-boundary sweeping, migration due to a thermal gradient, or migration due to elastic interaction of stress fields surrounding bubbles, must be considered.

The principal objective of this project is to determine the influence of a driving force on the migration and coalescence of bubbles. Again, the planned approach is to consider the change in some initial distribution due to the presence of a driving force, such as a thermal gradient, by application of finite-difference methods and numerical analysis.

Experimental programs are being planned to supplement the analysis of pore migration.

In Russia[62] it has been observed that the complex mechanism of swelling in fuels includes the formation of supersaturated solutions of inert gases in the system, resulting in the release of a gaseous phase; this is accompanied by the creation and subsequent growth of pores. The kinetics of the diffusion of the gases is controlled by the creep of the material subjected to the pressure of the gas held in the pores and the propagation of the vacancies toward the pores. The flow of the vacancies is assumed to be related to that of the gas atoms, and therefore the gas pressure within a given pore is compensated by the surface tension. If the diffusion of vacancies is the controlling factor in the pore growth, the volume change must follow an exponential law of time; if a creep mechanism prevails, the volume change remains independent from the pore-growth mechanism. An asymptotic solution of the swelling process was derived, determining the asymptote of the change in the number of the pores and in their average dimensions.

Ceramics

At Dounreay[63] results are reported of research into the irradiation behavior of cast uranium carbide with the following conclusions:

1. The saturation-resistivity and lattice-parameter increases for hypostoichiometric specimens irradiated at 80°C vary systematically with the excess concentration of uranium present in solution in the UC phase.

2. The temperature coefficient of resistivity (measured over the range 77 to 293°K), unlike the resistivity itself, is not significantly affected by irradiation.

3. A small resistivity annealing stage, in addition to those at 150 and 510°C, occurs between 1000 and 1200°C. The annealing out of the lattice-parameter change also occurs in two main stages of 150 and 510°C (5-hr anneals). A careful survey of the 400 to 800°C range has failed to reveal the stage postulated by other workers to occur at about 710°C. The significance of the results in determining the defect structure of irradiated uranium carbide is discussed.

The emission of ^{133}Xe from samples of uranium dioxide/yttrium oxide and thorium oxide/yttrium oxide solid solutions containing up to 30 mole % of yttrium oxide has been investigated at Harwell[64] by heating in the range 800 to 1600°C after a short irradiation. It is concluded that the migration of ^{133}Xe in these systems does not rely on the presence of vacancies in the oxygen sublattice.

The results of a series of experiments on the emission of ^{133}Xe from a stressed sample of uranium dioxide suggest that dislocations in the lattice also play no part in the migration of ^{133}Xe.

The release of fission xenon from UO_2 has been studied at Chalk River[65] during postirradiation annealing at 1400°C. Both single-crystal powders and sintered material were employed; suitable precautions were taken to ensure stoichiometric composition. In other postirradiation experiments the release of xenon from single-crystal powder specimens was followed during pulverization. The releases during annealing were analyzed by the commonly accepted diffusion equation, $f = \sqrt{(4Dt/\pi)}S/V$. The resulting diffusion coefficients decreased with increasing irradiation exposure. The decrease was most rapid in the range 10^{16} to 10^{17} fissions/cm^3 and had apparently saturated for sintered materials by 10^{19} fissions/cm^3. Anneals of long duration were performed on single-crystal specimens irradiated to exposures from 8.5×10^{14} to 3.0×10^{17} fissions/cm^3. The diffusion coefficients appeared to decrease abruptly during the period of 8 to 24 hr after the start of an experiment. A constant lower value was then indicated for the following period of three to seven days. The diffusion results are interpreted in terms of a distribution of existing, and irradiation-induced, trapping sites on a submicron scale. Pulverizing experiments with single-crystal specimens support the existence of the irradiation-induced trapping sites. The interpretation leads to an upper limit of 3×10^{-3} (xenon atoms/uranium atom)/atm xenon for the solubility of xenon in the UO_2 lattice at 1400°C.

At the Hahn-Meitner-Institut,[66] ideal diffusion has been observed for xenon in ThO_2 crystals above 1900°C. The activation energy is 85 kcal/mole between 1400 and 2000°C. (F. A. Rough)

References

1. J. P. Andre, P. Grenier, and P. Lacombe, Comparative Study of Creep in Imperfect Single Crystals and Polycrystals of α-Uranium (in French), *Mem. Sc. Rev. Met.*, 60: 888-894 (December 1963).
2. C. Rodriguez and J. A. Coll, Deformation Mechanism of β-Uranium Single Crystals, *J. Nucl. Mater.*, 11: 212-219 (February/March 1962).
3. W. J. Richmond, Fine-Grained Uranium by the Addition of Shot During Casting, USAEC Report NMI-7019, Nuclear Metals, Inc., May 31, 1963.
4. B. A. Loomis and D. W. Pracht, Swelling of Uranium on Postirradiation Annealing, *J. Nucl. Mater.*, 10: 346-359 (December 1963).
5. M. Anagnostidis, M. Colombié, and H. Monti, Metastable Phases in the Uranium-Niobium Alloys (in French), *J. Nucl. Mater.*, 11: 67-76 (January 1964).
6. R. F. Hills, B. R. Butcher, and B. W. Howlett, The Mechanical Properties of Quenched Uranium-Molybdenum Alloys, Part I: Tensile Tests of Polycrystalline Specimens, *J. Nucl. Mater.*, 11: 149-162 (February/March 1964).
7. B. R. Butcher and B. A. Haft, The Mechanical Properties of Quenched Uranium-Molybdenum Alloys, Part II: A Preliminary Survey of the Deformation Mechanisms, *J. Nucl. Mater.*, 11: 163-182 (February/March 1964).
8. G. Petzow and A. Junker, On the Structure of the System Uranium-Niobium-Chromium (in German), *J. Less-Common Metals*, 5: 462-476 (December 1963).
9. D. K. Khakimova, O. S. Ivanov, and Yu. S. Virgil'

yev, *Stroyeniye i Svoystva Splavov Urana, Toriya i Tsirkoniya (Structure and Properties of Uranium, Thorium, and Zirconium Alloys*, pp. 16-21, 47-60, 61-69, and 70-76, Gosatomizdat, Moscow, 1963.

10. P. R. Roy, Determination of α-Aluminum Solid-Solubility Limits in the Aluminum-Uranium and Aluminum-Plutonium Systems, *J. Nucl. Mater.*, 11: 59-66 (January 1964).
11. D. F. Bowersox, The Solubility of Selected Elements in Liquid Plutonium. II. Tantalum, USAEC Report LAMS-2952, Los Alamos Scientific Laboratory, July 18, 1963.
12. L. J. Wittenberg and G. R. Grove, Reactor Fuels and Materials Development Plutonium Research: 1963 Annual Report, USAEC Report MLM-1184, Mound Laboratory, Dec. 31, 1963.
13. Argonne National Laboratory, Reactor Development Program Progress Report, March 1964, USAEC Report ANL-6880, Apr. 15, 1964.
14. Argonne National Laboratory, Reactor Development Program Progress Report, April 1964, USAEC Report ANL-6885, May 15, 1964.
15. Argonne National Laboratory, Chemical Engineering Division Summary Report, April–June 1963, USAEC Report ANL-6725.
16. C. E. McNeilly, The Electrical Properties of Plutonium Oxides, *J. Nucl. Mater.*, 11(1): 53-58 (January 1964).
17. Argonne National Laboratory, Annual Report for 1963, Metallurgy Division, USAEC Report ANL-6868.
18. T. D. Chikalla, Hanford Atomic Products Operation, May 6, 1963. (Unpublished)
19. L. E. Russell, Improvements in or Relating to the Production of Sintered Plutonium Dioxide, British Patent 948,948, Feb. 5, 1964.
20. F. W. Albaugh, Reactor and Fuels Laboratory Monthly Report, March 1964, USAEC Report HW-81472A, Hanford Atomic Products Operation, Apr. 15, 1964. (Classified)
21. M. M. Hendrickson and J. K. Green (Eds.), Research and Development Programs Executed for the Division of Reactor Development, Quarterly Progress Report, July–September 1963, USAEC Report HW-79280, Hanford Atomic Products Operation, October 1963.
22. F. W. Albaugh, Reactor and Fuels Laboratory Monthly Report, April 1964, USAEC Report HW-82001A, Hanford Atomic Products Operation, May 15, 1964. (Classified)
23. A. E. Kmetko, Los Alamos Scientific Laboratory, May 6, 1963. (Unpublished)
24. Hanford Atomic Products Operation, Ceramics Research and Development Operation. Quarterly Report, October–December 1963, USAEC Report HW-76304, May 1963.
25. P. E. Potter, The Volatility of Plutonium Carbides, British Report AERE-M-1356, February 1964.
26. R. G. Sowden, Improvements in or Relating to the Production of Uranium and Plutonium Monocarbides, British Patent 948,791, Feb. 5, 1964.
27. Argonne National Laboratory, Reactor Development Program Progress Report, February 1964, USAEC Report ANL-6860, Mar. 15, 1964.
28. J. R. Thomson, Alloys of Thorium with Certain Transition Metals. I. The Systems Thorium-Ruthenium and Chromium-Rhodium, *J. Less-Common Metals*, 5: 437-442 (December 1963).
29. Hanford Atomic Products Operation, Research and Development Programs Executed for the Division of Reactor Development, Quarterly Progress Report, October–December 1963, USAEC Report HW-80284, April 1964.
30. Union Carbide Corporation, Nuclear Division, Y-12 Plant, March 1964. (Unpublished)
31. H. E. Rollig, Compatibility of Uranium Dioxide and Aluminum, Part 2, Studies on the Inhibition of the UO_2-Al Reaction in Fuel Elements of the Dispersion Type, *Kernenergie*, 7(1): 11-18 (January 1964).
32. D. J. Sandstrom, Consolidating Metal Powders Magnetically, *Metal Progr.*, 86(3): 91-94 (Septemper 1964).
33. J. W. Prados and J. L. Scott, Analysis of Stress and Strain in Spherical Shells of Pyrolytic Carbon, USAEC Report ORNL-3553, Oak Ridge National Laboratory, June 1964.
34. R. W. Dayton and R. F. Dickerson, Progress Relating to Civilian Applications During April 1964, USAEC Report BMI-1669, Battelle Memorial Institute, May 1, 1964. (Classified)
35. R. W. Dayton and R. F. Dickerson, Progress Relating to Civilian Application During March 1964, USAEC Report BMI-1668, Battelle Memorial Institute, Apr. 1, 1964. (Classified)
36. R. W. Dayton and R. F. Dickerson, Progress Relating to Civilian Applications During May 1964, USAEC Report BMI-1672, Battelle Memorial Institute, June 1, 1964.
37. W. O. Harms, Oak Ridge National Laboratory, personal communication, May 6, 1964.
38. J. B. Sayers, Behavior of Fuels at High Burn-up Levels: Thermal Reactor Fuels, B-Coated Particle Fuels, *Nucl. Eng.*, 9: 135-141 (April 1964).
39. H. K. Lonsdale and J. N. Graves, Coated-Particle Fuels Research at General Atomic From December 1, 1963 through April 30, 1964, USAEC Report GAMD-5216, Part 1, General Atomic Division, General Dynamics Corp., Apr. 30, 1964.
40. J. P. Blakely, N. V. Smith, and L. G. Overholser, Compatibility of Unsupported Pyrolytic-Carbon-Coated Uranium Dicarbide Particles with Water Vapor, USAEC Report ORNL-3598, Oak Ridge National Laboratory, April 1964.
41. G. Nilsson, Ejection of Uranium Atoms from UO_2 by Fission Fragments, Swedish Report AE-136, February 1964.
42. R. C. Daniel and I. Cohen, In-Pile Effective Ther-

mal Conductivity of Oxide Fuel Elements to High Fission Depletions, USAEC Report WAPD-246, Westinghouse Electric Corp., Bettis Atomic Power Laboratory, April 1964. (Unpublished)

43. M. Yunus, The Recrystallization of UO_2 at High Temperature, USAEC Translation HW-tr-66, Hanford Atomic Products Operation, July 1963.
44. A. T. Chapman and R. E. Meadows, The Volatility of $UO_{2\pm x}$ and Phase Relations in the Uranium-Oxygen System, USAEC Report ORNL-3587, Oak Ridge National Laboratory, April 1964.
45. K. Hagemark, The Partial Free Enthalpy, Enthalpy, and Entropy of Oxygen in the UO_{2+x} Phase at Higher Temperatures, Norwegian Report KR-67, February 1964.
46. J. G. Morgan, M. F. Osborne, and E. L. Long, Jr., Examination of UO_2 Irradiated at High Temperatures, USAEC Report ORNL-TM-763, Oak Ridge National Laboratory, March 1964.
47. L. Stieglitz, Studies of Release of ^{131}I from Neutron Irradiated UO_2, Thesis, Munich Technische Universität, 1963.
48. H. E. Roellig, Compatibility of UO_2 and Aluminum. Kinetic Studies of UO_2-Al Reactions in Mixed Powder Compacts, *Kernenergie*, 6: 685-691 (December 1963).
49. Atomic Energy of Canada, Ltd., 1964. (Unpublished)
50. I. Amato, R. L. Colombo, and A. M. Protti, Sintering Alumina-Urania Compositions, *Bull. Am. Ceram. Soc.*, 43(2): 125-217 (February 1964).
51. W. J. O'Leary and E. A. Fisher, Process of Making Shaped Fuel for Nuclear Reactors, U. S. Patent 3,121,128, Feb. 11, 1964.
52. D. Naumann, W. Heyne, G. Tschirne, and W. Bark, Uranium Dioxide Precipitation in Alkali Chloride Fuses and Its Properties in the Production of Swaged UO_2 Fuel Elements, *Kernenergie*, 6: 691-693 (December 1963).
53. F. W. Albaugh, Reactor and Fuels Laboratory Monthly Report, May 1964, USAEC Report HW-82428A, Hanford Atomic Products Operation, June 15, 1964. (Classified)
54. General Atomic Division, General Dynamics Corp., Investigations of Carbides as Cathodes for Thermionic Space Reactors. Quarterly Progress Report for Period Ending May 31, 1963, USAEC Report GA-4391, Sept. 25, 1963.
55. J. Crane and E. Gordon, The Development of Uranium Carbide as a Nuclear Fuel. Final Report, USAEC Report UNC-5080, United Nuclear Corp., Feb. 29, 1964.
56. Oak Ridge National Laboratory, Mar. 5, 1964. (Unpublished)
57. N. A. Hill and O. B. Cavin, Monoclinic-Cubic Transformation in Thorium Dicarbide, USAEC Report ORNL-3588, Oak Ridge National Laboratory, April 1964.
58. Oak Ridge National Laboratory, Apr. 6, 1964. (Unpublished)
59. Argonne National Laboratory, Chemical Engineering Division Research Highlights, May 1963–April 1964, USAEC Report ANL-6875.
60. Argonne National Laboratory, Reactor Development Program Progress Report, May 1964, USAEC Report ANL-6904, June 15, 1964.
61. R. S. Barnes, A Theory of Swelling and Gas Release for Reactor Materials, *J. Nucl. Mater.*, 11(2): 135-148 (February/March 1964).
62. V. M. Agranovich, E. Ya. Mikhlin, and L. P. Semenov, The Kinetics of the Swelling of Fissionable Materials Produced by the Release of a Gaseous Phase from the Supersaturated Solid Solution, *At. Energ. (USSR)* (in Russian), 15: 393-403 (November 1963).
63. B. G. Childs and J. C. Ruckman, Radiation Damage Effects in Uranium Carbide, in *New Nuclear Materials Including Non-Metallic Fuels*, Vol. II, International Atomic Energy Agency, Vienna, 1963.
64. G. Long, W. P. Stanaway, and D. Davies, Experiments Relating to the Mechanism of the Diffusion of Xenon-133 in Uranium Dioxide, British Report AERE-M-1251, January 1964.
65. J. R. McEwan and W. H. Stevens, Xenon Diffusion in UO_2–Some Complicating Factors, *J. Nucl. Mater.*, 11(1): 77-93 (January 1964).
66. Hahn-Meitner-Institut für Kernforschung, Diffusion of Fission Gases in Nuclear Fuels, Quarterly Report No. 13, July 1–September 30, 1963, USAEC-Euratom Report EURAEC-875, October 1963.

Section

II

Reactor Materials

Moderator Materials

Graphite

Experimental data on deposition of graphite by sublimation, recently reported by the National Carbon Company,[1] are of interest since very little had previously been reported on deposition of thick layers by this method. In contrast, voluminous literature has appeared on coatings of pyrolytic graphite formed by gas decomposition. The study reported by National Carbon was an exploratory one, but it indicated interesting property capabilities for this form of carbon. It appears possible to vary widely the anisotropy of the deposit through process control, and deposition rates about an order of magnitude greater than for gas decomposition have been demonstrated.

The reported high-temperature creep data for graphites have included a wide range in activation energies, varying with the grade of graphite, the type of creep test, and the method of analysis. There is also considerable disagreement in the literature regarding the stress dependence of the creep rate.

High-temperature tensile creep data, recently reported by National Carbon, led to several important conclusions.[2] The creep experiments, usually 90 min in duration, were conducted on several types of graphite under conditions of constant load and constant temperature in the range 2300 to 2900°C. The graphites tested were fine-grained grade ATJ, high-density grade ZTA, a low-density coke-based extruded graphite, and lampblack-base grade CEP. The most interesting conclusions were as follows:

1. From the temperature dependence of the creep rate, an activation energy of 124 kcal/mole was obtained, which was the same for all the materials tested. The activation energy was found to be independent of the grain orientation and the crystalline structure of the graphite. This contrasts with previous data on flexural creep, which showed a different activation energy for each grade of graphite.

2. For graphites with different proportions of filler and binder, the magnitudes of the creep strain and creep rate depended on the average bulk density, being insensitive to the relative proportions of filler and binder carbon. As the density increased, the creep strain and creep rate of specimens oriented "with the grain" both decreased. The activation energy and stress dependence of the creep rate were independent of the density.

3. At a given temperature the creep rate of ATJ varied with the fourth power of the stress for specimens oriented both "with the grain" and "against the grain." In contrast, the creep rate of the extruded coke-base graphite oriented "with the grain" varied with the 2.6 power of the stress. No stress dependence was determined for the ZTA and CEP graphites.

Limited information on the effects of irradiation on graphite cloth has been reported by Hanford.[3] A sample of National Carbon Company Grade WCA cloth was irradiated to 6750 Mwd/adjacent ton. Although the rolled-up cloth tended to retain its curvature, it seemed as flexible after the exposure as before irradiation. The limited test data indicated no detectable changes in weight, thickness, thread count, or electrical resistance. The breaking strength increased by about a factor of 2, a change analogous to that observed in bulk nuclear graphite.

A brief, interesting review[4] of research and development of nuclear graphite in Japan summarizes the advances made since 1955.

(M. C. Brockway)

Beryllium Metal and Alloys

Fuel-Element Cladding

Hanford[5] has fabricated several beryllium-clad UO_2 fuel elements, utilizing high-purity beryllium supplied by CEA (France), by magnetic-force resistance welding of beryllium end closures. The UO_2 fuel was vibratory packed into the beryllium tubing prior to final closure of the element by magnetic-force welding. After an extensive investigation, parameters were developed which produced end cap-to-cladding bonds with recrystallized grains at the cap-to-cladding interface no greater in size than the parent metal. However, detailed examination revealed that the joint was not reactor grade and that it contained small longitudinal microcracks in the upset metal. It was felt that these microcracks could be eliminated by further studies and several modifications to the magnetic-force welder. These modifications include a controlled preheating and postheating of the beryllium and increased magnetic current. When these changes were made, crack-free end closures were obtained with the CEA beryllium.

Joining

In a study of solder compositions, fluxes, and soldering procedures for beryllium at the Beryllium Corp.,[6] surface-preparation treatments and their effects on joint strengths were evaluated. Treatment variables evaluated included degreasing, acid etching, and rinse cycles. Solder compositions investigated included various percentages of silver, lead, tin, zinc, and indium.

Flowability was found to be sensitive to temperature and was best with solders containing high zinc, indium, or lead. Wettability was observed to be best with high-zinc and lead solders and was not as temperature sensitive as flowability. Joint strengths varied with the different solders; the high-zinc solders produced shear strengths above 10,000 psi, which approaches the strengths normally achieved in brazed joints.

Joining of beryllium plates by gas tungsten (TIG) or braze welding and fusion welding with alternating current for applications at temperatures up to 1300°F was investigated by Avco Corp.[7] Oxidation during welding was effectively controlled by means of an argon atmosphere inside a vacuumtight dry box. Braze welds were made with the use of filler strips of an aluminum–12 wt.% silicon alloy and with unalloyed silver arc melted in place. With the filler metal under optimum joining conditions, room-temperature tensile strengths in the direction traverse to the weld were found to be 20,000 to 25,000 psi. The melting point of the aluminum–12 wt.% silicon alloy limits the temperature capabilities of braze-welded beryllium structures. However, it was found that the silver braze welds had strengths of 11,000 psi at 1300°F, which is more than 80% of the beryllium base-metal strength at this temperature. Joint working or tearing during fusion welding was reduced by increasing preheat temperature and by decreasing speed and current for any specified section size and geometry.

Beryllium-metal tubing has been considered for cladding nuclear fuel elements because of its compatibility with fluids and fuels of interest. Consequently it was necessary to develop joining and closure techniques for beryllium. Prior to 1959 the joining of beryllium was best accomplished by utilizing an intermediate material such as aluminum. However, this type of joint has limited temperature capabilities for high-temperature reactor operation and is not compatible with most reactor coolant systems. During 1959 and 1960, people at Oak Ridge conducted solid-state bonding studies on beryllium by utilizing a molybdenum-jig differential-expansion technique to generate the pressure needed for bonding beryllium at temperature. Excellent bonds were achieved at Oak Ridge after 1 to 4 hr at 1000 to 1100°F in vacuum.

Workers[8] at Atomics International have made additional studies of techniques used by Oak Ridge and experimented with TIG welding of beryllium. Beryllium end plugs and tubes were machined from QMV grade beryllium for the welding and diffusion-bonding studies. Prior to welding and bonding, the beryllium was cleaned with a mixture of ammonium acid fluoride, dilute nitric acid, and distilled water.

Welding was accomplished in a pure-argon-atmosphere box with 25 volts direct current, and 30 amp straight polarity. Copper chill blocks were used around the area just below the section exposed for welding. Single-pass welds contained some porosity, but were helium leaktight. Multiple-pass welding increased the porosity in the weld area.

Diffusion bonding was achieved by holding the parts at 1000 to 1050°C for 1 to 2 hr under a pressure of 15 μ Hg or less. Some grain growth across the bond interface was obtained, and there were no unbonded areas in the diffusion-bonded specimens. Helium pressure testing of the bonds at 1400°F under a pressure of 300 psi revealed no leaks in the bond interface.

Fabrication of Beryllium

Brush Beryllium[9] is investigating techniques for the fabrication of very high-strength beryllium wire. Beryllium containing alloying additions of 0.8 to 1.2 wt.% iron did not fabricate well, and efforts are now being directed to the fabrication of an alloy containing only 0.5 wt.% iron. In addition, studies are in progress on the fabrication of high-strength wire from solid-solution alloys of beryllium and beryllium containing a fine-grained BeO dispersion. Copper, gold, cobalt, and nickel alloying additions will be made to beryllium to produce material for wire-fabricability studies.

In a report by Brush Beryllium[10] on techniques required to forge unclad beryllium, results are presented for forging runs with the use of different die designs, billet designs, and beryllium materials as a function of fabrication sequence, die and billet lubricants, and die and billet temperatures. The effects of these variables on room- and elevated-temperature properties in tension and compression are reported.

Beryllium-powder forging of parts ranging in size from 5 to 1200 lb has been accomplished by Wyman-Gordon.[11] Forging of beryllium powders was investigated by three techniques, which included forging powder, forging press-sintered material, and forging ingot material. The input powder and bonding of source material in all cases were prime considerations in achieving good physical properties. Consequently great care was taken in quality control during selection and processing of the powder in preparation for forging.

For forging, the beryllium powder is loaded into a vented can and preheated to 1000°F. The can is then sealed and transferred to a furnace for a 4- to 5-hr soak at 1800°F. All heat-treating operations are carefully controlled to minimize oxygen and nitrogen pickup. After soaking at temperature, the heated parts are removed from the furnace and hydraulically press forged in one pass to final shape. Pressures of 25,000 psi produce full densification of the beryllium.

The can is stripped from the forged beryllium either chemically (by leaching) or mechanically (by splitting or machining it away). The beryllium part is then finish machined to final dimensions. Further work is still in process on (1) the effect of improved starting material, (2) different forging techniques, and (3) sizing of starting material as it affects powder forging of beryllium.

Beryllium Alloys

Alloys of beryllium containing from 0.5 to 3.0 wt.% titanium or zirconium were found by Raine and Robinson[12] to have improved resistance to corrosion in hot carbon dioxide and increased ductility when compared with pure beryllium. These alloys were tested in the fabricated condition and were prepared by consumable-electrode arc melting.

Nuclear Metals is investigating the preparation and evaluation of extremely high-purity beryllium.[13] Material will be subjected to greater purification than was previously obtained with the 12-pass zone-refinement purification steps on single-distilled beryllium, to determine whether increased resistance to basal cleavage can be obtained with the higher purity material.

The effect of additions of nickel on solid-solution strengthening of zone-refined single-crystal beryllium was also studied at Nuclear Metals. It was found that nickel was not so effective a strengthener as iron.

Thin Beryllium Foil

Walters and Fuller of Harwell[14] have developed chemical and mechanical techniques for preparing beryllium thin films. Beryllium foil, mechanically thinned to 0.005 in., can be further reduced or surface finished by chemical cleaning in a system containing orthophosphoric acid, CrO_3, distilled water, and glycerol. The electropolished beryllium film then received final treatment by washing, trimming, and ultrasonic cleaning in absolute alcohol.

Beryllium-Gas Reaction Kinetics

A constant-volume system for studying the high-temperature reactions of beryllium with gases has been designed and fabricated by Sandia.[15] With this equipment, experiments are being made to determine the effects on the beryllium oxidation rate of gas-phase pressure,

sample temperature, and surface coverage. The temperature range of 1000 to 1500°C has been investigated, and the pressure range of 0.070 to 490 mm Hg has been studied. From the data presented by Sandia, it is apparent that the beryllium oxidation rate is very strongly temperature dependent. In the temperature range studied, the oxidation rate increased by a factor of 5 for every 100°C.

The temperature dependence of the beryllium oxidation rate can be satisfactorily represented by an exponential function of the form

$$r = K(P,\theta)\, e^{-E/RT}$$

where r = reaction rate, mg/(cm^2)(min)
$K(P,\theta)$ = a temperature-dependent function
T = absolute temperature
R = universal gas constant
E = activation energy, a temperature-independent constant

The effect of the oxygen-gas pressure on the rate of beryllium oxidation was investigated over the pressure range from 0.070 to 0.490 mm Hg. The oxidation rate was found to be nearly independent of pressure at temperatures below 1200°C, but at temperatures of 1400°C and above, the rate of oxidation was proportional to approximately the square root of the oxygen-gas pressure. (H. D. Hanes)

Beryllium Oxide

Several experimental observations are reported by Atomics International,[16] which suggest the possibility that neutron irradiation of BeO yields a disorder structure that has characteristics like those of the high-temperature crystalline form of BeO. First, it is noted that, when the high-temperature form of BeO is formed under electron bombardment in the electron microscope, it can be quenched rapidly to room temperature without reverting to the hexagonal form. Second, the high-temperature form of BeO has been observed by electron microscopy in extremely fine particles derived from irradiated and crushed BeO crystals of the low-temperature form. Third, disappearance of the (1 0 3) reflection is noted with the phase transition, and the early loss of the sharp component of the (1 0 3) reflection with neutron irradiation has been repeatedly observed. Finally, the anisotropic expansion resembles the dimensional changes that occur when BeO transforms from the low-temperature form to the high-temperature form. The c-axis expansion due to irradiation has been observed to exceed one-third that due to the transformation. It is hypothesized that, in the wake of displacement cascades, many beryllium atoms are left in tetrahedral sites other than those normally occupied. Such occupancy would be statistically and perhaps nonuniformly distributed; whereas, in the high-temperature form, the beryllium atoms have shifted to alternative tetrahedral sites in a regular fashion. Local relaxation associated with this disorder could partially account for the dimensional and diffraction effects. Upon crushing, some very small regions might possess sufficient disorder to relax into the high-temperature BeO form rather than the low-temperature BeO form and, thus, become evident by electron microscopy.

(M. C. Brockway)

Beryllium Intermetallic Compounds

In a final report from the Denver Research Institute,[17] the oxidation of $ZrBe_{13}$ and Zr_2Be_{17} in the temperature interval between 650 and 900°C and the oxidation of $NbBe_{12}$ and Nb_2Be_{17} in the temperature interval between 900 and 1050°C are associated with the stresses generated by the formation of polymorphs of ZrO_2 or Nb_2O_5 in the oxide coating. The immunity to severe oxidation in these temperature intervals of modified beryllides containing aluminum-alloy additions is attributed to the protective qualities and stability of the thin oxide coatings that were obtained.

The Australians[18] irradiated $(U_{0.33}, Th_{0.67})Be_{13}$ at 400 to 700°C to burnups of 7 to 11 at.% uranium in a predominantly thermal flux. Both massive beryllide and dispersions of 20, 35, and 50 vol.% beryllide in beryllium were studied. The massive beryllide and beryllide within the matrix were unaffected by the irradiation; however, the dispersions swelled 3 to 18% and released up to 33% of the gaseous fission products formed. The cause of the swelling of the dispersions were attributed, in part, to the hot-pressing operation used to fabricate the specimens, and it was suggested that the poor irradiation stability of these specimens was not

typical of $(U_{0.33}, Th_{0.67})Be_{13}$-beryllium dispersions prepared by other techniques.

(R. W. Getz)

Solid Hydrides

Zirconium Hydride

A set of standard micrographs for the quantitative estimation of hydrogen in hydrided Zircaloy-2 has been developed at Hanford.[19] The micrographs show the hydride structure patterns at seven hydrogen levels from 15 to 810 ppm. A magnification of 250× is suitable for revealing the hydrides, while retaining a reasonable area to minimize sampling error. Although sampling error is unavoidable, it is felt that the micrographs represent the sample hydrogen concentrations within the limits of error that usually accompany the metallographic technique of analysis. The quantitative estimation of hydride becomes more difficult at high hydrogen concentrations, i.e., above 400 ppm, as differences in hydride densities become more difficult to distinguish.

Hydrided Zirconium-Uranium Alloys

Thermal migration of hydrogen in compositions having a Zr : H : U ratio of 1 : 1.6 : 0.3 was studied at General Atomic.[20] No detectable hydrogen redistribution was found in these samples, which were subjected to gradients in the temperature range 425 to 675°C for periods up to 770 hr. Other compositions, having an H/Zr atom ratio less than 1.4, underwent rapid migration of hydrogen toward the cold end. The absolute heat of transport of hydrogen in the hydride phase was determined to be less than 500 cal/mole near the composition H/Zr = 1.6 and at least +350 cal/mole for H/Zr = 1.4 at a temperature of 500°C.

Information on SNAP reactor fuel elements has been published by Atomics International.[21] The elements nominally consist of 90 wt.% zirconium–10 wt.% highly enriched uranium rods. The rods are hydrided to an N_H of 6.0 to 6.5 and machined. Alloying of the zirconium and uranium is accomplished by triple arc melting, and forming is done by extrusion. The alloy is hydrided in massive form by specially developed techniques and then clad by conventional means.

The feasibility of changing the properties of hydrided zirconium-uranium fuels by the use of alloying additions has been examined at Battelle.[22] The objective of this study was to enhance the atmospheric burnup of these fuels during reentry from orbit. Twenty-seven metals were studied as additions of the zirconium–10 wt.% uranium hydride. It was concluded that the ablation characteristics of the hydride fuel can be changed, but that alloying additions made directly to the melt reduce the ablation tendency. It is believed that the most attractive avenue for improved burnup properties lies in increasing the thermal-shock susceptibility of the fuel.

Other Ternary Hydrides

A systematic study of compounds formed by zirconium, hydrogen, and elements of the first row of the periodic table is being conducted at Atomics International.[16] The composition $ZrC \cdot ZrH_2$ has been confirmed and its cell constants determined: $a_0 = 3.347$, and $c_0 = 5.469$. There apparently is a compound in the zirconium-nitrogen-hydrogen system also, and possibly in the zirconium-boron-hydrogen system, but these have not yet been characterized.

(H. H. Krause)

References

1. P. H. Higgs et al., Research and Development on Advanced Graphite Materials, Vol. XXXVII—Studies of Graphite Deposited by Pyrolytic Processes, Report WADD-TR-61-72 (Vol. XXXVII), May 1964.
2. E. J. Seldin, Research and Development on Advanced Graphite Materials, Vol. XVII. High-Temperature Tensile Creep of Graphite, Report WADD-TR-61-72, Vol. XVIII, July 1963.
3. F. W. Albaugh, Reactor and Fuels Laboratory Monthly Report, March 1964, USAEC Report HW-81472A, Hanford Atomic Products Operation, Apr. 15, 1964. (Classified)
4. T. Mukaibo, T. Saito, T. Takeshima, and Y. Ueda, Research and Development of Nuclear Graphite in Japan, *J. Electrochem. Soc. Japan*, 31(3): 79-87 (1963).
5. Hanford Atomic Products Operation, Ceramics Research and Development Operation, Quarterly Report, October–December 1963, USAEC Report HW-76304, December 1963.
6. E. E. Weismantel and K. C. Taber, The Soldering of Beryllium Metal, *Welding J. (N. Y.)*, 43: 57-62 (February 1964).
7. E. M. Passmore, Fusion Welding of Beryllium, *Welding J. (N. Y.)*, 43: 116-125 (March 1964).
8. N. H. Katz and E. L. Reed, Terminal Report on the Development of Techniques for Fabricating

High-Temperature Fuel and Cladding Material for Application in Advanced Nuclear Reactor Concepts, USAEC Report NAA-SR-Memo-8528, Atomics International, Aug. 15, 1963.

9. E. A. Murphy and R. G. O'Rourke, Development of Very-High-Strength Beryllium Wire. Bimonthly Report No. 1, December 6, 1963, to February 6, 1964, Report AD-432273, Brush Beryllium Co., Feb. 6, 1964.
10. M. B. Hornak and R. G. O'Rourke, Developing Technology To Forge Unclad Beryllium. Phase II, Interim Engineering Progress Report, December 1, 1962–November 30, 1963, Report NP-13500, Brush Beryllium Co., Nov. 30, 1963.
11. N. G. Orrell, The Fabrication of Beryllium Powder Forging, Report RD-63-105, Wyman-Gordon Co., Mar. 8, 1963.
12. T. Raine and J. A. Robinson, Beryllium Alloys, British Patent 952,488, Mar. 18, 1964.
13. Nuclear Metals, Inc., Fundamental and Applied Research and Development in Metallurgy, USAEC Report NMI-2124, Feb. 26, 1964.
14. G. P. Walters and W. C. Fuller, Preparation of Beryllium Thin Films, *Met. Soc., Am. Inst. Mining, Met. Petrol. Engrs., Inst. Metals Div., Spec. Rept. Ser.*, 227: 1462-1463 (December 1963).
15. J. L. Blumenthal and M. Santy, Beryllium Study Program, Quarterly Progress Report, September 23–December 31, 1963, USAEC Report SC-DC-64-303, Sandia Corp., Jan. 7, 1964.
16. Atomics International, AEC Unclassified Program, Quarterly Technical Progress Report, January–March 1964, USAEC Report NAA-SR-9700, May 19, 1964.
17. F. C. Perkins, Intermediate-Temperature Oxidation of Beryllides, Final Report, USAEC Report DRI-2128, Denver Research Institute, September 1963.
18. G. L. Hanna, B. S. Hickman, and R. I. Hilditch, The Irradiation Behavior of Hot-Pressed Dispersions of (U,Th)Be_{13} in Beryllium. Second Irradiation Experiment, Australian Report AAEC/E-112, November 1963.
19. L. A. Hartcorn and R. E. Westerman, Quantitative Metallography of the Hydride Phase in Zircaloy-2 Process Tubes, USAEC Report HW-74949, Hanford Atomic Products Operation, November 1963.
20. U. Merten, J. C. Bokros, D. G. Guggisberg, and A. P. Hatcher, Thermal Migration of Hydrogen in Zirconium-Uranium-Hydrogen Alloys, *J. Nucl. Mater.*, 10: 201-208 (November 1963).
21. T. S. Kirsch, Feasibility Report for Fabrication of SNAP Fuel Elements, USAEC Report NAA-SR-Memo-9299, Atomics International, Dec. 11, 1963.
22. E. L. Foster, Jr., Re-entry Burnup Enhancement of Hydrided Zirconium-Uranium Alloy Fuel, paper presented at Aerospace Nuclear Safety Meeting, October 1–4, 1963, USAEC Report SC-DC-3553, pp. 295-327, Sandia Corp., January 1964.

Section III

Reactor Materials

Nuclear Poisons

Metallic Poison Materials

Microstructure, thermal, thermomagnetic, and X-ray analyses were made of cerium-gadolinium alloys, and a constitution diagram was constructed for this binary.[1] The diagram exhibited a compound Ce_2Gd_5 with a samarium type lattice.

A possible approach toward decreasing the cost of reactor control rods is to use a rod whose economic worth at the end of its life is greater than its original cost.[2] Cobalt-base control rods may meet this criterion because of the production of ^{60}Co during their use. The potential of the rods was evaluated by irradiating sintered pellets of 30 wt.% dysprosium oxide dispersed in cobalt. The specimens were compacted by powder-metallurgy techniques and sintered at 1300°C. The first two capsules have been irradiated and tested in compression. Results of these tests are given in Table III-1.

Table III-1 COMPARISON OF ROOM TEMPERATURE PREIRRADIATION AND POSTIRRADIATION COMPRESSIVE STRENGTH OF COBALT–30 WT.% Dy_2O_3 PELLETS IRRADIATED[2] AT 300°C

Specimen	Integrated effective thermal-neutron flux, 10^{20} neutrons/cm^2	Ultimate compressive strength, kg/cm^2	Total decrease in length at fracture, %
Unirradiated		7520 to 7878	19.4
51-1-1	3.3	6100	7.6
51-1-2	3.3	5300	16.2
51-1-3	3.3	5000	13.8
51-1-4	3.3	5580	16.9
51-1-7	3.3	5270	13.8
51-1-8	3.3	5600	16.4
51-2-1	4.4	4700	10.4
51-2-2	4.4	4470	14.4
51-2-3	4.4	4590	12.0
51-2-5	4.4	8020	17.6

One pellet from each capsule was analyzed for production of ^{60}Co. The values of ^{60}Co in these two specimens were $190 and $260, as compared with a cost of about $1 for the original cobalt and dysprosium oxide.

(M. Kangilaski)

Dispersion Poison Materials

Studies being made at the Albany Metallurgical Research Center[3] have been directed toward producing sound castings of hafnium carbide. Although spin-casting techniques have been effective in increasing the density of fused hafnium carbide, some porosity and voids were still present. The ingots exhibiting the lowest porosity contained either greater or smaller carbon concentrations than the stoichiometric amount. Oxidation studies were made on specimens having 5.1, 7.7, 8.7, and 11.7 wt.% carbon at temperatures to 1000°C. Oxidation to HfO_2 began at 500°C and became catastrophic at 1000°C. The oxidation rate appears to be independent of carbon content.

Studies at Argonne[4] have been concerned with urania-gadolinia phase relations, inasmuch as gadolinia is being considered as a burnable poison for urania fuels. X-ray diffraction techniques have been used to establish the existence of a solid-solution phase between 30 and 70 mole % gadolinia, whereas in the regions of less than 30 and greater than 70 mole % gadolinia, two phases exist, the solid solution and the base components. The lattice parameter of the solid solution remains relatively constant at 5.405 A up to 30 mole % gadolinia. At higher gadolinia concentrations, the lattice parameter decreases linearly to 5.382 A at 60 mole % gadolinia.

Aerojet[5] is considering the use of thin burnable-poison foils, containing europia-titania mixtures dispersed in a stainless-steel matrix and clad in stainless steel, for the ML-1 reactor concept. The foils are 0.010 in. thick, and the cladding is from 0.0015 to 0.002 in. thick. The active portion of the foils is 22.12 by 5.147 in. The burnable absorber is a mixture of 68.8 wt.% europia and 31.2 wt.% titania. This mixture is blended with elemental stainless-steel powders to form the desired dispersion.

A recent report[6] describes the results of experiments to determine the compatibility of boron carbide with potential cladding materials for the Advanced Organic-Moderated Reactor concept. The compatibility of boron carbide with copper, types 304 and 430 stainless steels, and AISI 4130 steel was investigated at temperatures from 750 to 1300°F and for times up to 10,000 hr. The results indicate that copper and type 430 stainless steel are compatible with boron carbide at 1300°F for 10,000 hr. The type 304 stainless steel was compatible with boron carbide for 10,000 hr at 1100°F, but not at 1300°F. No reactions were observed in the AISI 4130 steel for 10,000 hr at 750°F, but at higher temperatures a hard reaction zone developed which was identified by X-ray diffraction techniques as Fe_2B.

The results of a comprehensive study of some properties of high-purity TiB_2, ZrB_2, HfB_2, NbB_2, and TaB_2 were recently reported.[7] The properties measured include lattice parameter, thermal expansion, electrical resistivity, and microhardness. The measurements were generally made between room temperature and 1000°C. Thermal-conductivity measurements between 1000 and 2000°C are now in progress. Thermal properties measured include specific heat, vapor pressure, and heat of formation. On the basis of current oxidation data, HfB_2 and ZrB_2 are shown to be the most likely candidates for high-temperature applications requiring oxidation resistance.

A recent report issued by Oak Ridge[8] described the postirradiation evaluation of a neutron-absorber plate containing 3 wt.% enriched boron in iron and clad in stainless steel. The plate was irradiated in the Engineering Test Reactor at 180°F to 29% burnup of the ^{10}B atoms. Dimensional and metallographic examination of the irradiated specimens revealed that, in the range of 5 to 8 wt.% burnup, the bond between the absorber core and cladding began to deteriorate and swelling occurred. Postirradiation heat-treatment at 570°F caused additional swelling. The early failures of the bonds are attributed to localized burnup greater than 35% of the ^{10}B atoms in the region adjacent to the stainless-steel cladding. Because of the burnup limitations, the continued use of this boron-iron combination as a serviceable neutron absorber for the SM-1 reactor is not recommended. (E. G. Smith, Jr.)

References

1. I. V. Burov et al., Constitution Diagram of Ce-Gd Alloys, *Zh. Neorgan. Khim.*, 8: 2658-2663 (December 1963).
2. Argonne National Laboratory, Annual Report for 1963, Metallurgy Division, USAEC Report ANL-6868.
3. Bureau of Mines, Quarterly Metallurgical Progress Report No. 21 for period of October 1–December 31, 1963, USAEC Report USBM-U-1091.
4. Argonne National Laboratory, Reactor Development Program Progress Report, March 1964, USAEC Report ANL-6880, Apr. 15, 1964.
5. Aerojet-General Nucleonics, Army Gas-Cooled Reactor Systems Program, Quarterly Progress Report, October 1–December 31, 1963, USAEC Report IDO-28621, Feb. 15, 1964.
6. R. D. Hahn, Compatibility of Boron Carbide with Potential AOMR Control Rod Cladding Materials, USAEC Report NAA-SR-8702, Atomics International, Mar. 1, 1964.
7. L. Kaufman and E. V. Clougherty, Investigation of Boride Compounds for Very High-Temperature Application, Report RTD-TDR-63-4096 (Pt. I), ManLabs, Inc., October 1963.
8. A. E. Richt, C. F. Leitten, Jr., and R. J. Beaver, Postirradiation Evaluation of Stainless Steel-Clad Plate-Type Specimens Containing 3 Wt.% Enriched Boron in Iron, USAEC Report ORNL-TM-815, Oak Ridge National Laboratory, June 1964.

Section IV

Reactor Materials

Cladding and Structural Materials

Corrosion

Zirconium Corrosion

A family of curves summarizing the long-term corrosion and hydrogen-uptake behavior of alpha-annealed and beta-quenched Zircaloy-2 and Zircaloy-4 has been released by Bettis.[1] The data presented are for water temperatures of 500 to 680°F and steam temperatures of 750 to 950°F. The corrosion behavior of Zircaloy-2, Zircaloy-4, and nickel-free Zircaloy-2 in 680°F water at *p*H 10.5 (LiOH) also has been reported.[2] After extended exposure of about 300 days, alpha-annealed and beta-quenched specimens of all three alloys exhibited weight gains that were more than two standard deviation limits greater than the corrosion weight gain of coupons exposed to neutral water at the same temperature.

In a study of the effect of oxygen and nitrogen on the aqueous corrosion resistance of consolidated Zircaloy-2 powder by Knolls,[3] it was found that increasing the oxygen content above 2300 ppm or the nitrogen content above base level shortened the time to transition in 680°F water. A similar deleterious effect of nitrogen was observed in 750°F steam. Although oxygen also had an adverse effect in 750°F steam, it was not so pronounced as that of nitrogen.

Impact and fretting studies have been conducted with Zircaloy-2 in 280°C water at Hanford.[4] A 13-mil penetration was observed after 4,000,000 impacts at a frequency of two impacts per second. Penetration of 1 mil in one month due to fretting was observed on Zircaloy-2 pressure tubes and $^1/_{16}$-in.-wide Zircaloy-2 supports with an induced vibration of 25 cps.

The absorption by zirconium alloys of a lower percentage of corrosion-product hydrogen in steam at 650°C than at 540°C has been attributed by Argonne scientists[5] to increased thermionic emission at the higher temperature which promotes hydrogen-ion discharge, possibly just outside of the corrosion film surface. This theory was based on the results of electrical measurements which suggested the presence of both electrons and gas ions. The measurements were made between a corroding zirconium surface and a platinum electrode spaced 50 μ away.

Experimental and literature data have been used to determine the upper temperature of usefulness for zirconium alloys in steam by Vallecitos.[6] Taking into account hydrogen pickup, embrittlement by oxygen dissolved from the oxide film, high-temperature strength, and effect of the oxide film on heat-transfer rates, it was concluded that there is good promise for developing zirconium alloys for fuel-cladding applications in steam at temperatures up to 475°C.

The corrosion behavior of zirconium alloys in CO_2 has been studied by French scientists.[7,8] Unalloyed zirconium was found to be strongly oxidized at 500°C, exhibiting breakaway corrosion with the linear postbreakaway rate depending upon the CO_2 pressure. Binary alloys containing 1, 1.6, and 2.5 wt.% copper, 2 wt.% vanadium, or 0.05 and 0.5 wt.% calcium, and ternary alloys containing copper-molybdenum or copper-phosphorus were more oxidation resistant. They did not exhibit breakaway after 3000 hr at 600°C. (W. E. Berry)

Aluminum Corrosion

The increase in corrosion rate of aluminum with increasing heat-transfer rate was found by Hanford[9] to stem from an increase in the temperature of the oxide-water interface, thereby providing a driving force for dissolution of the protective oxide. Measured corrosion rates of X8001 aluminum-clad fuel elements were found

to agree fairly well with calculated oxide dissolution rates.

Sintered aluminum-silicon-nickel powder products containing 7 to 13 wt.% silicon have been found[10] to possess good hot strength and good corrosion resistance in experiments conducted in Germany. An alloy containing 9 wt.% silicon–1 wt.% nickel–1 wt.% titanium exhibited weight gains of 2 mg/cm^2 after 1600 hr of exposure to static water at 300°C and 400 hr of exposure to static water at 350°C.

(W. E. Berry)

Corrosion of Iron-Base, Nickel-Base, and Miscellaneous Alloys

OXIDATION

Maximum oxidation penetration of 0.0044 in. has been observed by Aerojet-General[11] in Hastelloy X cladding on an ML-1 prototype fuel element after 10,151 hr in the AGN-GETR gas-cooled loop. The element was exposed to reference coolant (99.5 vol.% nitrogen–0.5 vol.% oxygen) during the first 6415 hr and to air during the remainder of the test. Average exposure conditions were 53.1 kw power generated, 90,000 Btu/(hr)(sq ft) heat flux, and 800°F inlet, 1200°F outlet gas temperature.

The oxidation behavior of platinum and platinum–10 wt.% rhodium alloys as cladding materials for molybdenum and niobium is being studied by Metals and Controls.[12] Oxidation rates of 1.98 and 2.40 μin./hr were obtained for platinum and the platinum-rhodium alloy, respectively, in air at 2550°F flowing at 480 in./min. An increase in the dew point from –40 to 120°F had no effect on the oxidation of platinum in 2200 and 2550°F air at 24 in./min. Coated molybdenum specimens failed by diffusion of molybdenum to the oxide surface, where it oxidized and volatilized. Oxygen penetrated the coating on niobium and caused oxide blisters, which eventually ruptured the coating surface. Several barrier layers have been investigated but with little success to date.

The effect of incoherent twin boundaries on diffusion rates during thin-film oxidation of copper has been studied by Oak Ridge.[13] Upon oxidizing the (111) plane, it was found that the oxide was heavily oriented and twinned, with the two possible twin orientations occurring in about equal amounts. This resulted in an array of incoherent twin boundaries along which enhanced diffusion could occur. Small concentrations of certain substances, such as CCl_4, on the surface increased the fraction of one twin orientation relative to the other, resulting in a reduction in the total length of the incoherent twin boundaries. At twin concentration ratios of 8 to 9, oxidation rates after 30 min at 185°C were reduced to about one-half those of uncontaminated specimens.

Studies on the oxidation of nickel–2 vol.% ThO_2 in the temperature range of 900 to 1400°C have revealed a dense outer oxide layer and a porous inner layer.[14] The oxidation was believed to have occurred by the diffusion of nickel ions outward to produce the outer layer and the diffusion of oxygen gas inward to produce the inner layer. The source of the oxygen gas was attributed to decomposition of NiO in the outer layer at the boundary between the inner and outer oxides. It was also suggested that the effect of thoria particles was to inhibit plastic flow in the oxide layer.

AQUEOUS CORROSION

The corrosion resistance of TD nickel in degassed pure water at 360°C and oxygenated superheated steam at 650°C was found to be comparable with that of pure nickel in studies conducted at Argonne.[15] Weight gains averaged 0.35 mg/cm^2 after 104 days' exposure to 360°C water and about 1.4 mg/cm^2 after 70 days in 650°C steam.

The solubility of Inconel corrosion products in high-temperature water over the temperature range of 80 to 650°F has been reported by Knolls.[16] Spectrophotometric and neutron activation analytical techniques were employed. The solubility for any of the metallic components did not exceed 22 ppb. Among the significant effects observed was that the solubility of nickel in *p*H 9.5 water was nine times greater at 80°F than at 650°F. In another program the solubility of iron corrosion products from a carbon-steel loop in *p*H 10 water at 260°C has been determined at Chalk River.[17] Analysis of the filtrate after passage through a colloidal silver filter revealed 3×10^{-3} mg/liter (3 ppb). The filtrate may have included particles less than 0.01 μ in size.

The factors affecting the removal of the corrosion film (high-temperature water) from Inconel 600 by electrolytic descaling in inhibited sulfuric acid have been investigated at Knolls.[3]

Included in the variables were: balance precision, inhibitor effectiveness, current density, nitric acid immersion to remove lead deposits, mechanical brushing, and blank corrections.

(W. E. Berry)

Corrosion of Coated Refractory Metals

Design data for coated niobium alloys D-43 (niobium–10 wt.% tungsten–1 wt.% zirconium) and B-66 (niobium–5 wt.% molybdenum–5 wt.% vanadium–1 wt.% zirconium) were determined in work conducted at Thompson Ramo Wooldridge (TRW).[18] These alloys were coated with Pfaudler's modified silicide and TRW's chromium-titanium-silicon coating. The protective lives of these coatings were determined at temperatures up to 2600°F at 1-atm air pressure. Table IV-1 summarizes the test results. Exposing the coatings at reduced air pressures of 0.1 and 1 mm for 2 hr at 2500°F was found to significantly degrade their 1-atm protective lives. In addition to the oxidation tests, tensile and creep properties of coated sheet were determined in air-atmosphere tests at temperatures up to 2600°F.

Weibull statistical analysis has been found to be a versatile method for describing the oxidation behavior of protective coating systems. A recent report prepared by the University of Dayton discusses how this statistical technique is used to determine the type of coating failure (i.e., random or wear-out) and also the reliability levels of the coating.[19] Figures IV-1 and IV-2 are Weibull plots of the 2600°F cyclic-oxidation-test results[20] for the General Telephone & Electronics R-508 silver-silicon-aluminum slurry silicide coating on niobium alloys C-129Y (niobium–10 wt.% tungsten–10 wt.%

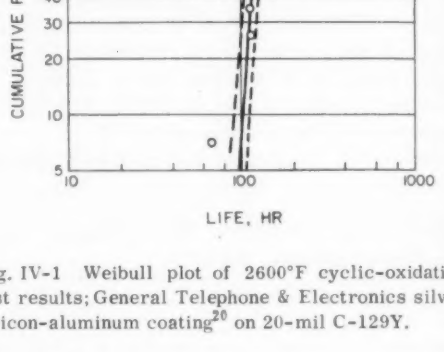

Fig. IV-1 Weibull plot of 2600°F cyclic-oxidation-test results; General Telephone & Electronics silver-silicon-aluminum coating[20] on 20-mil C-129Y.

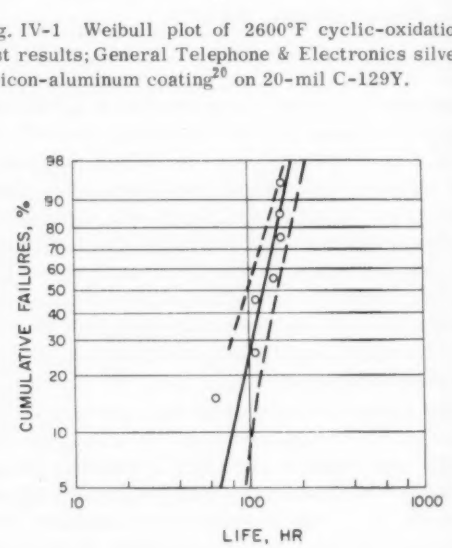

Fig. IV-2 Weibull plot of 2600°F cyclic-oxidation-test results; General Telephone & Electronics silver-silicon-aluminum coating[20] on 20-mil D-43.

Table IV-1 CYCLIC-OXIDATION-TEST* RESULTS OF PFAUDLER AND TRW COATINGS ON D-43 AND B-66 ALLOY SHEET TESTED IN AIR[18] AT 1600, 2000, 2300, AND 2600°F

Coating	Substrate	Protective life,† hr			
		1600°F	2000°F	2300°F	2600°F
Pfaudler	B-66	150,[a]‡ 150,[a] 150,[a] 150[a]	150,[a] 150,[a] 150,[a] 150[a]	24,[b]§ 24,[b]§ 24,[b]§ 24[b]§	4,[c]§ 4,[c]§ 4,[c]§ 4[c]§
	D-43	1,[d]§ 28,[d]§ 72,[d]§ 150[a]	1,[c]§ 24,[e]§ 144,[d]§ 144[d]§	40,[d]§ 56,[d]§ 56[d]§	24,[f]§ 24,[f]§ 24,[f]§ 24[f]§
TRW	B-66	150,[a] 150,[a] 150,[a] 150[a]	150,[a] 150,[a] 150,[a] 150[a]	150,[a] 150,[a] 150,[a] 150[a]	24,[f]§ 24,[f]§ 24,[f]§ 27[e]§
	D-43	150,[a] 150,[a] 150,[a] 150[a]	150,[a] 150,[a] 150,[a] 150[a]	77,[e]§ 98,[e]§ 98,[e]§ 120[e]§	24,[f]§ 24,[f]§ 24,[f]§ 24[f]§

*Cyclic oxidation: 8-hr cyclic exposure plus 16-hr static exposure in each 24-hr period.

†Failure criteria: first visual evidence of coating failure and growth of columbium oxide.

‡The superscript *a* denotes no visible coating failure; test terminated.

§Mode of coating failure: *b*, face, general; *c*, edge, spot; *d*, edge, spalling; *e*, face, spot; *f*, specimen melted, failure origin not evident.

hafnium) and D-43. The 95% reliability levels of 95-hr coating life on C-129Y and 68 hr on D-43 are the highest obtained to date for any substrate-coating combination in the University of Dayton program. The R-508 coating was rather thick, 7 to 14 mils, as compared with 2 to 4 mils for most protective coatings.

High-Temperature Inorganic Coatings, a Reinhold publication,[21] contains current information on the technology of protective coatings for materials operating at temperatures above 1500°F. Included are chapters on properties of coating materials, techniques for applying the coatings, testing methods, and phenomena important to the behavior of coated systems, such as oxidation, fatigue, and diffusion.

(J. J. English)

Corrosion by Liquid Metals

Workers at Vallecitos found[22] that specimens of UO_2 clad with molybdenum or tungsten did not exhibit a UO_2–refractory-metal interaction when exposed in vacuum and in cesium vapor at temperatures up to 1900°C (for molybdenum) and 2000°C (for tungsten). Similar lack of interaction was noted with Al_2O_3, BeO, ThO_2, and Y_2O_3 in contact with either molybdenum or tungsten and exposed to cesium vapor at pressures of 1 to 4 torrs. It was also found that the evaporation of UO_2 through a vent hole in the cladding into a cesium environment at a pressure of 2 torrs occurred at a rate approximately 100 times lower than that for the corresponding evaporation into a vacuum.

Valves capable of 10,000-hr operation with NaK up to 1200°F and with lithium up to 1000°F have been developed at Pratt & Whitney.[23] The designs utilize sealing surfaces of Stellite No. 6 against Stellite No. 12. These surfaces have been shown through extensive experimentation to be resistant to corrosion and to self-welding and galling. One type of valve combines sealing surfaces with a diaphragm type seal located in the opening. In service, the diaphragm can be sheared to open a flow path, and, after this event, the valve can be used in the standard way to control fluid flow.

An investigation at Atomics International[24] is directed toward evaluating the failure behavior of type 304 stainless-steel tubes that are subjected by internal pressurization to a gradually increasing hoop stress (for example, zero to maximum stress in 90 days). The tubes contain sodium-bonded uranium carbide, and thus the stressed steel is subjected to gradual carburization. The experiments are conducted in the 950 to 1250°F range. To date four failures have occurred after applied-stress periods of up to about 4500 hr; the hoop stress at failure in each case was approximately 13,500 psi. The character of the failures is particularly interesting. The description by the author is as follows: "The first four failures ... exhibited a very slow pressure loss at the time of failure. Several hundred psi could be easily maintained from the inside to the outside. This and subsequent metallurgical examination indicated a pinhole-type failure in the sodium bond region. Similar failure in a fuel element would allow bond loss down to the level of the pinhole. During operation at 1250 and 1100°F, the type 304 steel becomes sensitized; i.e., complex carbides of chromium and iron precipitated at the grain boundaries. The chromium carbide may have been leached from the boundaries by the sodium. Removal of the material, along with the applied stress, could then lead to the 'fine' pinhole failures at the grain boundaries ...."

An apparatus utilizing pressurized tubes to study biaxial creep of alloys in an environment of high-temperature lithium (to 2500°F) was built by Aerojet-General.[25] Employing a two-stress capsule (two different wall thicknesses in the same capsule) made of type 304L stainless steel and containing lithium at 1600°F, an 11-hr trial run was made, with shutdowns after 1, 2.5, 5.5, and 7 hr to make diameter measurements. Posttest examination showed a roughening of the interior surface of the capsule, but the authors concluded that: "In general, effects due to lithium exposure appear minor, and no significant effect on the creep strength is discernible."

The compatibility of containment materials with liquid cesium is being investigated at MSA Research Corp.[26,27] The following solubilities of structural-alloy constituents in cesium have been found:

1. Metallic species comprising Haynes 25 alloy (equal to or less than 10 ppm at 1800°F)
2. Niobium from niobium–1 wt.% zirconium alloy (approximately 20 ppm at 2500°F)
3. Molybdenum from molybdenum–0.5 wt.% titanium (approximately 20 ppm at 2500°F)

Pronounced isothermal mass transfer of metallic constituents of bimetallic combinations such

as Haynes 25 alloy–niobium–1 wt.% zirconium, TD nickel–niobium–1 wt.% zirconium, and TD nickel–molybdenum–0.5 wt.% titanium has been observed at 1800°F. The characteristic transfer is that of the refractory-metal constituent to the Haynes 25 alloy or to the nickel. Interstitial elements also transfer, but a characteristic pattern is not apparent. Some interstitial-element transfer between niobium–1 wt.% zirconium and molybdenum–0.5 wt.% titanium has been observed at 2500°F. (J. H. Stang)

Metal-Water Reactions

Additional analysis of work reported by Argonne[28] has been performed on data obtained by both the pressure-pulse and levitation methods for obtaining information on the reaction of aluminum with steam. The extent of reaction at 1200°C by the pressure-pulse method was approximately twice the extent in the levitation studies. The greater reaction obtained by the pressure-pulse method very likely resulted from the diffusion of steam through the slightly porous alumina crucibles used to contain the molten aluminum, which allowed reaction to occur over an increased surface. The cubic rate law was fitted to the levitation data, and the following equation was obtained:

$$W^3 = 4.0 \times 10^9 t \left(\exp \frac{-73{,}500}{RT}\right) \qquad (1)$$

where W = metal reacted, mg of aluminum/cm^2
t = time, min
R = gas constant, 1.987 cal/(mole)(°K)
T = temperature, °K

The activation energy, 73,500 cal/mole, found experimentally is approximately the same as the values reported for the heat of vaporization of aluminum. A similar coincidence between the activation energy for oxidation and the heat of sublimation of magnesium was taken as evidence for a vaporization-controlled reaction.

Equation 1 describes, within a factor of 2, the reaction of aluminum and two alloys* of aluminum with steam at 1-atm pressure over the range 800 to 1300°C (see discussion under Fuel-Water Reactions in Sec. I). Pure aluminum appears to follow a linear rate law at 1400, 1500, and 1600°C. It is also possible, however, to fit the data satisfactorily to a curve that follows a cubic rate law initially and then undergoes a smooth transition to a linear rate law after 2.3 mg of aluminum per square centimeter has reacted. The linear portion of the curve is described by the following equation:

$$W = 2.5 \times 10^8 t \left(\exp \frac{-73{,}500}{RT}\right) \qquad (2)$$

where W is greater than 2.3 mg of aluminum per square centimeter. Values of the extent of reaction of 6061 aluminum alloy were very scattered and were generally greater at 1400, 1500, and 1600°C than those given by Eq. 2. This greater reaction was probably due to the disruption of the protective oxide film by vaporizing magnesium.

Pure aluminum and the two alloys studied ignited immediately in steam (and also in air) when the metal temperature reached 1750°C. The burning reaction that followed was evidently a combustion process in which aluminum was first vaporized (vapor pressure ~7 mm at 1750°C) and then reacted as a vapor. Very fine aluminum oxide powder was formed during the burning. Pellets that had been ignited in air or steam, and had been subsequently dropped into liquid water, continued to burn with increased vigor under the water surface and later at the water-air interface. The consumption time of pellets was measured as a function of diameter; the surface burning rate was found to be independent of diameter. The rate was constant at 0.96 g of aluminum/(cm^2)(min). Pellet consumption, however, was not complete. An oxide shell of irregular thickness formed around the pellets during the latter stages of burning, and the equivalent of a 2.3-mm-diameter sphere of aluminum remained unreacted after the burning had ceased.

At present the extent of the aluminum-water (or steam) reaction at high temperatures must be viewed as being very dependent upon environmental conditions, such as pressure, water temperature, particle size, and the presence of turbulence. Thus, in steam at 1-atm pressure and in the absence of turbulence, aluminum forms a very protective oxide up to temperatures of 1750°C, at which temperature ignition occurs. Under more violent conditions, such as

*SL-1 (81 wt.% aluminum–17 wt.% uranium–2 wt.% nickel) and 6061 (1 wt.% magnesium–0.6 wt.% silicon–0.25 wt.% cerium–0.25 wt.% chromium, balance aluminum).

those prevailing in laser-heating experiments or in TREAT experiments, the extent of reaction is considerably greater at temperatures below 1750°C. It is not presently known whether this increased reaction under turbulent conditions results from repeated fracturing of the oxide film or by sporadic vapor burning. The failure to observe a very rapid pressure rise in TREAT experiments indicates that the reaction under turbulent conditions is not extremely rapid. The extent of reaction is increased further when the reaction takes place in heated water at a high overpressure of steam, suggesting that either the reaction rate is greatly increased or the ignition temperature is lowered. The sharp energy threshold for reaction in TREAT experiments suggests that the lowering of the ignition temperature is the most likely cause of the increased reaction, although it is difficult to find a mechanistic explanation for this behavior.

In other experiments at Argonne,[29] small cylindrical specimens of molybdenum, rhenium, tungsten, tantalum, and niobium were supported on an alumina rod, which also acted as a sheath for a platinum, platinum-rhodium thermocouple. Specimens were heated in flowing steam by an external induction coil. The rates of the reactions of steam with the refractory metals were too high at temperatures above 1200°C to allow the use of these metals as high-temperature structural materials.

The molybdenum-steam reaction was studied in greater detail than were the reactions with the other structural materials because it served as an example of a metal that oxidized by the formation of a volatile oxide. The molybdenum-steam reaction followed a linear rate law. Rate constants as a function of reciprocal temperature are plotted in Fig. IV-3. The metal surface acquired only a slight tarnish. The principal oxide formed was found by X-ray analysis to be the volatile MoO_3. Overall stoichiometry as determined by comparison of the metal weight loss and the quantity of hydrogen generated indicated the formation of $MoO_{2.85}$. The stoichiometry was consistent with the slight blue color of the condensed oxide, indicating the presence of polymeric suboxides.

(A. W. Lemmon, Jr.)

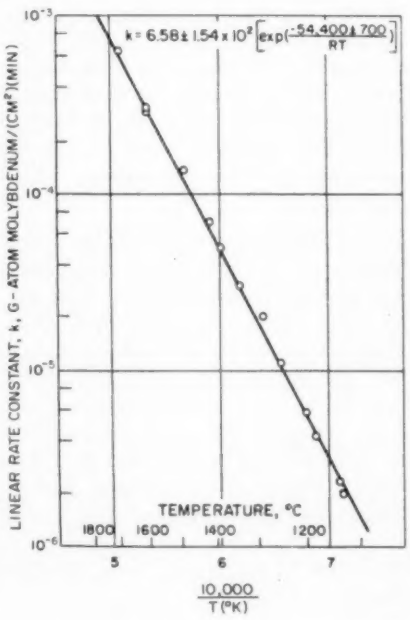

Fig. IV-3 Linear rate constants for the molybdenum-steam reaction (1100 to 1700°C).[29]

Selected Mechanical Properties of Refractory Metals

The creep behavior of niobium–0.6 wt.% zirconium in a cantilever-beam slow-bend test at 1000°C was found by workers at Oak Ridge[30] to be strongly dependent upon the test vacuum. A systematic increase in the test pressure within the range 7×10^{-8} to 6×10^{-5} torr promoted an increase in contamination rate which was reflected in a progressive weakening of the alloy during the early test stages. Later the alloy was strengthened by dispersed phases such as ZrO_2 and/or niobium carbides or nitrides, and possibly by interstitials in solution. This effect was more pronounced at higher test pressures.

It was noted that the alloy was weakened when oxygen contamination proceeded to the point where NbO precipitated.

During a single test it was reported to be possible to alternately accelerate or decelerate the creep of the alloy by systematically varying the pressure between the range of 10^{-5} and 10^{-7} torr. It appears that vacuums of better than 1×10^{-7} torr are required to minimize the

Table IV-2 STRESS-RUPTURE DATA FOR TANTALUM–9.6 WT.% TUNGSTEN–2.4 WT.% HAFNIUM–0.01 WT.% CARBON ALLOY[31]

(Reduced 90%; Recrystallized 1 Hr at 3000°F)

Stress, 1000 psi	Minimum creep rate, %/hr	Transition time,* hr	Rupture time, hr	Elongation, %
		2400°F		
40	4.39	1.4	2.15	33
40	2.55	1.2	2.55	33
35	0.52	4.6	12.3	42
35	0.46	3.2	9.95	39
32.5	0.129	5.6	15.6	31
32.5	0.048	8.6	26.0	31
		3000°F		
20	35.5	0.06	0.26	25
15	5.7	0.29	1.11	23

*From second- to third-stage creep.

environmental effects observed for the test conditions described by the authors.

Stress-rupture properties of T-222 alloy (tantalum–9.6 wt.% tungsten–2.3 wt.% hafnium–0.01 wt.% carbon), as reported by Westinghouse,[31] are presented in Table IV-2.

(J. A. DeMastry)

Selected Metallurgical Aspects of Cladding and Structural Materials

Aluminum

The behavior and properties of aluminum-alumina composite materials have been of considerable interest recently. Europeans have conducted studies[32] of the fundamental mechanisms of plastic deformation in the SAP alloys which have resulted in the determination of the activation energy and activation volume from room temperature to 600°C. On the basis of their results, they propose that dislocations move by cross slip and climb up to about 350°C; at higher temperatures a process of pinning-unpinning dislocations by the alumina particles begins.

In addition, SAP was studied in the temperature range above the melting point of aluminum,[33] with a view to assessing the limits for the appearance of the typical dispersed-phase structure of the SAP itself. Various heat-treatments were used. A partial transformation was observed in the alumina from the finely dispersed initial gamma structure into an alpha structure of relatively larger crystals, at a growth rate proportional to the temperature. The $\gamma \rightarrow \alpha$ alumina transformation, which normally occurs at temperatures of the order of 1000°C, takes place in SAP at just above 660°C. The trends followed by this phenomenon in relation to temperature and time were studied, and the activation energy of the transformation was calculated as 61 kcal/mole.

Zirconium and Titanium

Argonne[15] studies on the effects of temperature on the C_{11}, C_{33}, C_{44}, C_{66}, and C_{13} moduli of titanium, zirconium, hafnium, and other hcp metals have been completed over the temperature range from 4°K to the hcp → bcc transformation temperature. The shear moduli, with few exceptions, are more sensitive to temperature variation than are the C_{11} and C_{33} moduli. Anisotropy is evidenced by the different effects of temperature on the shear and elastic moduli. Transformations of hcp to bcc are induced thermally in the hcp metals with a c_0/a_0 ratio of less than 1.598, except in ruthenium and osmium. A generalization is that the anisotropy factor, C_{44}/C_{66}, increases with temperature in those hcp metals which undergo hcp → bcc transformations and that both phenomena occur only when the c_0/a_0 ratio is less than 1.598. Anharmonicity in lattice vibrations is suggested as a possible source for the thermodynamic driving force for the martensitic hcp → bcc transformation.

Luke and coworkers[34] examined the metastable constitution of titanium- and zirconium-base alloys from a theoretical point of view and correlated with existing experimental data. The electron-to-atom ratio was deduced as a criterion for predicting 100% beta stabilization in quenched alloys. The same criterion also establishes the composition range over which the omega phase is expected to form in conjunction with either alpha-prime or beta phase. The proposed theory allows quantitative predictions to be made regarding the effects of minor concentrations of contaminants on the constitution of binary alloys.

Transmission electron microscopy has been used by researchers[35] to follow the formation and reversion of the metastable omega phase in

a zirconium–15 wt.% niobium alloy. In a fully aged specimen, the omega is shown to consist of noncoherent platelets lying on {1 1 1} planes of the retained beta phase. The platelets form a regular three-dimensional network having an average spacing of approximately 1000 A. The retained-beta-phase regions contain a line structure similar to that observed in specimens aged at lower temperatures when the omega phase is coherent. Aging of the foils in the electron microscope resulted in partial reversion of the noncoherent platelets and formation of the coherent structure. Possible mechanisms for the formation of the two types of omega phase are discussed, along with an explanation of the changes in mechanical properties which accompany their formation.

The effects of zirconium additions on room-temperature mechanical properties of selected alpha, alpha-dispersed, alpha-beta, and beta titanium alloys have been examined at Battelle.[36] Zirconium additions of up to 50 wt.% in the binary system and up to 15 wt.% in the ternary system were found to have a mild strengthening effect. Russian investigators[37] have measured the hardness of titanium-zirconium alloys as a function of temperature. Diagrams for $\alpha \rightarrow \beta$ transitions were constructed, and the effects of structure at the $\alpha \rightarrow \beta$ transition point on mechanical properties were determined.

An investigation on the strengthening of zirconium[38] alloys by use of carbide or oxide dispersants showed that highly promising materials can be produced by standard powder-metallurgy techniques. The dispersants used included ZrC, VC, Al_2O_3, La_2O_3, Y_2O_3, Ce_2O_3, CaO, and ThO_2. The stress-rupture data developed for these materials at 1200°F show that the addition of particle dispersions to zirconium markedly increases the time to rupture; it may, in fact, double the stress for a given time to rupture of undispersed zirconium.

The susceptibility of zirconium and certain zirconium alloys to delayed failure (static fatigue), as caused by a combination of absorbed hydrogen and applied stress, was studied at Illinois Institute of Technology Research Institute.[39] Specimens of unalloyed zirconium, Zircaloy-2, zirconium–1.25 wt.% aluminum–1 wt.% tin–1 wt.% molybdenum, and zirconium–2.5 wt.% niobium were hydrogenated in a Sieverts apparatus and evaluated in static tests at room temperature. For notched and unnotched specimens of unalloyed zirconium and Zircaloy-2 containing up to 500 ppm hydrogen, no time-dependent, brittle fractures occurred that could be attributed to the delayed-failure phenomenon. The high-strength quaternary alloy with 500 ppm hydrogen, however, exhibited a high degree of susceptibility to delayed failure at room temperature. Data for heat-treated zirconium–2.5 wt.% niobium with the same hydrogen content indicated that this material is moderately susceptible to delayed failure. The results are explained in terms of dislocation pileup at hydride platelets and the ability of these matrices to allow crack propagation.

Refractory Metals

Union Carbide European researchers[40] have studied the tensile properties of flash-annealed and conventionally recrystallized niobium at room temperature and at 77°K. Twinning at 77°K at stresses lower than the predicted value of the Peierls-Nabarro force proved that it is not this which causes the large temperature dependence of the yield stress. Electron-microscopic examination of foils loaded at room temperature to <3 kg/mm^2 showed that edge dislocations are mobile before the apparent proportional limit of the flash-annealed niobium (about 3.5 kg/mm^2) is reached. At this temperature and 1%/min strain rate, the material was characterized by an absence of an upper yield point, high work-hardening rate, and high ultimate/yield stress ratio.

Studies at Battelle[41] have shown that carbon additions strengthen tantalum and tantalum-base alloys at the temperatures at which they form stable carbides. In conjunction with concurrent zirconium additions, the structural nature of the carbide phase may be altered, although it seems to have little effect on the strength. At very high temperatures of 3000°F or above, the carbon solubility in tantalum increases rapidly with temperature, and even the reactive metal carbides dissolve in the metal and lose their effectiveness.

Results of studies at the Massachusetts Institute of Technology[42] have shown that the ternary-phase diagrams for the zirconium-tungsten-tantalum system contain two planes of four-phase equilibrium and no ternary intermediate phases not in the component binary diagrams. One four-phase plane lies in the solidus surface at 1760°C and the other lies at 812°C, corresponding to the alpha-beta zir-

conium ternary solid-solution transformation. The W_2Zr compound extends into the system along a constant-zirconium-content line up to 12 at.% tantalum. Solid-solution regions are of very limited extent.

Studies at Oxford University[43] on the palladium-rich end of the molybdenum-palladium equilibrium diagram have confirmed the existence of an intermediate close-packed hexagonal epsilon phase over a narrow range of composition at about 52 at.% palladium. The palladium-rich terminal solid solution showed a maximum freezing point at about 60 at.% palladium and also gave rise to a lattice-spacing–composition curve with a minimum lattice spacing at about 10 at.% molybdenum. The results also confirmed that, in alloys of elements from group VI-A with those of group VIII-C, the solubility of the elements of group VIII-C is usually the greater.

Miscellaneous Alloys

Researchers at U. S. Steel[44] have determined the lattice parameters of solid solutions of niobium in nickel up to 8 at.% niobium. The plot of lattice parameter vs. composition yielded a straight line over the range investigated. A method based on atomic volumes of the solute and solvent, assuming a linear relation between concentration and atomic volumes, was capable of predicting the lattice parameters of nickel-niobium solid solutions with reasonable accuracy. In addition, the paramagnetic susceptibility of these alloys was measured up to about 1500°K. This paramagnetism is describable by a modification of the Curie-Weiss law by addition of another susceptibility contribution, X_a. The quantity X_a, which generally was assumed to be independent of the temperature, was found to increase with increasing temperatures. Niobium in nickel did not follow the Volkov-Chechernikov correlation between X_a and the valence and concentration of the solute metal in nickel.

Tensile specimens of impact-extruded strip of magnesium – 0.5 wt.% zirconium alloy[45] have been strained to failure at 500°C at a rate of 0.01%/hr in a CO_2 atmosphere containing approximately 200 ppm water vapor. Under these conditions hydrogen was absorbed, and extensive precipitation of ZrH_2 occurred. Denuded zones were formed preferentially at grain boundaries and were oriented approximately normal to the stress axis. Examination of the fractured specimens revealed that extensive cavitation had occurred and that the cavitation was confined to the denuded zones. The relatively brittle failure at such a high temperature was attributed to the particular mode of distribution of the hydride phase. Microhardness data at 300, 350, and 400°C were used to analyze aging in beryllium bronze[46] and the effects of tensile forces on the aging process. The effects of the tensile forces at these temperatures are related to a transition from a two-phase system to a single-phase system. (N. M. Griesenauer)

Diffusion Studies

Toth and Searcy[47] have developed a model of self-diffusion which attempts to predict Q_D, the activation energy for self-diffusion, for many metals. For fcc metals, $Q_D = 22.6B_sV_0 + 0.27L_s$ or $Q_D = 16.0T_m + 0.27L_s$; for bcc metals, $Q_D = 14.7T_m + 0.27L_s$ or $Q_D = 23.8B_sV_0 + 0.27L_s$. Here B_s is the bulk modulus, V_0 is the atomic volume, L_s is the heat of sublimation, and T_m is the absolute melting temperature. All of these are readily measured parameters. Reasonably close agreement with experimental data was observed for many metals, but several large discrepancies were not explained for platinum and gold when $Q_D(V_0B_s)$ was used, for tungsten when $Q(T_m)$ was used, and for zirconium. Only fair agreement with empirical values was noted for nickel, iron, and magnesium.

Additional data on the diffusion in bcc metals is provided by Wolfe and Paxton[48] as a result of their investigations to test ring-mechanism theories in bcc metals and to explain the deviations from linearity of diffusion coefficient, D, vs. reciprocal temperature, $1/T$, for several systems. Diffusion was measured by radioactive tracer methods with ^{51}Cr and ^{55}Fe in four different materials: iron–12 wt.% chromium, iron–17 wt.% chromium, chromium, and vanadium. Resulting activity-concentration curves were used to determine the diffusion coefficients. The authors observed sharp deviations from linearity in plots of D vs. $1/T$ in the temperature range 950 to 1600°C. A vacancy mechanism was suggested as a possible cause for these deviations, but the authors did not elaborate.

The influence of crystal orientation and of concentration on the diffusivity of tungsten in niobium is discussed by Gebhardt and Kirner in

a German publication.[49] The concentration of tungsten in niobium was determined from microhardness measurements of annealed alloy buttons. Matano analyses were made of concentration-penetration curves, using times to 390 hr at 2100°C and to 500 hr at 1900°C. Values of diffusivity at 2100°C varied from about 1.6×10^{-5} cm^2/sec in 10 at.% tungsten to 2.1×10^{-7} cm^2/sec in 90 at.% tungsten. The strong effect of concentration on the diffusivity of tungsten in niobium apparently eliminated any observable influence of crystal orientation.

Final results of diffusivity studies of palladium into silver and into copper are reported by Argonne,[15] along with preliminary values of self-diffusion of palladium. Values determined were: for palladium diffusion into silver, 9.57 exp $(-156{,}752 \pm 300/RT)$, and for diffusion into copper, 1.71 exp $(-54{,}370 \pm 300/RT)$. The self-diffusion rate for palladium was estimated at 0.1 exp $(-62{,}000/RT)$.

In other literature on directional-diffusion phenomena, Harris and Jones[50] found that after slow deformation of magnesium – 0.5 wt.% zirconium alloys at elevated temperatures, precipitate-free zones formed preferentially normal to the stress axis. The study reported in this article investigates whether this is due to a directional-diffusion process occurring during the creep tests and if directional-diffusion creep is likely to be an important deformation mode in reactor components.

Studies in the USSR in the field of diffusion of metals and alloys are described in a 528-page volume translated from Russian.[51] Much of the material has been supplemented by papers published during the 1954–1958 period. The chapters concerned with applications of diffusion phenomena and with the technique of determining diffusion are of fundamental interest. Applicable fields of diffusion are described under general headings of Metal Ceramics, Heat-Resistant Metals, and Protective Coatings. An extensive list of diffusion coefficients and activation energies for metals and alloy systems, plus boundary diffusion values, are given in the appendix.

Grisaffe and Spitzig[52] have suggested diffusion bonding as the cause of strong bonds resulting from plasma-arc spraying tungsten particles onto a stainless-steel substrate. Mechanical interlocking on the surface was previously thought to have been the primary source of bond strength. Hot tungsten particles at 3000°F were deposited onto a highly polished type 304 stainless-steel surface at room temperature. Metallographic, microhardness, and microprobe analyses indicated that a small reaction layer between the tungsten and stainless steel had a hardness between that of the two base metals and a measurable (5 to 6 wt.%) amount of tungsten. The results should be considered preliminary until additional data can substantiate their findings. (A. N. Ashurst)

Ceramic Technology

A compilation has been made by the National Bureau of Standards (NBS)[53] of the melting points of 70 metal oxides published prior to January 1963. No attempt has been made to choose between values in disagreement, but information is included on pertinent experimental details such as the method of temperature measurement, purity, furnace type, and environmental conditions. NBS plans to verify data experimentally and hopes ultimately to have national and international recognition of the melting points of several specific oxides for use as calibration standards.

Parikh[54] has summarized well the status of the understanding of the factors affecting the brittle behavior of ceramic oxides. He discusses the comparison of single crystals and polycrystals, the statistical theory of strength, microstructural effects, effects of surface condition, and fracture energy. He points out the need for further investigation of the detailed effects on strength of grain-size and pore-size distributions; pore size, spacing, and shape; impurity distribution; and surface condition in polycrystalline oxides.

Stokes[55] has studied the combined effects of both thermal and mechanical history on the mechanical behavior of MgO single crystals. He found that impurity-precipitate particles in single crystals can be redistributed by heat-treatment. Their size and density affect the lattice resistance to fresh dislocations and thus the yield strength at room temperature. Above 1200°C the impurities go into solid solution, and the strength drops to 0.7 of the as-received value. Fresh dislocations can be locked by heating above 600°C to produce yield phenomena at room temperature. The upper yield strength increases with time and temperature, particularly when aging temperature exceeds 1000°C. Locking is attributed to diffusion of impurities,

and point defects are attributed to dislocations. The basic temperature dependence of the yield strength contains two regions:

1. Up to 500°C the strength decreases rapidly, suggesting a dislocation-cutting mechanism during flow. Material preheated above 1200°C shows a stronger dependency of yield strength on temperature than as-received material, due to finer dispersion of impurities in solid solution.

2. Above 500°C the strength decreases linearly at a rate proportional to the decrease in elastic modulus, suggesting long-range interaction of dislocations with internal stress fields.

Superimposed on this basic temperature dependence there is, for material preannealed above 1200°C, a hump due to reprecipitation between 500 and 1000°C.

The tensile behavior of MgO single crystals in the temperature range from 1000 to 2000°C has been investigated by Day and Stokes.[56] The crystals show a wide variety of deformation and fracture modes under tension at high temperatures. These modes are determined by the number of slip systems operating concurrently in a given volume. At low temperatures slip is confined to a single {1 1 0} system, and plasticity is limited by stress concentrations that develop where slip switches from one plane to another. At intermediate temperatures the {1 1 0} slip systems at 90° to each other can interpenetrate, but those at 60° cannot. Mechanical properties depend on initial slip distribution. When slip is confined to two 90° systems, there is little work hardening before crystals neck down to a knife-edge ductile fracture. When slip is confined to 60° systems, crystals work harden and fracture by cleavage. At high temperatures dislocations can interpenetrate on all systems, and polygonization can occur. After easy glide the crystals work harden and elongate over 100% before fracturing in a completely ductile manner.

The present state of knowledge on the mechanical behavior of sapphire has been reviewed by Conrad.[57] Sapphire deforms plastically at temperatures above 900°C. The most common mode of deformation is slip on the basal plane in the ⟨1 1 2 0⟩ direction. A yield point is often observed. This appears to be related to the multiplication of dislocations by a mechanism that is controlled by the motion of dislocations through the lattice, rather than by the tearing of dislocations from an impurity (or defect) atmosphere. In the temperature range from 1100 to 1500°C, the tensile fracture stress decreases with increase in plastic strain, independent of temperature and strain rate. The mechanism of failure in this case seems to be the interaction of edge dislocations with preexisting cracks.

A fundamental study of the ductile-brittle behavior of the transition-metal monocarbides is being made by Williams.[58] The plastic deformation of single crystals of TiC, ZrC, and NbC is being investigated. Compression measurements in the range 800 to 1600°C are being made. In experiments to date the three carbides behaved similarly, but NbC was several times harder than TiC and ZrC. It was found that the critical resolved shear stress decreases exponentially with increasing temperature, increases approximately linearly with increasing carbon content in the range from $MC_{0.7}$ to MC, is little affected by surface condition, and increases as the logarithm of the strain rate. No yield point was observed.

The thermal conductivities of titanium carbide, zirconium carbide, and titanium nitride in the range from 200 to 2000°C have been measured by Atomics International.[59] The titanium nitride conductivity at 1000°C is higher by a factor of 4 than previously published values. Also the tests showed a positive temperature coefficient for the thermal conductivity, rather than the negative coefficient previously reported.

The nitriding of TiC, ZrC, HfC, NbC, and TaC powders and carburization of TiN, ZrN, HfN, NbN, and TaN powders at 1500 to 2500°C are described by Portnoi and Levinskii.[60] X-ray and chemical analyses of the obtained solid solutions of refractory metal-carbonitrides were made to study equilibrium states, activation energies of carburization and nitriding, temperature dependence of lattice parameters, and thermal stability.

Ceramic structural materials of lead oxide combined with other oxides for the absorption of gamma rays and neutrons have been prepared by Schumann.[61] Ceramic bodies of lead oxide and zirconium oxide have about half the capacity of metallic lead to attenuate gamma radiation. Lead oxide and rare-earth oxide combinations have specific gravities up to 5.9 and large neutron-capture cross sections.

The stabilization of rare-earth oxides in perovskite-like compounds (ABO_3) by combining them with other oxides has been studied by

Argonne.[15] Dy_2O_3 and Eu_2O_3 were combined with oxides of cobalt, iron, and nickel by heating in air at 1400°C. X-ray analysis showed complete reaction of Fe_2O_3 with both Dy_2O_3 and Eu_2O_3 to form $FeDyO_3$ (not reported previously in the literature) and $FeEuO_3$. $CoEuO_3$ (also not reported previously) formed but melted below 1400°C. No reaction was observed between the NiO and either of the rare-earth oxides or between Co_3O_4 and Dy_2O_3.

Bodies of high compressive strength and steel-cutting ability have been made at Oak Ridge[62] by forming a number of oxides and carbides at unusually high pressures and by sintering them at temperatures lower than normal. Isostatic pressing at 200,000 to 300,000 psi has been used. (D. J. Bowers)

Radiation Effects in Nonfuel Materials

Defects: Structure and Properties

METALS

The recovery of nickel after plastic deformation, neutron irradiation, and quenching was investigated by measuring the initial susceptibility and, on quenched samples, the coercive force.[63] The following stages of recovery were observed: (1) a stage near 0°C in deformed nickel, in accordance with previous investigations, probably due to the separation of vacancy pairs from impurity atoms with an activation energy of 0.82 ev; (2) a stage (III) near 100°C in deformed and in irradiated nickel, in accordance with previous investigations, probably due to the annihilation of interstitial atoms with an activation energy of 1.02 ± 0.03 ev; (3) stage IV in deformed nickel, the annihilation of vacancies with an activation energy of 1.6 ± 0.1 ev; (4) between these stages, in deformed and in irradiated nickel, some more or less continuous recovery, probably due to the annihilation of vacancies coupled to solute atoms; (5) a stage near 100°C in quenched nickel, possibly explained by the separation of vacancy pairs either from vacancy clusters or from impurity atoms with an activation energy of 1.26 ± 0.03 ev; and (6) at 180 ± 30°C in irradiated nickel, the annihilation of some particular lattice defect, which gives rise to strongly temperature-dependent relaxation near −15°C. Possibly this defect is an interstitial pair, consisting of an impurity atom and a nickel atom. Its activation energy is 0.82 ± 0.08 ev.

The recovery of cold-worked or neutron-irradiated pure iron was investigated[64] using stored-energy measurements over the temperature range 20 to 450°C. In both cases a single recovery stage was found, which lies in the same temperature range for both types of treatment. On the basis of the experimental results, and a comparison with other bcc metals, the nature of the defects that anneal out in the observed recovery stage is discussed. Foils of iron have been neutron irradiated in the Swedish research reactor R2 to integrated doses in the range 10^{17} to 10^{19} neutrons/cm^2 (>1 Mev) and examined by transmission electron microscopy.[65] Features have been observed having diffraction contrast similar to that of the prismatic dislocation loops formed in fcc metals by the collapse of point-defect clusters. The features have been shown to be due to precipitation of impurities at radiation-damage centers in the iron matrix.

Muller has again demonstrated the effectiveness of field-ion microscopy in studying radiation damage on an atomic scale. His report[66] discusses the damage produced in tungsten by 20-kev helium atoms. About one-half of the number of atoms calculated to have received a displacement energy of 50 ev in the interior appear as surface defects. The surface integrates the damage by focusing collisions coming from as deep as 1000 A. Stress-enhanced mobility of subsurface interstitials is detectable at 21°K, and a rapid thermal diffusion from the depth occurs at 90°K. Another new technique, small-angle scattering of subthermal neutrons ($\lambda \approx 9$ A), was used to investigate the damage produced in polycrystalline, pile-irradiated copper.[67] The observed scattering was due to regions of high vacancy densities or dislocations and disappeared after annealing at 570°C. It was assumed that one primary recoil atom produces one of these vacancy agglomerates. If this zone is vacancies, the results require the order of 20 vacancies in each zone; if dislocations, the results require about 40 vacancies in a loop of about 15 A diameter.

Experiments were performed to investigate the feasibility and usefulness of using the Barkhausen effect as a tool for studying radiation damage in magnetic materials.[68] The re-

sults indicate that the Barkhausen effect is a more sensitive indicator of radiation damage than the coercive force. However, the smallness of the effect after neutron irradiation is puzzling. On the basis of estimates of the number of high-energy primary recoils produced by neutrons, the observed changes were several orders of magnitude too small. This result may indicate that the concentration of defects generated in the path of high-energy primary recoils is too small to impede domain wall motion appreciably.

DEFECTS IN METAL ALLOYS

The electrical-resistivity changes that occur upon annealing quenched iron-carbon (0.011 wt.%) after irradiation at −100°C in a reactor have been compared[69] to the changes that occur in unirradiated specimens. In unirradiated specimens two stages of resistivity are noted, one at about 170°C, associated with the formation of a metastable carbide, and one at about 250°C, associated with the formation of Fe_3C. In contrast, five annealing stages are observed in the irradiated specimens between −80 and 300°C. These stages are discussed in terms of the migration history of the carbon atoms. It was observed that the carbon atoms are temporarily trapped by radiation-produced point defects and leave the traps only at a temperature higher than that at which the metastable carbide can form. The binding energy of carbon to these defect traps was measured by calorimetry[70] and found to be 0.41 ev/atom. It was verified, therefore, that no precipitate with a binding energy for carbon of less than 0.41 ev/atom will be formed in an iron-carbon alloy irradiated to a dosage sufficient to trap all of the carbon atoms. In unirradiated iron-carbon the energy released per carbon atom in forming the metastable carbide precipitate was 0.27 ev/atom, which explains why this carbide is not formed in irradiated alloys. Electron microscopy also revealed[71] that irradiation prevents the formation of the metastable carbide precipitate, which occurs at about 160°C in the unirradiated alloy, but does not alter the temperature of the Fe_3C precipitation process. An accelerated growth of the Fe_3C precipitate particles occurs between 300 and 330°C in the irradiated specimens. With a similar system point-defect calculations were made using a high-speed computer to minimize the energy of an array of about 500 lattice atoms.[72] Configurations of interstitial-carbon and vacancy-carbon complexes were obtained, and temperature of their formation and dissociation and the expectation of internal friction arising from their reorientation were estimated.

The redistribution of atoms segregated by neutron irradiation (3.8×10^{18} neutrons/cm^2, $E > 1$ Mev) in copper−35.7 at.% nickel has been studied by measuring the changes in $\bar{\alpha}$ (the average temperature coefficient of resistance) during annealing.[73] The recovery occurs in two stages: one at about 300°C, associated with the redistribution of segregated atoms, and the second at about 600°C, associated with the annealing of the radiation-produced equilibrium vacancies as a result of self-diffusion.

X-ray diffraction, electron diffraction, and microscopy, metallography, and thermal methods were utilized to study transmutation effects in a group of crystalline solids.[74] Nearly homogeneous distributions of transmuted species were introduced in small crystals of ^{197}Au, ^{107}Ag, and ^{115}In, and in powder samples of ^{193}Ir, $^{115}In_2O_3$, and $^{176}Lu_2O_3$. The crystals were irradiated in a thermal-neutron flux of 4.0×10^{14} neutrons/(cm^2)(sec) at a temperature of ~85°C for periods of a few days to several months, so that considerable fractions of transmuted species were formed. Small metal single-crystal spheres were converted to alloy single crystals in their solid-solution ranges at temperatures up to several hundred degrees below those required by normal laboratory methods in $Au_{0.82}Hg_{0.18}$, $Ag_{0.78}Cd_{0.22}$, and $In_{0.95}Sn_{0.05}$. A powder sample of ^{193}Ir was transformed into the solid-solution alloy $Ir_{0.68}Pt_{0.32}$, a high-temperature alloy, which would require a temperature in excess of 2000°C for its formation by laboratory methods. The production of 22.5 at.% ^{198}Hg and ^{199}Hg in ^{197}Au through nuclear transmutation revealed the nucleation of Au_3Hg particles with the hcp structure, whereas the introduction of 29 at.% mercury caused a recrystallization into two unidentified phases. Long-range order in single crystals of ^{115}In was completely destroyed when 14 at.% ^{116}Sn was introduced through nuclear transmutation. Powder specimens of In_2O_3 enriched in ^{115}In were irradiated to produce concentrations of ^{116}Sn as high as 38 (metal) at.%, with the result that a new phase with a smaller fluorite structure was formed which contains oxygen vacancies. The original In_2O_3 structure was largely recovered upon annealing at 1200°C, and SnO_2

particles were precipitated. Powder samples of Lu_2O_3 containing ^{176}Lu were irradiated to produce 74 (metal) at.% ^{177}Hf, and the resultant material was cubic (fluorite) with a lattice parameter approximately one-half that of the original structure. This oxygen-deficient lattice was stable at temperatures up to 1200°C. The results are considered in terms of the original crystal structures and known phase-equilibrium systems, and possible future experiments are discussed.

The room-temperature strength of copper and alpha copper-aluminum single crystals containing 0.5 to 14 at.% aluminum has been studied[75] as a function of neutron irradiation from doses of 1.0×10^{15} to 0.98×10^{20} neutrons/cm^2. For a dose of 1.4×10^{17} neutrons/cm^2 or less, the amount of irradiation-induced strengthening decreases with increasing solute concentrations; the strength of copper–14 at.% aluminum crystals is independent of dose in this range. With a dose of 0.94×10^{18} neutrons/cm^2 or more, the strength of these crystals is independent of solute concentration. These observations are explained on the basis of solute additions increasing the dislocation-motion stress and neutron irradiation increasing the dislocation-generation stress. Annealed disks, 0.13 mm thick, of 99.999% copper and copper–14 at.% aluminum were irradiated[76] by 1.1×10^{19} fast neutrons/cm^2. The specimens were then electrolytically thinned and examined in an electron microscope. From the results it is concluded that the dislocation loops are not the source of the strengthening in neutron-irradiated copper or alpha copper-aluminum crystals.

DEFECTS IN OTHER MATERIALS

The split interstitial, which was predicted on the basis of computer calculations, has been verified experimentally[77] in 4-mm-thick slabs of single-crystal $SrTiO_3$ irradiated with fast neutrons from a plutonium-beryllium source ($\approx 8 \times 10^8$ neutrons/cm^2). The observation was that new Laue spots appeared, corresponding to the forcing of an interstitial onto other planes as a result of the formation of the split interstitial.

The additional elastic scattering of monochromatic neutrons, wavelength 7.5 A, produced by irradiating a sample of AGXP graphite to a dose of 6×10^{19} fast neutrons/cm^2 at 30°C has been measured as a function of the scattering angle.[78] If the reasonable assumptions are made that equal concentrations of vacancies and interstitials are present and also that the vacancies scatter isotropically, the state of agglomeration of the interstitials may be estimated, provided that allowance is made for the relaxation of the neighboring atoms. The result is 4 ± 2 interstitials per cluster; also the values of the interstitial and vacancy concentrations are each about 2%. The radiation-produced scattering disappears almost completely after an anneal at 1100°C for 1 hr, whereas at intermediate temperatures the shape of the scattering curve is identical to that obtained in the as-irradiated condition. This suggests that the predominant annealing mechanism in this temperature range is not the free migration of particular sizes of small interstitial clusters.

Thin films of metastable amorphous germanium (700 ± 100 A thick), prepared by evaporation on rock salt, were bombarded with either fast neutrons or monoenergetic Xe^+ ions at room temperature.[79] Subsequent examination by bright- and dark-field transmission electron microscopy revealed that small discrete crystallized regions (ranging up to several hundred angstroms in size) were produced throughout the amorphous matrix by the irradiation. The fast-neutron irradiation resulted in a linear increase in the density of crystallized regions with neutron doses ranging from 0 to 5.1×10^{16} neutrons/cm^2 and a most probable crystallized region size of 190 A. The monoenergetic Xe^+-ion bombardment (covering a range of incident energies) resulted in a most probable crystallized region size very closely equal to the calculated ion range for incident-ion energies from 40 to 90 kev. Also a low (<40 kev) and a high ($\geq$ 140 kev) Xe^+-ion energy cutoff for the production of crystallized regions were observed. Other furnace-annealing experiments with similar amorphous films showed that they crystallized completely near 400°C as a result of ordinary homogeneous heating. The results were explained on the basis of "displacement spike crystallization," where the concentration of kinetic energy in the displacement cascade region was capable of inducing crystallization of the amorphous structure. Experimental evidence was presented which indicated that the crystallization was confined to the displacement cascade region and therefore required the intense atomic agitation characteristic of the early stages of a displacement spike.

(T. G. Knorr)

Theories of Radiation Effects

The migration energies and atomic configurations for monointerstitials and diinterstitials and monovacancies and divacancies in alpha iron have been calculated using a classical model.[80] About 530 atoms surrounding the defect were treated as individual particles, each with three degrees of freedom, and the remainder of the crystal was treated as an elastic continuum with atoms embedded in it. A two-body central force was devised which matched the elastic moduli, was sharply repulsive at close separation, and went to zero midway between the second and third neighboring atoms. Configurations were found by choosing a starting configuration roughly approximating the situation under consideration and successively adjusting the value of each variable occurring in the energy equation so that the magnitude of the generalized force associated with it was zero until equilibrium was reached. The energy calculations include changes in bond energy in the discrete region, energy in the elastic field, and work done against cohesive forces; however, changes due to the redistribution of electrons are neglected. Calculated activation energies for the motion of monointerstitials and diinterstitials and monovacancies and divacancies were 0.33, 0.18, 0.68, and 0.66 ev, respectively, and binding energies of diinterstitials and divacancies were 1.08 and 0.20 ev, respectively. The stable interstitial was a "split" configuration in which two atoms were symmetrically spiit in a (1 1 0) direction about a vacant normal lattice site, and the stable diinterstitial consisted of two parallel split interstitials at nearest neighbor lattice sites with their axes perpendicular to the line joining their centers. In the vacancy configuration an atom was missing from a normal lattice site, and the divacancy consisted of two vacancies at second nearest neighbor lattice sites.

The displacement efficiency $K(E)$ for damage production by energetic iron atoms in alpha iron was computed by simulating complete elastic collision cascades in a bcc atomic array on a high-speed computer.[81] Energies in the range $0.1 < E < 30$ kev were considered. Above 1 kev, $K(E)$ decreased monotonically as a consequence of progressively more frequent knock-on channeling. The extrapolated $K(E)$ value at 50 kev is 0.6 that at 1 kev. Damage production by primary knock-ons per se was attenuated by quasi channeling. Pure channeling was observed only for higher order knock-ons. For reactor irradiation the computed $K(E)$ leads to an overall damage reduction of 35% relative to that predicted by simple cascade theory. This indicates that ignoring channeling effects (crystal structure) in simple cascade theory is not totally responsible for its overestimation of damage production by at least a factor of 2.

Adamovich[82] points out that knowledge of the fast-neutron flux is not sufficient per se to determine radiation-induced damage in metals. The number of point defects was previously used as an indicator of the dose, but these defects are not sufficient because they do not affect most of the important physical and mechanical properties. Therefore an attempt was made to estimate the effectiveness of the radiation on the basis of changes of these properties, including yield strength, tensile strength, or elongation. From considerations advanced by J. Brinkman [*J. Appl. Phys.*, 25: 961 (1954); *Am. J. Phys.*, 24: 246 (1956)], it is shown that, since the displacement of the peaks and the accumulation of vacancies created by fast neutrons equal the number of knocked-out atoms, which have an energy E_l higher than a certain threshold value, for displacement peaks $E_l = 400$ ev. To accumulate vacancies, set $E_l = 6E_d$, where E_d designates the energy required for the displacement. If the energy of the atom is less than $6E_d$, only single or double vacancies are created. A formula was derived for determining the number of primary knocked-out atoms having an energy higher than E_l. The formula dose not allow the determination of the number of complex defects at high radiation dose levels because absorption starts at 10^{20} neutrons/cm^2. The point defects do affect markedly certain properties, such as electrical resistivity, modulus of elasticity, and diffusion.

General Electric workers[83] have extended their machine calculations to consider saturation effects (overlap damage zones from multiple primaries) in displacement spikes produced by primary knock-on atoms. One reason for the experiment was an attempt to correlate theories of radiation hardening. The general results of the calculation for 5-kev iron primaries in iron indicate: (1) the number of displacements produced by each succeeding primary in a multiple-pass calculation was less than that produced in the single-pass calcula-

tion, (2) the minimum separation distance between mobile defects in a multiple-pass damage state was less (about 20%) than that in a single-pass damage state, (3) the relative number of monovacancies in a multiple-pass damage-state region was smaller than that in a single-pass region, and (4) the largest vacancy-cluster size observed increased in proportion to the number of passes.

A binary collision simulation of the radiation-damage problem has been proposed.[84] Energy thresholds and parameter adjustment are discussed. Preliminary results show strong focusing in the (1 1 0) direction and weaker focusing in the (1 0 0) direction. Although not complete, the model is expected, with suggested modifications, to adequately represent the radiation-damage problem. (T. G. Knorr)

Surveys on Radiation-Induced Defects

A theoretical review has been presented[85] which discusses the effect of irradiation on the crystal lattice of metals and the means of direct and indirect investigation of irradiation effects by field ion microscopy, electron microscopy, low-angle X-ray scattering, and measurement of the Hall effect and electrical resistance, modulus of elasticity, and internal friction as affected by irradiation. Examples are given for zirconium, aluminum, copper, MnSi steel, CrNi-189 steel, lead alloys, and semiconductors such as germanium and graphite.

Dienes[86] has published a series of six lectures outlining the basic knowledge of point defects in metals and the current work designed to expand this knowledge. The subjects of the lectures are: general theory, physical properties and point defects, concentration of point defects in metallic crystals, annealing theory, annealing experiments, and diffusion with external generation of defects.

The dimensional, mechanical, and thermal effects of reactor irradiation of beryllium oxide have been collected.[87] Gas production by transmutation and its role in these changes are considered. A state-of-knowledge summary is presented.

Radiation-induced phase transformations have been discussed[88] for heteropolar and homopolar compounds, metals, and alloys. Point defects and displacement spikes due to irradiation are also considered. (T. G. Knorr)

Radiation Effects on Mechanical Properties

The effect of periodic in-service annealing for the relief of radiation-induced embrittlement of pressure-vessel steels is being investigated by the Naval Research Laboratory.[89] Three steels, types A-350-LFI (modified), A-212B, and A-302B, have been irradiated under special conditions and tested subsequently to determine their notch-ductility characteristics. Type A-350-LFI (modified) steel was irradiated at 430°F, whereas the A-212B and A-302B steels were irradiated at 550°F. The total exposure for all materials was approximately 3.4×10^{19} neutrons/cm^2 (>1 Mev). The study was designed to investigate the relative influence of frequent and infrequent annealing operations. The results for type A-350-LFI (modified) steel indicated a significant reduction, approximately 30%, in radiation-induced changes in the nil-ductility transition temperatures with frequent intermediate annealing at 600°F. A similar response to intermediate annealing at 750 and 800°F was found for the A-212B and A-302B steels. About a 40 to 45% improvement was observed.

A patent[90] has been issued for a radiation-resistant steel. It is indicated that small additions of a rare-earth element make steels suitable for use as reactor construction materials. However, no irradiation-effects data are presented to demonstrate this.

The Russians[91] have reviewed and analyzed the radiation-induced mechanical-property changes for low-carbon steels, low-alloyed steels, austenitic stainless steel, zirconium, and zirconium alloys. This analysis shows a pronounced dependence of properties on irradiation time and temperature.

Workers at General Electric[83] report that the creep-rupture properties of tungsten at 1100°C are increased considerably by an exposure of 8.2×10^{19} neutrons/cm^2 (>1 Mev), but there is no significant change in properties at an exposure of 1.6×10^{19} neutrons/cm^2 (>1 Mev). Tungsten–25 wt.% rhenium alloys similarly heat-treated did now show a significant difference in creep-rupture properties at 1100°C after irradiation to 3.7×10^{19} neutrons/cm^2 (>1 Mev).

Additional studies[83] have been made on the radiation effects in A-286, a precipitation-hardening stainless steel. Tensile specimens of A-286 were irradiated at 650°C to 3.5×10^{19} neutrons/cm^2 (>1 Mev) neutron flux. Part of

the specimens were shielded with cadmium, and the remainder were unshielded. Cadmium prevents the majority of the lower energy neutrons (<0.4 ev) from penetrating to the samples. Post-irradiation stress-rupture properties showed a significant difference between the shielded and unshielded samples. These data indicate that the reduction in rupture time after irradiation is related to a reaction involving the thermal flux. (F. R. Shober)

References

1. Westinghouse Electric Corp., Bettis Atomic Power Laboratory, Pressurized Water Reactor (PWR) Project, Technical Progress Report, October 24, 1963–January 23, 1964, USAEC Report WAPD-MRP-107.
2. Westinghouse Electric Corp., Bettis Atomic Power Laboratory, Pressurized Water Reactor (PWR) Project, Technical Progress Report, January 24–April 23, 1964, USAEC Report WAPD-MRP-108.
3. Knolls Atomic Power Laboratory, Reactor Technology Report No. 24, USAEC Report KAPL-2000-21, May 1964.
4. Hanford Atomic Products Operation, Research and Development Programs Executed for the Division of Reactor Development, Quarterly Progress Report, October–December 1963, USAEC Report HW-80284, April 1964.
5. Argonne National Laboratory, Reactor Development Program Progress Report, March 1964, USAEC Report ANL-6880, Apr. 15, 1964.
6. H. H. Klepfer and D. L. Douglass, The Factors Limiting the Utilization of Zirconium Alloys in Superheated Steam, USAEC Report CONF-187-36, General Electric Company, Vallecitos Atomic Laboratory, Nov. 20, 1963.
7. P. Baque, R. Dominget, and J. Bossard, Research on Zirconium Alloys Which Are Compatible with Carbon Dioxide Under Pressure Up to 600°C, *Energie Nucl.*, 6(2): 89-106 (March/April 1964).
8. P. Baque, R. Dominget, and J. Bossard, Research into Zirconium Alloys Resistant to Carbon Dioxide Under Pressure at Temperatures of Up to 600°C, French Report CEA-2393, 1963.
9. D. R. Dickinson and R. J. Lobsinger, Effect of Oxide Dissolution and Heat Transfer on the Corrosion of Aluminum Fuel Cladding, USAEC Report HW-77529, Hanford Atomic Products Operation, December 1963.
10. H. Spindler, Aluminum-Silicon Special Alloys with Good Corrosion Resistance Against High-Temperature Water, *J. Nucl. Mater.*, 11(2): 203-211 (February/March 1964).
11. G. T. Geering, S. Nakazato, and H. T. Watanabe, A 10,000-Hour Test of a Nitrogen- and Air-Cooled High-Temperature Fuel Element, USAEC Report AGN-TP-66, Aerojet-General Nucleonics.
12. Metals and Controls, Inc., Study of Ductile Coatings for the Oxidation Protection of Columbium and Molybdenum Alloys, Fourth Bimonthly Progress Report, January 1–February 29, 1964. Report AD-43441, Mar. 31, 1964.
13. Oak Ridge National Laboratory, May 6, 1964. (Unpublished)
14. F. S. Pettit and E. J. Felten, The Oxidation of Ni-ThO_2 Between 900 and 1400°C, *J. Electrochem. Soc.*, 111(2): 135-139 (February 1964).
15. Argonne National Laboratory, Annual Report for 1963, Metallurgy Division, USAEC Report ANL-6868.
16. M. E. Jones, The Solubilities of Ni-Cr-Fe Alloy 600 Corrosion Products, USAEC Report KAPL-3017, Knolls Atomic Power Laboratory, Feb. 10, 1964.
17. Atomic Energy of Canada Ltd., 1964. (Unpublished)
18. D. B. Warmuth and R. A. Jefferys, Design Study for Coated Columbium Alloys, Final Summary Technical Report to Bureau of Naval Weapons RRMA-232, Thompson Ramo Wooldridge, Inc., Apr. 1, 1964.
19. J. C. Wurst, The Evaluation of High Temperature Materials, Report ML-TDR-64-62, University of Dayton, March 1964.
20. J. C. Wurst, J. A. Cherry, and N. L. Hecht, The Evaluation of High-Temperature Materials, First Quarterly Progress Report, University of Dayton, January 1–March 31, 1964, Apr. 10, 1964.
21. J. Huminik, Jr. (Ed.), *High-Temperature Inorganic Coatings*, 310 pp., Reinhold Publishing Corp., 1963.
22. General Electric Company, Vallecitos Atomic Laboratory, Development of a Nuclear Thermionic Fuel Element, Annual Summary and Quarterly Progress Report No. 4, March 1–May 30, 1963, USAEC Report GESR-2017.
23. D. E. Smith, LCRE Valve Development, Final Report, USAEC Report PWAC-401(Pt. II), Pratt & Whitney Aircraft Division, May 4, 1964.
24. Atomics International, AEC Unclassified Program, Quarterly Technical Progress Report, January–March 1964, USAEC Report NAA-SR-9700, May 19, 1964.
25. Aerojet-General Nucleonics, Development of an Apparatus To Measure Biaxial Creep of Materials in Lithium, Report APL-TDR-64-73 (AGN Report AN-1175; AiResearch Report SY-5472-4), July 1964.
26. F. Tepper and J. S. Greer (Eds.), Factors Affecting the Compatibility of Liquid Cesium with Containment Metals, Report ASD-TDR-63-824 (Pt. I), MSA Research Corp., September 1963.
27. F. Tepper and J. S. Greer, Factors Affecting the Compatibility of Liquid Cesium and Containment Metals, Sixth Quarterly Progress Report, December 1963–February 1964, Report MSAR-64-27, MSA Research Corp., Mar. 16, 1964.

28. Argonne National Laboratory, Reactor Development Program Progress Report, May 1964, USAEC Report ANL-6904, June 15, 1964.
29. Argonne National Laboratory, Chemical Engineering Division Research Highlights, May 1963–April 1964, USAEC Report ANL-6875.
30. T. K. Roche, The Effect of Degree of Vacuum on the Slow-Bend Creep Behavior of Columbium–0.6 Wt.% Zirconium at 1000°C, USAEC Report ORNL-3569, Oak Ridge National Laboratory, June 1964; also USAEC Report CONF-373-10, December 1963.
31. E. S. Bartlett and F. F. Schmidt, Review of Recent Developments in the Technology of Columbium and Tantalum, Battelle Memorial Institute, Defense Metals Information Center, Jan. 10, 1964.
32. P. Guyot, Study of the Plastic Deformation Mechanisms of SAP, Report CONF-167-4, Joint Nuclear Research Center, Ispra, Italy, 1964.
33. G. Beghi, G. Piatti, and D. Quataert, Structural Changes in Alumina in Molten SAP, Report CONF-425-1, Joint Nuclear Research Center, Ispra, Italy, 1964.
34. C. A. Luke, R. Taggert, and D. H. Polonis, The Metastable Constitution of Quenched Titanium and Zirconium-Base Binary Alloys, *Trans. Am. Soc. Metals*, 57: 142-149 (March 1964).
35. J. O. Stiegler, J. T. Houston, and M. L. Picklesimer, Transmission Electron Microscopy of Omega Phase in a Zr–15% Nb Alloy, *J. Nucl. Mater.*, 2(1): 32-40 (January 1964).
36. D. N. Williams, R. A. Wood, R. I. Jaffee, and H. R. Ogden, The Effects of Zirconium in Titanium-Base Alloys, *J. Less-Common Metals*, 6: 219-225 (March 1964).
37. V. V. Glazova and N. N. Kurnakov, Temperature Effects on Hardness of Titanium-Zirconium Alloys, *Izv. Akad. Nauk SSSR, Otd. Tekhn. Nauk, Met i Gorn. Delo*, 6: 152-154 (November/December 1963).
38. Atomics International, Annual Technical Progress Report, AEC Unclassified Programs, Fiscal Year 1963, USAEC Report NAA-SR-8888, Apr. 1, 1964.
39. D. Weinstein and F. C. Holtz, Susceptibility of Zirconium and Zirconium Alloys to Delayed Failure Hydrogen Embrittlement, *Trans. Am. Soc. Metals*, 57: 284-293 (March 1964).
40. A. Fourdeux and A. Wronski, Some Observations of the Deformation Mechanisms of Niobium, *J. Less-Common Metals*, 6: 11-20 (January 1964).
41. H. R. Ogden, F. F. Schmidt, and E. S. Bartlett, The Effects of Carbides on Mechanical Properties of Tantalum, *Rev. Metal Lit.*, 21(2): (February 1964).
42. L. F. Pease and J. H. Brophy, The Zirconium-Tungsten-Tantalum System, *J. Less-Common Metals*, 6: 118-131 (February 1964).
43. E. Anderson, The Equilibrium Diagram of the System Molybdenum-Palladium, *J. Less-Common Metals*, 6: 81-84 (January 1964).
44. S. Arajs, H. Chessin, and R. V. Colvin, Lattice Parameters and Paramagnetic Susceptibility of Nickel-Rich Nickel-Niobium Solid Solutions, *Phys. Status Solidi*, 3: 2337-2346 (1963).
45. J. H. Day, Grain Boundary Cracking in a Magnesium-Zirconium Alloy, *J. Nucl. Mater.*, 11(2): 249-251 (February/March 1964).
46. Effects of Tensile Forces on Aging Processes in Beryllium Bronze, *Fiz. Metal. i Metalloved.*, 16: 366-369 (September 1963).
47. L. E. Toth and A. W. Searcy, Prediction of Activation Energies for Self-Diffusion in Metals, USAEC Report UCRL-10581, University of California, Lawrence Radiation Laboratory, Mar. 5, 1963.
48. R. A. Wolfe and H. W. Paxton, Diffusion in BCC Metals, Report NP-13738(AD-434751), Carnegie Institute of Technology, Mar. 1, 1964.
49. E. Gebhardt and K. Kirner, Diffusion Investigations in the Niobium-Tungsten System for Polycrystal, Single Crystal, and Spray Couples. II. Single-Crystal Couples (in German), *Z. Metallk.*, 54: 698-704 (December 1963).
50. J. E. Harris and R. O. Jones, Directional Diffusion in Magnesium Alloys, *J. Nucl. Mater.*, 10(4): 360-362 (December 1963).
51. S. D. Gertsriken and I. Ya. Dekhtyar, Solid State Diffusion in Metals and Alloys, USAEC Translation AEC-tr-6313, 1960.
52. S. J. Grisaffe and W. A. Spitzig, As-Plasma-Sprayed Diffusion Bonding Between Tungsten and Cool Stainless-Steel Substrates, Technical Reprint, NASA Lewis TR-22-63, NASA Lewis Research Center, January 1964.
53. S. J. Schneider, Compilation of the Melting Points of the Metal Oxides, Report NBS-MON-68, National Bureau of Standards, Oct. 10, 1963.
54. N. M. Parikh, Factors Affecting the Brittle Behavior of Ceramic Oxides, paper presented at the 1964 Golden Gate Metals Conference; published in *Materials Science and Technology for Advanced Application*, Vol. II, American Society for Metals, Golden Gate Chapter, Berkeley, Calif., February 1964.
55. R. J. Stokes, Thermal-Mechanical History and the Strength of Magnesium Oxide Single Crystals. I. Mechanical Tests, Report HR-64-258, Honeywell Research Center, March 1964.
56. R. B. Day and R. J. Stokes, The Mechanical Behavior of Magnesium Oxide at High Temperatures, Report HR-64-253(AD-431615), Honeywell Research Center, January 1964.
57. H. Conrad, Mechanical Behavior of Sapphire, Aerospace Corp., Mar. 23, 1964.
58. W. S. Williams, Influence of Temperature, Strain Rate, Surface Conditions, and Composition on the Plasticity of Transition-Metal Carbide Crystals, *J. Appl. Phys.*, 35: 1329-1338 (April 1964).
59. R. E. Taylor and J. Morreale, Thermal Conductivity of Titanium Carbide, Zirconium Carbide, and

Titanium Nitride at High Temperatures, *J. Am. Ceram. Soc.*, 47: 69-73 (Feb. 21, 1964).

60. K. I. Portnoi and Yu. V. Levinskii, Interaction in System Refractory Metal-C-N, *Issled. Splavov Tsvetn. Metal. Akad. Nauk SSSR, Inst. Met.*, 4: 279-285 (1963).
61. H. Schumann, Ceramic Structural Materials for the Absorption of Gamma Rays and Neutrons, *Ber. Deut. Keram. Ges.*, 40: 113-117 (February 1963).
62. R. P. Levey, Jr., A Survey of High-Compressive-Strength Oxides and Carbides, USAEC Report Y-1450, Union Carbide Corp., Nuclear Division, Sept. 26, 1963.
63. H. Jaeger, The Relaxation of the Initial Susceptibility and Its Recovery in Nickel, Investigated Using Polycrystalline Specimens After Deformation, Quenching, and Neutron Irradiation, *Z. Metallk.*, 55: 17-29 (January 1964).
64. F. Bell and O. Krisement, The Recovery of Iron After Cold Working or Neutron Irradiation Between 20 and 450°C, *Phys. Status Solidi*, 3: 2241-2252 (1963).
65. B. Solly, Radiation-Induced Precipitation in Iron, Swedish Report AE-138, February 1964.
66. M. K. Sinha and E. W. Muller, Bombardment of Tungsten with 20 Kev Helium Atoms in a Field Ion Microscope, *J. Appl. Phys.*, 35: 1256-1261 (April 1964).
67. W. Schilling and W. Schmatz, Small-Angle Scattering of Neutron-Irradiated Copper, *Phys. Status Solidi*, 4: 95-101 (1964).
68. S. I. Taimuty and J. B. Swedlund, Barkhausen Effect in Irradiated Pure Iron and Nickel, Report NP-13771(AD-433849), Stanford Research Institute, Feb. 28, 1964.
69. F. E. Fujita and A. C. Damask, Kinetics of Carbon Precipitation in Irradiated Iron. II. Electrical Resistivity Measurements, *Acta Met.*, 12: 331-339 (April 1964).
70. R. A. Arndt and A. C. Damask, Kinetics of Carbon Precipitation in Irradiated Iron. III. Calorimetry, *Acta Met.*, 12: 341-345 (April 1964); also USAEC Report BNL-7069.
71. H. Wagenblast, F. E. Fujita, and A. C. Damask, Kinetics of Carbon Precipitation in Irradiated Iron. IV. Electron Microscope Observations, *Acta Met.*, 12: 347-353 (April 1964); also USAEC Report BNL-7070.
72. R. A. Johnson and A. C. Damask, Point Defect Configurations in Irradiated Iron-Carbon Alloys, *Acta Met.*, 12: 443-445 (April 1964); also USAEC Report BNL-7519.
73. A. Ascoli, M. G. Belloni, and G. T. Queirolo, Rehomogenization Kinetics of Irradiated-Segregated Copper-Nickel, *Phys. Letters*, 9(4): 305-306 (May 1, 1964).
74. M. C. Wittels, J. O. Stiegler, and F. A. Sherrill, An Investigation of Transmutation Effects in Crystalline Solids, *Phys. Status Solidi*, 4: 533 (1964).
75. T. J. Koppenaal, The Effect of Neutron Irradiation on the Strength of αCu-Al Single Crystals, *Acta Met.*, 12: 487 (May 1964).
76. R. M. J. Cotterill and T. J. Koppenaal, Effects of Type and Density of Defects on Yield Strength of Neutron-Irradiated Copper and Copper–14 At.% Aluminum Alloy, *Appl. Phys. Letters*, 4: 156-157 (Apr. 15, 1964).
77. H. Weik, Split Interstitial Configuration Induced in Perovskite Type Single Crystals by Neutron Bombardment, *Phys. Letters*, 9(2): 92-93 (Apr. 1, 1964).
78. D. G. Martin and R. W. Henson, The Scattering of Long Wavelength Neutrons by Defects in Neutron Irradiated Graphite, *Phil. Mag.*, 9: 659 (April 1964).
79. J. R. Parsons and R. W. Balluffi, Displacement Spike Crystallization of Amorphous Germanium During Irradiation, *J. Phys. Chem. Solids*, 25: 263-272 (1964).
80. R. A. Johnson, Interstitials and Vacancies in α-Iron, *Phys. Rev.*, 134: A1329 (June 1, 1964).
81. J. R. Beeler and D. G. Besco, Effects of Channeling on Damage Production in Iron, *Phys. Rev.*, 134: A530 (Apr. 20, 1964).
82. V. K. Adamovich, Estimation of the Neutron Radiation Dose Which Changes the Mechanical Properties of Pure Metals, *At. Energ. (USSR)*, 15: 430-432 (November 1963).
83. General Electric Company, Advanced Technology Services, High-Temperature Materials Program, Progress Report No. 35, Part A, USAEC Report GEMP-35A, May 28, 1964.
84. J. P. Bird and R. L. Kronz, Computer Programs for the Two-Body Approximation to the Radiation Damage Problem (thesis), Report AD-416313, Naval Postgraduate School, Monterey, Calif., 1963.
85. E. Schmid and K. Lintner, Irradiation Effects in Metals, *Radex Rundschau*, 4: 519-534 (1963).
86. G. J. Dienes, Point Defects in Metals, USAEC Report BNL-7623, Brookhaven National Laboratory, 1963.
87. F. J. P. Clarke, Irradiation Damage in Beryllium Oxide, *Progr. Nucl. Energy, Ser. IV*, 5: 221-248 (1963).
88. O. Hauser and M. Schenk, Radiation-Induced Phase Transformations, *Kernenergie*, 6: 655-667 (December 1963).
89. L. E. Steele, J. R. Hawthorne, and H. E. Watson, Irradiation Effects on Reactor Structural Materials, Report NRL-1534, Naval Research Laboratory, May 15, 1964.
90. H. J. Kirschung, Radiation Resistant Steel, U. S. Patent 3,119,687 (to Klockner-Werke A. G.), Jan. 28, 1964.
91. N. F. Pravdyuk and A. D. Amaeev, Some Regularities in the Change of Fundamental Mechanical Properties of Contractive Materials Under Neutron Irradiation (translation of Russian), Akademiya Nauk SSSR, Institut Atomoni Energii, 1962.

Section V

Reactor Materials

Special Fabrication Techniques

Melting, Casting, and Working

The conversion to 18-in.-wide sheet of the niobium–27 wt.% tantalum–10 wt.% tungsten–1 wt.% zirconium alloy (FS-85) has been completed by Fansteel.[1,2] The other alloy of interest, niobium–5 wt.% vanadium–5 wt.% molybdenum–1 wt.% zirconium (B-66), has proved less amenable to the fabrication techniques employed. The 6-in.-diameter FS-85 ingots were forged at 1290°C, surface conditioned, wrapped in tantalum foil, and vacuum annealed for 1 hr at 1475°C. After they were annealed, the $1\frac{3}{8}$-in.-thick slabs were rolled at 370°C in air to $\frac{3}{8}$-in.-thick slabs. These slabs were then annealed and cold rolled to 0.060-in.-thick sheet. The sheet exhibited an as-rolled hardness of 272 DPH. An anneal in vacuum at 1300°C for 1 hr yielded 100% recrystallized sheet material, with a DPH of 190. An attempt to forge the B-66 alloy was unsuccessful; therefore the ingots were extruded to sheet bar by Du Pont at their Baltimore facility. An extrusion temperature of 1430 to 1460°C and a reduction ratio of 2.51:1 were employed. The resulting sheet bar was of very poor quality, requiring heavy conditioning prior to further processing. An evaluation of the FS-85 sheet and further processing of the B-66 sheet bar is in progress at Fansteel.

The extrusion of the molybdenum-base alloy tubes used in a study of refractory-alloy sheet materials has been accomplished at Climax Molybdenum.[3] The 4-in.-diameter vacuum arc-cast ingots were extruded at temperatures of 1425 to 1540°C, with reduction ratios of 4 to 1. The as-cast material had massive carbide inclusions in the grain boundaries and acicular carbides within the grains. A redistribution of these carbides might be expected as a result of further fabrication to sheet and the concomitant heat-treatments.

The fabrication of tungsten and tungsten-base alloys is being investigated at numerous sites. Thompson Ramo Wooldridge[4] has reported a yield of 98% in their forging studies on thin sections of tungsten. The billets employed in the study were cast and extruded by Climax Molybdenum. Upset forging of stress-relieved extrusions resulted in a nonuniform worked structure and in a larger grain size than that exhibited by recrystallized extrusions. The upset forging was accomplished at 1260 to 1290°C. The closed-die forging and coining that followed the upset forging was done at 1200°C. Nuclear Metals[5,6] continued their extrusion studies on both unalloyed tungsten and the tungsten-rhenium alloys. As reported previously, the tungsten was extruded successfully at 1200°C, and the tungsten–25 wt.% rhenium alloy, at 1800°C. Further reduction of the tube blanks was accomplished by drawing. The drawing constant for the alloy appeared to be 2 to 3 times that required for similar tungsten draws.

Melting and fabrication of tungsten-base alloys are being investigated at Wah Chang[7] and Westinghouse.[8] Wah Chang produced $9\frac{1}{2}$-in.-diameter ingots of tantalum–30 wt.% niobium–7.5 wt.% vanadium by master alloying the tantalum and niobium and then consumably melting this master alloy with the vanadium. Electron-beam melting of the alloy resulted in a reduction of the vanadium content on the order of 93%, whereas attempts to prepare the alloy without master alloying resulted in segregation in the ingot. The program in progress at Westinghouse Astronuclear[8] is concerned with the development of alloys for use in the 1315 to 1650°C temperature range. The alloy is to be developed primarily from the tantalum-tungsten-hafnium-carbon system, with limited substitution or

addition of rhenium and molybdenum, zirconium, and nitrogen for tungsten, hafnium, and carbon, respectively. The 800-g button castings exhibited an as-cast structure cored in the outer portions and essentially homogeneous in the center. These buttons were forged at 1250 to 1490°C. Alloys selected for further study were prepared in the form of 2-in.-diameter ingots by double consumable-electrode arc melting. All the ingots except those containing zirconium exhibited the typical columnar structure usually obtained with this melting technique. The zirconium-containing ingot exhibited obvious grain refinement.

The effects of aluminum, iron, and silicon on the fabrication behavior of uranium are of interest.[9,10] National Lead Company of Ohio has reported that billet temperature and the levels of carbon, iron, and silicon all caused significant differences in either the amount of recrystallization of the alpha-rolled rods or in the grain size of the β-heat-treated fuel cores. High iron, high silicon, high carbon, and low rolling temperatures reduced the grain size of the β-heat-treated cores. It was also noted that chemistry had more influence than rolling temperature on the grain size of finished fuel cores. Battelle has been conducting rolling studies in conjunction with the studies at National Lead. These studies indicate that the β-heat-treated uranium is easier to fabricate than as-extruded material and that the additions of iron, silicon, and aluminum tend to increase the difficulty of fabrication. It was also noted that, whereas thin-walled tubes tend to thicken, the wall thickness of thick-walled tubes was relatively unaffected by rolling.

Fabricability of the uranium–14 wt.% molybdenum alloy for blanket rod stock is being investigated at Argonne.[11] The erratic fabrication behavior of the as-cast material was attributed to the large dendrites noted in the ingots. Heat-treatment studies showed that an anneal of 20 hr at 1000°C produces homogeneous single-phase material and should overcome this problem. Argonne also reported the successful casting by injection-molding techniques of various uranium-plutonium-fizzium alloys. A yield of 81.87% was obtained, utilizing a melt temperature of 1270 to 1375°C and a mold temperature of 100 to 260°C.

The APM alloys are being evaluated by Atomics International[12] for cladding UO_2 fuel and for process tubes. Both conventional extrusion and impact extrusion have been shown to be capable of producing satisfactory 14-fin tubes. A magnetic pulse-forming process has been used to lock the end plugs mechanically in the fuel tubes prior to closure. Magnetic pulse swaging of finned APM-clad UO_2 fuel rods was found to be suitable for producing intimate contact between fuel and cladding. However, this process was unsuccessful in applying the cladding with a 1- to 2-mil annular gap in selected regions where a thermal barrier was desired.

(N. E. Daniel)

Cladding

Rolling, Swaging, and Coextrusion

A hot-extrusion technique for producing stainless-steel-clad UO_2 fuel elements was developed at Nuclear Metals.[13] It utilizes the concept that UO_2 can be hot extruded in a manner analogous to that for metals. The process, based on the multitemperature coextrusion technique, involves the coextrusion of UO_2 at 1875°C within the cladding at 760°C. The coextrusion of a low-carbon steel can over the cladding is required to prevent its melting and to exert a high isostatic pressure on the ceramic core. Any type of UO_2 material of reasonable purity can be used, and refractory metals such as molybdenum or tantalum can be coextruded with UO_2.

Belgian investigators[14] carried out a study on the use of plutonium as a fuel in water reactors. Fuel fabrication methods employed were densification by vibration and vibration swaging. High-density UO_2-PuO_2 fuel elements were produced by defining different powder granulations. Elements measuring 150 cm in length, 8.7 mm in diameter, and having a cladding thickness of 0.5 mm employed size fractions of 60 wt.% −7 +8 mesh, 25 wt.% −70 +80 mesh, and 15 wt.% −400 mesh. PuO_2 was incorporated in the fine fraction of the mixture, eliminating recycling of the PuO_2. Densities of 86 to 90% of theoretical, varying from 2 to 3% longitudinally, were produced. The distribution homogeneity of the PuO_2 was investigated, and it was determined that it is related to the frequency of the system used for vibration, the dimensional range of the powder particles, and the loading system of the tubes. The authors concluded that calcination in the preparation of a completely homogeneous powder mixture was not significant. Additional studies

were carried out on the transverse distribution of PuO_2 in vibrated fuel rods and on the distribution in vibrated, cold-swaged fuel.

Vibratory compaction has been employed at Argonne[11] to fabricate irradiation test specimens of solid-solution uranium-plutonium carbides. Twenty 5-cm-long specimens 0.366 cm, 0.4 cm, and 0.65 cm in diameter were compacted. A density of 80% of theoretical was achieved by the use of three size fractions in the following proportions: 60 wt.% coarse, 20 wt.% medium, and 20 wt.% fine. For the 0.4-cm-ID tubes, the ratio was 60 wt.% −20 +60 mesh, 20 wt.% −120 +120 mesh, and 20 wt.% −320 mesh.

Codrawing and coextrusion were investigated[11] as fabrication methods for a duplex tube consisting of stainless steel or Hastelloy X on the exterior of a refractory-metal tube (or liner). A vanadium rod canned in type 304 stainless steel was extruded at 1200°C. A hole was drilled in the vanadium core to form a duplex tube, 1.268 cm in outside diameter and 0.873 cm in inside diameter. After the tube was ironed on a nondeformable mandrel, vacuum annealed at 850°C, ironed again, reannealed, and a ductile copper core inserted, the duplex tube was finished to a final size of 0.442 cm in inside diameter and 0.047 cm in wall thickness. (R. J. Diersing)

Pressure Bonding

Beryllium armor was gas-pressure bonded to tubular liners to provide composite hypervelocity impact targets measuring 1.220 in. in diameter by 6 in. in length.[15] Liners of type 316 stainless steel and a niobium−1 wt.% zirconium alloy were employed in this work. The beryllium for these composites consisted of either QMV-grade beryllium powder hydrostatically pressed in place or extruded beryllium tubing. Bonding conditions of 1400°F and 10,000 psi for 1 hr were used to densify and bond the assemblies. After the mild-steel jacketing material was removed by pickling, the targets were machined to final size. Although bonding parameters were not optimized and the character of the bonds was not established in this effort, the fabrication of the beryllium-clad targets appeared successful. (S. W. Porembka)

Canning

A purely mathematical method to predict achievable densities of vibratory-compacted spherical shapes is reported by Argonne.[11] The relation between void packing efficiency, P_f, and the diameter ratios is given for single-, binary-, and ternary-component packing. The packing efficiency of a single-component system is given by the equation

$$P_f = 0.635 - 0.216\, e^{-0.313 D/d_1}$$

where D/d_1 is the ratio of the diameter of the container, D, to the diameter of the first component spheres, d_1. The value of 0.635 in the relation above is the limiting value to which the spherical bodies will fill a void space.

The relation between P_f and d_1/d_2, the ratio of diameter of the first component to the second component, is given as follows:

$$P_f = 0.635 - 0.737 e^{-0.201 d_1/d_2}$$

The total packing efficiency, P_e, of any multicomponent system of spheres as a function of diameter ratios is

$$P_e = 0.867 - 0.079 e^{-0.313 D/d_1} - 0.269 e^{-0.201 d_1/d_2} - 0.159 e^{-0.313 D/d_1 - 0.201 d_1/d_2}$$

with the value of 0.867 being the limited density for a binary system.

The void packing efficiency for the ternary system is given by

$$P_f = 0.951 - 0.029 e^{-0.313 D/d_1} - 0.098 (e^{-0.201 d_1/d_2} + e^{-0.201 d_2/d_3}) - 0.198 e^{-0.201 [(d_1/d_2)+(d_2/d_3)]}$$

where 0.951 is the ternary-system limiting density.

The packing efficiency of vibratory-compacted irregularly shaped particles of one size classification is reported by Argonne[16] to be proportional to the particle size down to diameters of 0.25 mm. The function is of the form

$$P_e = A + (K/d_1)$$

where A is the limiting density, d_1 is the diameter of the single size classification, and K is a constant. The above relation was found for the region where the boundary condition is negligible. In the binary system of irregular shapes, P_e as a function of d_1/d_2, the ratio of diameter

of the first component to the diameter of the second component, was found to be of the same shape as that for a spherical system.

Following the installation of a 5000-lb-force vibrator unit at Hanford,[17] fuel-rod fabrication for the Experimental Boiling-Water Reactor was successfully initiated. To date more than 300 fuel rods containing UO_2-PuO_2 of 86 to 89% of theoretical density have been fabricated with this unit; 850 kg of UO_2–1.5 wt.% PuO_2, with a density of over 98% of theoretical, was produced by blending fused depleted UO_2 (–65 mesh) with PuO_2 (–325 mesh) and pneumatically impacting at 1180°C.

Bulk densities of compacted ThO_2 particles in excess of 88% of theoretical are reported by Oak Ridge.[18] The densities were achieved in 8-ft-long ¾-in.-diameter stainless-steel tubes by using the floating-anvil principle.

A recent U. S. patent[19] describes a process that permits cladding of reactor fuel elements without variation in sheath thickness during forming. Parallel rods are spaced between metal sheets and are held in place by a plastic, relatively incompressible substance disposed between the rods within the sheets. The metal sheets are compressed around the rods with lateral displacement during sheath formation.

A German patent[20] describes the following steps for encasing a nuclear fuel element in a sheath of sintered material: (1) insertion of a concavely shaped plug into the open end of the sheath; (2) welding of the sheath, the inserted plug, and the convexly shaped counter plug simultaneously; and (3) removal of the counter plug by machining. (V. D. Linse)

Electroplating

Electroplating and electroforming of refractory metals is possible by a proprietary process developed by Union Carbide.[21,22] Niobium has been electroformed on a copper mandrel in fused salts heated to 1400°F. Wall thickness has been built up to ¼ in., and densities were reported to be 99.9% or more of theoretical. Electroforming of niobium and tantalum is offered commercially. Tungsten, molybdenum, vanadium, zirconium, and hafnium may be deposited from the fused-fluoride-salt bath, but some development work might be required before the process could be considered commercial.

A deposit of thorium dioxide[23] was obtained on aluminum plates by electrolyzing thorium from a solution of ethanol (8 to 10 mg thorium/100 ml C_2H_5OH) at a current of about 3 ma/cm^2, and heating of the deposits to 500 to 550°C for 1 hr transformed the deposits to white ThO_2.

A laboratory method of stripping nickel from and replating of nickel on uranium was reported by Dow Chemical personnel[24] to produce smooth, adherent, dense deposits. The preferred method includes chemically dissolving the old nickel in a solution of 20 g of $Ni(NO_3)_2 \cdot 6H_2O$ and 20 g of $Hg(NO_3)_2 \cdot H_2$ in 250 ml of HNO_3, 250 ml of H_2SO_4, and 500 ml of H_2O, rinsing, anodic cleaning, rinsing, and replating with fresh nickel. The process was said to be (1) safe, because uranium salts do not build up from uncontrolled dissolution, (2) quick, from 4 to 10 mm required, and (3) satisfactory, because the plate is continuous and firmly bonded to the uranium. (G. R. Schaer)

Nonelectrolytic Chemical Plating

Equipment was developed[25] for depositing and for evaluating tungsten prepared by hydrogen reduction of WF_6. The density of the material varied from 18.90 to 19.20 g/cm^3, compared with the theoretical value of 19.3 g/cm^3. Resistivity appears to be about 5.5 μohm-cm, in agreement with published values on bulk material. Tensile-property values were presented[26] for annealed pyrolytic tungsten over the temperature range 1370 to 2980°C in vacuum.

Joining and seaming of fibrous materials (for example, woven-metal screen) were described.[27] The deposit resembles a weld nugget and is formed at temperatures well below those deleterious to the substrate. Thin sheets (lamellae) of chromium can be formed by chemical vapor deposition on a molten substrate.[28] The substrate must possess a boiling point higher than the decomposition temperature of the metal-organic compound used as the source of chromium and must also be chemically inert and nonwetting to chromium metal.

Various properties of bulk pyrolytic graphite were evaluated. It was learned, for example,[29] that deposition temperature significantly alters both the magnitude and temperature dependence of the thermal conductivity of this material. Fast-neutron irradiation[30] at about 20°C (10^{18} neutrons/cm^2) reduces the a-axis electrical conductivity of recrystallized pyrolytic graphite by a ratio of 3:1 and reduces the elec-

trical conductivity in the *c* direction by a ratio of 5 : 2.

High-purity metal oxides can be prepared in finely divided form by chemical vapor deposition employing vapor-phase hydrolysis of volatilized halides.[31] These include Al_2O_3, TiO_2, SiO_2, BeO, and ZrO_2. Filaments of boron, silicon carbide, and titanium carbide were deposited by chemical vapor deposition.[32] These usually are overlays on fine tungsten-wire substrates.

Much activity continued in the area of silicide type diffusion coatings for the protection of refractory metals and alloys against high-temperature oxidation. Coating is performed primarily by pack cementation[33] and by fluidized-bed chemical vapor deposition.[34] In evaluating coated specimens, it has been found[35] that degradation and accelerated attack by moving air at reduced pressure (0.01 to 1.0 torr), compared to air at 1 atm, take place for all coating systems investigated. In the case of silicide-coated molybdenum, the failure mechanism is described[36] as follows. At pressures below atmospheric, SiO(g) is more stable than SiO_2, and active oxidation and weight loss occur. The preferred oxidation of silicon instead of molybdenum depletes the surface silicon, and formation of lower silicides begins. The silicon content becomes so low that catastrophic oxidation of molybdenum is finally initiated.

The results of many studies of silicide type diffusion coatings for refractory metals and alloys continue to demonstrate that much remains to be done in this area to provide adequate protection under the extreme environments contemplated. The alloy-base materials most frequently studied are tantalum[37] and tungsten.[38,39] Although less satisfactory than the big four (molybdenum, niobium, tantalum, and tungsten) as a high-temperature structural material, vanadium[40,41] also is receiving attention for some applications.

Refractory metals can themselves be employed as coatings for special applications. Difficulty is experienced, however, in preparing coatings of such metals as tungsten on graphite. Unless a graphite with controlled thermal expansion is chosen for a substrate, vapor-deposited tungsten is highly prone to cracking. An investigation[42] was started to determine the effect of plating parameters on this tendency.

The behavior of chemically deposited (electroless) nickel on aluminum alloys was investigated[43] in high- and low-flow aqueous systems at 300 and 330°C. The effects of heat-treatment on corrosion properties of the nickel plate were studied. It was found that relatively thick nickel/aluminum diffusion layers suppressed catastrophic failure of 1245 aluminum alloy at 330°C.

(E. M. Sherwood)

Explosive Forming

A production technique utilizing explosive methods to form contoured honeycomb panels has been developed by the Martin Co.[44] The technique can be used with metallic or phenolic core materials having honeycomb, square, or multiwave cell shapes. The process involves bonding one faceplate to the honeycomb, filling the honeycomb with paraffin, attaching (not bonding) the other faceplate, explosively forming, removing the paraffin, and finally bonding the other faceplate. This method of forming is compared to more conventional methods and the advantages discussed.

Among the 18 metals and alloys tested at North American Aviation, in a program on the explosive formability of metals,[45] are 1100-0 aluminum, Inconel X, 4130 steel, and type 321 stainless steel. The testing method used involved clamping a circular blank of the metal to be investigated over a hemispherical cavity and impacting under water with a standoff explosive charge. The amount of deformation caused by this impact was measured and used as a relative measure of the formability of that metal. It was found that the formability of metals with similar crystal structure and process history can be approximately predicted from a single theoretical relation. Also investigated were the effects of two die design parameters: the radius of the draw plate and the pressure required to clamp the outer edge of the workpiece. The optimum "hold-down pressure" was found to vary with the material, being very slight for 1100-0 aluminum and rather large for type 321 stainless steel.

General Dynamics[46] has been investigating the explosive bonding of dissimilar metals. Successful bonds that have been produced include: K-Monel to type 321 stainless steel, an aluminum alloy to a copper alloy, and 6061 aluminum to itself. In addition, a semimechanical, semimetallurgical bond has been reported between 6061 aluminum and commercially pure titanium. Current work predicts the successful metal-

lurgical bonding of these two materials. In the method used, a sheet of PETN is employed as a contact charge, and there is a uniform clearance of 25 mils between the pieces to be joined. The requirement of a clearance angle of 1 to 15° is discounted, and the heat produced is not considered detrimental. The design advantages of explosive bonds are discussed.

Perfection of a technique for cladding carbon steel with Hastelloy or Stellite has recently been announced by Du Pont.[47] At present, the major application for these cladding steels is for chemical processing equipment; pressure vessels and heat-exchanger tube sheets have been successfully manufactured.

The current status of shock-wave research is discussed in a paper by Duvall.[48] An overview is given of the present accomplishments and achievements in this field. The shock-generation methods and measurement techniques in common use are described, as are some of the problems inherent in this type of work. Also discussed is the use of Rankine-Hugoniot curves to determine the transmission and propagation characteristics of shock waves in matter. The mutual interaction of shock waves and the transmitting medium is pointed out. Various sources of more detailed information are listed.

A translation[49] of a Russian paper describing work done at the Institute of Hydrodynamics discusses Soviet efforts at welding flat plates. The parameters required to weld various steel, copper, titanium, and aluminum alloys were studied by varying the thickness of the granular explosive, hexogen (trimethylene trinitramine, density 1.2 g/cm^3), the interfacial clearance, and the interfacial angle. Successful joints were produced with angles of 2 to 7°, a clearance of 2 mm, and a charge thickness of 5 to 20 mm. More powerful explosives, TNT and 50-50 fusions of TNT and hexagen, were also tested but were found to be too powerful and resulted in considerable specimen destruction. Also discussed were the physical requirements necessary for flat-plate explosive welding and the dynamics of the explosive-welding process.

The metallurgical bonding of tubular sections of tantalum–10 wt.% tungsten to 4330 steel by explosive techniques was the objective of a two-phase research program[50] conducted at Battelle. The initial phase was concerned with the feasibility of joining these two materials and the establishment of the basic process parameters required to achieve a bond. The second phase had as its goal the successful bonding of 24-in. lengths of tubular sections of 20-mil tantalum–10 wt.% tungsten alloy to 0.775-in.-thick (6.210-in.-OD) 4330 steel.

The variables investigated were explosive-charge density, initial interface clearance, and method of achieving the initial interface clearance. These tests were conducted in air and employed contact charges of EL 506 C sheet explosive. The results, which were evaluated by means of visual examination and metallography, showed that the best joints were obtained with a charge density of 5 g/sq in., clearances of 0.030 to 0.103 in., and clearance shims spaced $\frac{1}{4}$ in. apart, perpendicular to the direction of travel of the detonation front. (D. Laber)

Welding and Brazing

Refractory-metal joining continues to receive much of the attention of investigators in the welding field. Niobium and niobium alloys are the subject of most of this attention.

A final report[51] by Westinghouse investigators covers work directed toward the determination of the weldability of production-scale quantities of the niobium alloys B-66 (niobium–5 wt.% molybdenum–5 wt.% vanadium–1 wt.% zirconium) and FS-85 (niobium–27 wt.% tantalum–10 wt.% tungsten–1 wt.% zirconium). The base metal was 0.040- to 0.060-in.-thick 18-in.-wide sheet, fabricated from 300-lb ingots. Welds were made by the tungsten-arc process in a helium atmosphere. The results indicated that the as-welded ductility of FS-85 was superior to that of B-66. After the welded sheets were annealed, the longitudinal welds in B-66 had low elongations and ultimate strengths, but the transverse weld strength was satisfactory. High joint efficiencies were obtained in both testing directions for welded FS-85 up to annealing temperatures of 2500°F. The poor ductility of welds in B-66 was attributed to aging of the heat-affected zone during annealing.

General Electric[52] has been studying the structural stability of welds in niobium alloys B-66 and D-43 (niobium–10 wt.% tungsten–1 wt.% zirconium). Welding variables such as speed, voltage, and current are being evaluated to determine their effect on interdendritic spacing because of its relation to bend ductility and aging

kinetics. Tentatively the investigators have concluded that:

1. Interdendritic spacing is more dependent on welding-heat input and cooling rate than on alloy composition.
2. Bend-transition temperatures are dependent on welding speed. Fast welding gives lower transition temperatures.
3. Kinetics of aging are strongly influenced by interdendritic spacing and, consequently, by welding variables. Large spacings promote sluggish aging reaction.

A simple method of satisfactorily spot-welding refractory-metal alloys without using an inert atmosphere has been reported by researchers at the University of Pennsylvania.[53] An aqueous solution of potassium hydroxide is placed on the surfaces to be welded, and the weld is made before the surface dries. The technique is applicable, especially when welding molybdenum.

Investigators[54] have reported on the development of brazing filler metals for use to 930°C. The work was concentrated on the ternary-alloy systems titanium-zirconium-beryllium and zirconium-niobium-beryllium. Tests utilizing wettability, flowability, thermal cycling, aging, and shear as criteria showed that 48 wt.% zirconium–48 wt.% titanium–4 wt.% beryllium and 75 wt.% zirconium–19 wt.% niobium–6 wt.% beryllium alloys were particularly promising. Strength data published for these and some of the other alloys evaluated are tabulated in Table V-1.

At Knolls Laboratory[55] studies are under way to evaluate brazing filler metals for joining the nickel-chromium-iron Alloy 600 that is to be used in reactor-core applications. Initial results indicate that a nickel-germanium-chromium-palladium-copper (J-8900) alloy is best for a high-flux area and the gold-nickel eutectic alloy (Premabraz 130) is best for low-flux areas. The use of precious metals in areas of significant radiation would seem questionable.

Most available data are on the effect of brazing on the short-time properties of high-temperature alloys. Consequently investigators at NASA[56] made a study to determine the effect of brazing on the long-time properties of such alloys. Stress-rupture tests of brazed joints in L-605, A-286, and Inconel 700 were used. The brazing alloys were of the nickel-chromium-silicon-boron and nickel-chromium-silicon types. It was found that the thermal treatments required for brazing improve the stress-rupture life of L-605 but lower the life of A-286 and Inconel 700. The boron-bearing filler metal improves the stress-rupture strength of L-605 and Inconel 700 but decreases that of A-286. The boron strengthens by diffusing into the base metal. The boron-free filler metal was less harmful to A-286 than the boron-bearing alloy. (R. M. Evans)

Table V-1 ALLOY COMPOSITION, BRAZING TEMPERATURE, AND SHEAR-STRENGTH TEST RESULTS[54] OF REFRACTORY-METAL-BASE BRAZING ALLOYS FOR SERVICE TO 1700°F

Brazing alloy, wt.%	Brazing temp.		Shear strength,*† psi			
			Room temp.			
	°F	°C	As-brazed	Aged 100 hr at 1500°F (815°C)	1300°F (704°C)	2000°F (1093°C)
48 Ti–48 Zr–4 Be	1920	1049	33,300 (6)	24,500 (3)	13,600 (4)	Not tested
46 Ti–46 Zr–4 V–4 Be	1920	1049	27,800 (6)	32,500 (4)	13,775 (4)	Not tested
63 Ti–27 Fe–10 V	2375	1302	27,088 (6)	22,500 (4)	19,700 (4)	2230 (3)
68 Ti–28 V–4 Be	2280	1249	26,800 (6)	22,300 (4)	Not tested	700 (1)‡
63 Ti–27 Fe–10 Mo	2375	1302	24,900 (5)	19,500 (4)	16,500 (4)	475 (1)§
75 Zr–19 Cb–6 Be	1920	1049	24,000 (6)	24,800 (4)	19,000 (4)	Not tested
45 Ti–40 Zr–15 Fe	1920	1049	22,500 (3)	17,500 (4)	16,000 (4)	Not tested
60 Zr–25 V–15 Cb	2375	1302	21,500 (4)	12,400 (3)	11,910 (2)	3950 (3)
67 Zr–29 V–4 Fe	2375	1302	20,200 (5)	14,600 (3)	12,000 (2)	4400 (3)

*The room temperature and 1300°F shear tests were performed using pure niobium-base metal. The 2000°F shear tests were performed using the niobium alloy D-31 (niobium–10.8 wt.% titanium–10.6 wt.% molybdenum–0.13 wt.% carbon).

†Figures in parentheses indicate number of specimens tested.

‡Specimen tested required rebraze.

§Second specimen broke upon initiation of load.

Nondestructive Testing

Ultransonic Techniques

It may be possible in the near future to measure the temperature in the high-radiation environment of nuclear reactors by ultrasonic means. Aeroprojects[57] has conducted studies toward this end, based on the change in velocity of sound associated with a change in temperature in a metal. The theory is that two identical progressive waves propagating through identical transmission lines of equal temperature are in phase at all corresponding points. If a section of length l of only one rod is heated, the velocity decreases, causing the waves to be out of phase at corresponding points beyond the heated section. The phase angle ϕ between the traveling waves is given by the equation:

$$\phi = 2\pi f \left(\frac{1}{c} - \frac{1}{c_0}\right) l$$

where f = driving frequency, kcps
l = length of heated section, cm
c = velocity of sound in the heated section, cm/sec
c_0 = velocity of sound in the unheated section, cm/sec

The Aeroprojects' acoustic thermometer is a single rod driven at one end and terminated at the other in an acoustic absorber to minimize standing waves. The "cold leg" is a section between the driving transducer and a barium titanate pickup element placed between the driving transducer and the hot length. A second barium titanate pickup element is located on the opposite side of the hot length, and the section of rod between the first and second pickup elements is the "hot leg." This thermometer is still under development.

Hanford[58] has made use of ultrasonic techniques of measuring grain size to predict the outer zirconium-uranium interface roughness of NPR fuel elements. The smoothness of the zirconium surface on the extruded fuel element varies inversely with the size of grains near the surface of the billet.

The studies pertaining to ultrasonic boundary waves which have been conducted at Hanford[59–61] could lead into interesting basic research with very useful results. Boundary waves, which are similar to Rayleigh waves, are generated by ultrasound incident at the critical angles on interfaces between acoustically dissimilar media. In fact, these boundary waves may exist for all incident angles that exceed the critical angle for longitudinal waves in the solid. The existence of these boundary waves causes some unusual perturbations in the reflected waves. The Hanford researchers have been able to relate these effects, such as a lateral shifting of the reflected beam along the interface and a redistribution of energy across the reflected beam, to various physical conditions. For instance, these effects can be used to measure surface hydride in Zircaloy-2 in amounts as small as 300 ppm. They were also able to detect surface strains in brass and aluminum of about 300 μin./in. However, no effect was produced in stainless steel at strains of 500 μin./in.

Argonne[11,62] has an imaging technique in operation capable of inspecting clad fuels at 75 cm/min. They claim to detect routinely artificial edge defects 0.75 mm deep and 1.5 mm long, either moving or stationary. Nonuniform distribution of UO_2 can be detected by this technique in a moving specimen but not in a stationary specimen.

The system uses conventional ultrasonic techniques, with the test object far enough from the transmitter to avoid near-field nonuniformities. The detected signal is processed by conventional closed-circuit television methods, using 525 lines interlaced at 30 frames/sec.

The target is a 2-Mc piezoelectric plate. Quartz has been used, but most of the studies have been conducted with barium titanate targets with better resolution. Correlation between defect size and image size is poor below a defect size set by either the wavelength of the ultrasound or the thickness of the target, whichever is larger. For flaws larger than this lower limit, image size correlates well with defect size when the flaw and the detector are within approximately 4 cm of each other. At greater distances the image becomes larger and less sharp.

Best visual indications are obtained from flat samples angled at 15 to 20° from the perpendicular to the direction of propagation of the ultrasonic beam. (D. Ensminger)

NDT Techniques Other Than Ultrasonic

The pulsed electromagnetic test system under investigation at Argonne[63] for inspection of thin-

walled tubing has been reported to offer advantages of stability and resolution over sinusoidal equipment that is intended for parallel applications. Although other techniques offer greater inspecting speeds, the use of the mask-aperture system to restrict the field of view is reported to meet more critical reject levels than many higher speed systems. Details of design of the mask-aperture apparatus are presented, and typical detected flaws are described that are not generally detectable with X-ray or ultrasonic methods.

An interesting technique by which the effects of differences in thermal emissivity can be reduced, when making differential radiometric measurements, has been described[61] by investigators at Hanford. The method is employed during infrared inspection for nonbond. As heat is applied to the surface of a rotating specimen by means of a plasma jet, two radiometers are employed to view a given location and given area of the surface at different instants of time separated by a given time interval. When the first signal is compared with the second, their ratio, in principle, is independent of surface emissivity. The rate of cooling of the given inspected area is compared with that of other areas to detect nonbond in the presence of surface distortions. (A. F. Leatherman)

References

1. Fansteel Metallurgical Corporation, Columbium Alloy Sheet Rolling Program, Interim Report No. 3, July 7, 1963–September 6, 1963, Report AD-418992, Sept. 7, 1963.
2. H. L. Kohn and R. M. Curcio, Columbium Alloy Sheet Rolling Program, Interim Report No. 4, on Contract No. 63-0231-C, Fansteel Metallurgical Corporation, Nov. 7, 1963.
3. R. Q. Barr, P. R. Pfefferle, and M. Semchyshen, Studies of Refractory Alloy Sheet Materials. Quarterly Progress Report, March 15–June 15, 1963, Report AD-412904, Climax Molybdenum Co.
4. E. J. Breznyak, Tungsten Forging Development Program, Ninth Interim Progress Report, May 19, 1963–August 19, 1963, Report ASD-TR-7-797, Thompson Ramo Wooldridge Inc., August 1963.
5. Nuclear Metals, Inc., Fundamental and Applied Research and Development in Metallurgy, Progress Report, December 1963, USAEC Report NMI-2124, Feb. 28, 1964.
6. Nuclear Metals, Inc., Fundamental and Applied Research and Development in Metallurgy, Progress Report, January 1964, USAEC Report NMI-2125, Mar. 27, 1964.
7. M. D. McNabb and R. R. McFarlane, Tantalum Alloy Ingot Reliability and Sheet Rolling Development Program, Interim Report, April 25, 1962–June 30, 1963, Report IR-7-826 (III), Wah Chang Corporation.
8. R. W. Buckman, Jr., and R. T. Begley, Development of Dispersion-Strengthened Tantalum Base Alloy, Quarterly Progress Report No. 2, September 20–December 19, 1963, Report WANL-PR(Q)-002, Westinghouse Electric Corp., Astronuclear Laboratory, December 1963.
9. The National Lead Company of Ohio, Summary Technical Report for the Period, January 1–March 31, 1964, USAEC Report NLCO-905, Apr. 28, 1964.
10. E. G. Smith, Jr., Fabrication of Uranium and Uranium-Base Alloy Tubes and Rods. Final Report, USAEC Report BMI-X-294, Battelle Memorial Institute, June 9, 1964.
11. Argonne National Laboratory, Annual Report for 1963, Metallurgy Division, USAEC Report ANL-6868.
12. Atomics International, Annual Technical Progress Report, AEC Unclassified Programs, Fiscal Year 1963, USAEC Report NAA-SR-8888, Apr. 1, 1964.
13. J. Hunt and P. Loewenstein, The Hot Extrusion of UO_2 Fuel Elements, USAEC Report NMI-TJ-55, Nuclear Metals, Inc., Nov. 25, 1963.
14. E. Fossoul and E. Vanden Bemden, Vibration and Vibration-Swaging Fabrication of Nuclear Fuels Enriched in Plutonium for Water Reactors, USAEC Translation AEC-tr-6312, translated from paper presented at the Enlarged Colloquium Fuel Cycles for Power Reactors by the European AEC, Baden-Baden, Sept. 9–14, 1963.
15. R. J. Diersing, H. D. Hanes, and E. S. Hodge, Fabrication of Beryllium-Clad Tubular Hypervelocity Impact Targets by Gas-Pressure Bonding, Report NASA-CR-54058, Battelle Memorial Institute, Nov. 6, 1963.
16. Argonne National Laboratory, Reactor Development Program Progress Report, March 1964, USAEC Report ANL-6880, Apr. 15, 1964.
17. Hanford Atomic Products Operation, Ceramics Research and Development Operation Quarterly Report, October–December 1963, USAEC Report HW-76304A, Mar. 19, 1964. (Classified).
18. Oak Ridge National Laboratory, June 4, 1964. (Unpublished).
19. C. Beernaert, Processes for Sheathing the Fuel Elements of Nuclear Reactors, U. S. Patent 3,118,222 (to Commissariat à L'Énergie Atomique), Jan. 21, 1964.
20. J. A. Stohr and C. Bridoux, Method for Encasing Nuclear Fuel Elements, German Patent 1,159,105, Dec. 12, 1963.
21. Union Carbide Corporation, Electroforming Refractory Metals, *Iron Age*, 192: 158–59 (Oct. 10, 1963).
22. G. W. Mellors and W. Senderoff, Electrodeposi-

tion of Coherent Deposits of Refractory Metals, *Extended Abstracts of the Electrodeposition Division, The Electrochemical Society Fall Meeting*, 1: 12-13 (Sept. 30, 1963).

23. H. R. von Guten and W. Scherle, Electrodeposition of Thorium Oxide on Aluminum, Intern. *J. Appl. Radiation Isotopes*, 15: 167-168 (March 1964).
24. W. H. Roberts, A Method of Stripping and Replating Nickel Electroplated Uranium, USAEC Report RFP-342, Dow Chemical Co., Mar. 9, 1964.
25. J. Connor, and A. Brenner, Deposition of Tungsten by Reduction of the Hexafluoride with Hydrogen in the Vapor Phase, Quarterly Report for Period February 1–April 30, 1964, National Bureau of Standards, May 14, 1964.
26. J. Taylor and D. Boone, Tensile Properties of Pyrolytic Tungsten from 1370 to 2980 C in Vacuum, *J. Less-Common Metals*, 6(2): 157-164 (February 1964).
27. C. MacNeill, Gas-Plated, Fibrous Composites, paper presented at Eighth Meeting Refractory Composites Working Group, Ft. Worth, Texas, Jan. 14–16, 1964.
28. B. Miccioli, Production of Chromium Lamella on a Molten Supporting Vehicle, U. S. Patent 3,131,049 (to Union Carbide Corporation), Apr. 28, 1964.
29. J. Pappis and L. Hager, Thermal Conductivity of Pyrolytic Graphites, paper presented at American Ceramic Society 66th Annual Meeting, Apr. 18-23, 1964.
30. A. Ammar and D. Young, Electrical Conduction in Irradiated Pyrolytic Graphite, *Brit. J. Appl. Phys.*, 15(2): 131-141 (February 1964).
31. C. Stokes and G. Kistiakowsky, Method of Preparing Metallic Oxides by Hydrolysis of Metal Halides, U. S. Patent 3,130,008 (to Cabot Corporation), Apr. 21, 1964.
32. L. Davies and J. Withers, A Study of High Modulus, High Strength Filament Materials by Deposition Techniques, Bimonthly Progress Report No. 2, January 1–February 29, 1964, General Technologies Corp., Mar. 15, 1964; also Report AD-433501.
33. N. Tiner, Refractory Coatings, *Chem. Eng. Progr.*, 60(2): 56-58 (February 1964).
34. The Pfaudler Co., Investigation of Practical Techniques for Coating Refractory Metals, Quarterly Progress Report No. 3, November 1, 1963–January 31, 1964.
35. Lockheed Missiles and Space Co., Coatings for Refractory Materials in Aerospace Environments, Third Progress Report, December 1, 1963–February 29, 1964, April 2, 1964.
36. R. Bartlett and P. Gage, Investigation of Mechanisms for Oxidation Protection and Failure of Intermetallic Coatings for Refractory Metals, Seventh Quarterly Progress Report, Philco Research Laboratories, Apr. 15, 1964.
37. B. Ohnysty, A. Stetson, and J. Long, Development of Protective Coating for Tantalum Base Alloys, Quarterly Progress Report 3, December 1, 1963–February 29, 1964, Solar, Division of International Harvester Co., Mar. 20, 1964.
38. C. Dickinson, Protective Coatings for Tungsten at High Temperatures, paper presented at Eighth Meeting, Refractory Composites Working Group, Ft. Worth, Tex., Jan. 14–16, 1964.
39. Thompson Ramo Wooldridge Inc., Oxidation-Resistant High-Temperature Protective Coatings for Tungsten, Third Quarterly Progress Report, November 15, 1963–February 15, 1964.
40. Illinois Institute of Technology Research Institute, High-Temperature Oxidation Protective Coatings for Vanadium-Base Alloys, Bimonthly Report No. 2, December 1, 1963–January 31, 1964, Feb. 28, 1964.
41. Illinois Institute of Technology Research Institute, High-Temperature Oxidation Protective Coatings for Vanadium-Base Alloys, Bimonthly Report No. 3, February 1, 1964–March 31, 1964, May 1, 1964.
42. V. Nieberlein, Vapor-Deposited Tungsten Coatings on Graphite, paper presented at American Ceramic Society 66th Annual Meeting, Chicago, Ill., Apr. 18–23, 1964.
43. A. B. Johnson, Jr., Behavior of Chemical Nickel Plate on Aluminum Alloys in High-Temperature, Dynamic, Aqueous Systems, USAEC Report HW-81196, Hanford Atomic Products Operation, April 1964.
44. Anonymous, Fill It with Wax, Then Blast It, *Steel*, pp. 52-53 (Feb. 17, 1964).
45. E. E. Lockwood and J. Glyman, The Explosive Formability of Metals, Report SP 62-09, Creative Manufacturing Seminars, 1961–1962, American Society of Tool and Manufacturing Engineers.
46. W. C. Wilson, Explosive Bonding Gains Ground Through Simplified Setups, *Iron Age*, 189(22): 127-129 (May 31, 1962).
47. Anonymous, Hastelloy Alloys Bonded to Steel by New Explosive Process, *Haynes Alloys Digest*, 15(4): (April 1964).
48. G. E. Duvall, Shock Waves in Solids, *Intern. Sci. Technol.*, No. 16: 45-52 (April 1963).
49. V. S. Sedykh, A. A. Deribas, Ye. I. Bichenkov, and Yu. A. Trishin, Explosive Welding, NASA Technical Translation F 140 [translated from *Svarochno. Proizv.*, No. 5: 3-6 (1962)].
50. R. J. Carlson and C. C. Simons, Joining of Tubular Components of Ta-10W to 4330 Steel by Explosive Techniques, Final Report, Battelle Memorial Institute, Mar. 24, 1964.
51. R. A. Nadler, Processing and Evaluation of Pre-Production Quantities of Columbium Alloy Sheet, Final Report, N63-20341, Westinghouse Electric Corp., Jan. 20, 1964.
52. R. E. Yount, The Structural Stability of Welds in Columbium Alloys, Quarterly Progress Report No. 2, General Electric Company, Nov. 10, 1963.
53. A. P. Saunders, A Simple Technique for Spot

Welding Molybdenum, *J. Sci. Instr.*, 41: 112 (February 1964).

54. R. G. Gilliland, The Development of Refractory-Metal Brazing Alloys for Elevated-Temperature Service, paper presented at AIME Technical Conference on Applied Aspects of Refractory Metals, Los Angeles, California, Dec. 9–10, 1963, CONF-373-374, December 1963.
55. Knolls Atomic Power Laboratory, Reactor Technology Report No. 24–Metallurgy, USAEC Report KAPL-2000-21, May 1964.
56. J. S. Sinclair, and C. A. Gyorgak, Effect of Two Braze Coatings, Processing Variables, and Heat Treatments on 1200 F Stress-Rupture Strength of L-605, A-286, and Inconel 700 Sheet, Report NASA-TN-D-1880, NASA — Lewis Research Center, November 1963.
57. Aeroprojects, Inc., Applications of Ultrasonic Energy: Ultrasonic Instrumentation for Nuclear Applications, Bimonthly Progress Report No. 14, December 1, 1963–January 31, 1964, USAEC Report NYO-2910-2, February 1964.
58. G. L. Waldkoetter, Ultrasonic Inspection of Uranium Billets to Predict Coextrusion Performance, USAEC Report HW-70821, Hanford Atomic Products Operation, Aug. 22, 1961.
59. Hanford Atomic Products Operation, Research and Development Programs Executed for the Division of Reactor Development. Quarterly Progress Report, July–September 1963, USAEC Report HW-79280, October 1963.
60. C. E. Fitch, Jr., and B. W. Chettle, Critical Angle Ultrasonic Tests, USAEC Report HW-79928, Hanford Atomic Products Operation, Dec. 31, 1963.
61. Hanford Atomic Products Operation, Research and Development Programs Executed for the Division of Reactor Development, Quarterly Progress Report, October–December, 1963, USAEC Report HW-80284, April 1964.
62. Argonne National Laboratory, Reactor Development Program Progress Report, February 1964, USAEC Report ANL-6860, Mar. 15, 1964.
63. C. J. Renken, A Pulsed Electromagnetic Test System Applied to the Inspection of Thin-Walled Tubing, USAEC Report ANL-6728, Argonne National Laboratory, March 1964.

A-286, br
Admiralt
Alloy 600
Alloys, c
diffusio
explosi
Alloys (b
oxidati
Alloys (i
253
Alloys (r
creep,
engine
hardne
meltin
powder
spot w
tensile
Alloys (r
ties,
prepar
Alloys (r
191
Aluminiz
for, 74
Aluminu
burnin
compa
corros
diffusi
elonga
H and
He pr
reacti
with
solubi
ThO_2
ultras
weldi
wettin
Aluminu
55
corro
damag
damag
deuter
monov
mel
neutro
Aluminu
weldi
Aluminu
chang

Index

Reactor Materials

Volume 7

Note: The page range for each of the four issues of Vol. 7 is as follows: No. 1, pages 1 to 80; No. 2, pages 81 to 148; No. 3, pages 149 to 209; and No. 4, pages 211 to 267.

A

A-286, brazing effects on, 263
Admiralty metal, corrosion, 121
Alloy 600, brazing, 263
Alloys, creep in high-temperature Li, 241
  diffusion in, 195, 247
  explosive forming, 75-8, 261
Alloys (braze), corrosion, 50, 52
  oxidation, 51
Alloys (irradiated), phase transformations, 253
Alloys (refractory), corrosion, 124
  creep, 125
  engineering properties, 125
  hardness, 139
  melting, 71-2
  powder metallurgy, 71-2
  spot welding, 263
  tensile strength, 139
Alloys (refractory)(coated), mechanical properties, 181
  preparation, 261
Alloys (refractory)(irradiated), test results, 191
Aluminizing, pack-diffusion coating process for, 74
Aluminum, brazing to Al, 145
  burning, 31-2, 184
  compatibility with Pu, Th, and U, 14
  corrosion, 49, 124-5, 180, 238
  diffusion bonding to Ni and U, 202-3
  elongation during explosive forming, 77
  H and He permeability, 126-7
  He precipitation in, 127
  reaction, with steam, 184, 242-3
    with UN, 100
  solubility in zirconium beryllide, 42
  ThO_2 electrodeposition on, 260
  ultrasonic detection of surface strain, 264
  welding, 204
  wetting of Be, 75
Aluminum (irradiated), channeling effects, 55
  corrosion, 185
  damage, 253
  damage recovery, 129
  deuteron range, 185-6
  monovacancy-formation energy relation to melting point, 187
  neutron production, 41
Aluminum (SAP), plastic deformation, 244
  welding, 74
Aluminum (SAP)(molten), Al_2O_3 structural changes in, 244
Aluminum alloy (X8001)–boron carbide–uranium dioxide dispersions (Al alloy-clad) (irradiated), damage, 156
Aluminum alloy (X8001)–boron carbide–uranium octoxide dispersions (Al alloy-clad)(irradiated), damage, 156
Aluminum alloy (X8001)–boron carbide–uranium trialuminide dispersions (Al alloy-clad)(irradiated), damage, 156
Aluminum alloy (X8001)–uranium octoxide dispersions, mechanical properties, 156-7
Aluminum alloys, corrosion, 179-80
  explosive bonding to Cu alloys, 261
  explosive forming, 75
  explosive welding, 262
  H and He permeability, 126-7
  reactions with water, 225-6
Aluminum alloys (1100), corrosion, 179-80
Aluminum alloys (1100-0), explosive forming, 261
Aluminum alloys (1245) (Al-Ni coated), corrosion, 261
Aluminum alloys (1245)(irradiated), corrosion and film formation, 120
Aluminum alloys (5056-H343), welding, 74
Aluminum alloys (6061), corrosion, 179-80
  explosive bonding, 261-2
  mechanical properties, 156-7
  reaction with steam, 242
Aluminum alloys (APM), welding, 145
Aluminum alloys (HS 15), explosive forming, 76
Aluminum alloys (Ni-plated), behavior, 261
Aluminum alloys (X8001), corrosion, 180, 238-9
  mechanical properties, 156-7
Aluminum-beryllium-silicon system, ternary eutectic solidification, 111
Aluminum–boron carbide dispersions (S.S. 304L-clad), control-rod fabrication and assembly, 47
Aluminum-cerium-chromium-magnesium-silicon system, reaction with steam, 242
Aluminum-chromium-iron-yttrium alloys, corrosion, 121
Aluminum-chromium-titanium-vanadium alloys, brazing using, 206
Aluminum-copper alloys (irradiated), electrical resistivity, 129
Aluminum-copper single crystals (irradiated), strength, 251
Aluminum foils (irradiated), damage recovery and defect clusters, 53
Aluminum-iron-nickel alloys, corrosion, 180
Aluminum-iron-nickel-silicon system, polarization, 49
Aluminum-iron-uranium alloys, phase studies, 151, 213
  properties, 150
  structure, 150
Aluminum-magnesium alloys (irradiated), electrical resistivity, 129
Aluminum-manganese alloys (irradiated), electrical resistivity, 129
Aluminum-molybdenum-tin-zirconium alloys, H embrittlement, 245
Aluminum-nickel alloys, diffusion in, 196
Aluminum-nickel-plutonium alloys (Zircaloy-2-clad) (irradiated), properties, 85
Aluminum-nickel-silicon system, corrosion and hot strength, 239
Aluminum-nickel-uranium alloys, diffusion in, 196
  reaction, with steam, 225, 242
    with water, 31
Aluminum-niobium alloys, phase studies, 62-3
Aluminum-niobium intermetallic compounds, oxidation, effects of Si or Sn on, 50
Aluminum-niobium-titanium intermetallic compounds, oxidation, Sn effects on, 50
Aluminum oxide, brazing to Nb, 144
  compatibility with Pu-PuN cermet, 88
  corrosion, 52, 183
  fabrication, 45, 47
  fiber formation by chemical vapor deposition, 204
  fracture, 128
  mechanical behavior, 196
  preferred orientation, 128
  preparation by vapor deposition, 261
  stress-strain properties at high temperatures, 196
Aluminum oxide (irradiated), annealing, 114
  growth, 113-14
  stresses, 23
Aluminum oxide (W-metallized), brazing to Nb-Zr alloy, 144
Aluminum oxide–beryllium oxide ceramics, containment properties, 128
Aluminum oxide coatings, development for fuel particles, 158
Aluminum oxide crystals (irradiated), expansion, 130
Aluminum oxide films, polarization, 49
Aluminum oxide–gadolinium oxide cylinders, fabrication, 196-7
Aluminum oxide–gadolinium oxide mixtures, fabrication, 45, 47
Aluminum oxide–molybdenum ceramics, fabrication, 143

Aluminum oxide–nickel brazed joints, corrosion, 52
Aluminum oxide–niobium brazed joints, corrosion, 52
Aluminum oxide–pyrolytic carbon coatings, crack-stopping properties, 20
Aluminum oxide–uranium dioxide system, corrosion, 52
sintering, 224
Aluminum oxide–uranium dispersions, strength, 81
Aluminum oxide whiskers, formation by vapor deposition, 142
Aluminum-plutonium alloys, EBR-I core development and manufacture, 85
self-irradiation effects, 165
Aluminum-plutonium alloys (irradiated), annealing effects, 85
Aluminum-plutonium alloys (self-irradiated), annealing and electrical resistivity, 101
Aluminum-silicon system (irradiated), electrical resistivity, 129
Aluminum-silicon-uranium system, properties and structure, 150
Aluminum-silver alloys (irradiated), electrical resistivity, 129
Aluminum-thorium alloys, phase studies, 89, 154
Aluminum-tin alloys (irradiated), electrical resistivity, 129
Aluminum-titanium alloys, 61
Aluminum-titanium alloys (irradiated), properties, 61
Aluminum-uranium alloy powder (Al-clad)(irradiated), properties, 152
Aluminum-uranium alloys, phase studies, 213
Aluminum-uranium alloys (Al-clad), reaction with water, 31, 184-5
Aluminum-uranium alloys (irradiated), annealing effects, 82-3
Aluminum-uranium composites (Ni-plated), preparation, 143
Aluminum–uranium dioxide compacts, reactions in, kinetics of, 223-4
Aluminum–uranium dioxide dispersions, reactions in, inhibition of, 218-19
Aluminum–uranium octoxide compacts, reaction sintering, 66
Aluminum–uranium octoxide dispersions, interactions, 89
phase identification, 157
Aluminum–uranium octoxide dispersions (irradiated), swelling, 89
Aluminum-zinc alloys (irradiated), electrical resistivity, 129
Aluminum-zirconium alloys, 61
Aluminum-zirconium alloys (irradiated), properties, 61
APM alloys, cladding applications, 258
Arc melting, thermodynamics of cold-mold, 201

B

B-66, diffusion bonding, 144
fabrication, 71, 257
ingot preparation, 201-2
oxidation of coated, 240
welding, 144-5, 204-5, 262-3
B-77, mechanical properties, effects of C on, 125
B120VCA, brazing using, 206
Beryllium, activation analysis, 107
bend properties, 107-8
brazing, 37-8, 109
coatings on, 40, 110, 173
compatibility with Pu, Th, and U, 14
corrosion, 40, 112, 173
deformation, 38, 109, 110
diffusion bonding, 37
diffusion in Nb, 110
ductility, 39, 109
electrical resistance, 111
electron microscopy, 39
electrorefining, 106-7
fabrication, 37-8, 107-9, 172
forging, 232
fuel-can applications and properties, 112-13
hardness, 39
impurity distribution, thermal-treatment effects on, 172-3
Fe solubility in, 40
joining, 231-2
lattice parameters, 39
liquid phase in commercial, 111
machining, 109
mechanical properties, 38, 172-3
melting, 107
metallurgy, 107
microstructure, 109, 172
N solubility in, 39-40
Ni solubility in, 39-40
O effects on lattice parameters, 39
O solubility in, 39-40
oxidation, 40, 112, 232-3
oxide films on, 173
physical metallurgy, 38-40, 109-12, 172-3
plasticity, 39
preparation of high-purity, 232
pressure bonding, 259
purification, 107
reactions with gases, 232-3
redrawing of extruded, 107-8
self-diffusion in BeO, 174
specific heat, 111
structure, dissolved gas and Ni effects on, 40
tensile properties, 107-8
ternary phases in commercial, 110-11
Ti solubility in, 39
toxicology, 113
U diffusion in, 172
welding, 108-9
wetting of, 75
Y solubility in, 39
Zr solubility in, 39
Beryllium (coated), corrosion, 112
Beryllium (irradiated), ductility, 41
He-bubble formation, 41
mechanical properties, 41
neutron production, 40-1
properties, 112-13
Beryllium acetate, activation analysis, 107
Beryllium alloys, corrosion, 111-12, 173
Beryllium bronze, aging, tensile force effects on, 246
Beryllium-calcium alloys, corrosion, 40, 173
Beryllium carbide, thermodynamics, 197
Beryllium-chromium alloys, properties, 172-3
Beryllium compounds, evaporation and Seebeck coefficients, 115
Beryllium-copper alloy sheet, mechanical properties, 112
Beryllium-copper alloy single crystals, tensile properties, 38-9
Beryllium crystals, impurities, 110
lattice parameters, 110
mechanical properties, 109
thermal evaporation, 110
Beryllium films, preparation, 232
slip, 39
Beryllium foils, solubility of Ni, Ti, Y, and Zr in, 39
Beryllium-iron alloys, annealing effects, 173
impurity distribution, thermal-treatment effects on, 172-3
matrix ductility, 39
mechanical properties, alloying element effects on, 172-3
microstructure, 172
Beryllium-nickel alloys, corrosion, 40, 173
lattice parameters, O effects on, 39
solubility of Ni, O, Ti, Y, and Zr in, 39
Beryllium-niobium alloys, phase studies, 110
Beryllium-niobium intermetallic compounds, oxidation, 233
Beryllium-niobium-zirconium alloys, brazing applications, 263
Beryllium-nitrogen-oxygen solid solutions, decomposition, 40
Beryllium oxide, applications, 174
Be self-diffusion in, 174
corrosion, 183
fabrication, 115
fiber formation by chemical vapor deposition, 204
fracture stress-temperature relation, 114-15
mechanical behavior, 196
preferred orientation, 128
preparation by vapor deposition, 261
properties, 115, 174
Beryllium oxide (irradiated), annealing, 114
damage, 55, 132, 253
disorder structure, 233
electron photomicrography, 41
He-bubble formation, 41
properties, 42, 113-14, 173-4
stability, 115
strength, 41
stresses, 23
tunneling, 131
volume expansion, 41
Beryllium oxide (UO_2-fueled)(irradiated), damage, 174
Beryllium oxide–calcium oxide ceramics, containment properties, 128
Beryllium oxide crystals (irradiated), damage and debris, 115
Beryllium oxide–magnesium oxide ceramics, containment properties, 128
Beryllium oxide–nickel brazed joints, corrosion, 52
Beryllium oxide powder, hot pressing, 115
Beryllium oxide single crystals, growth, 42
Beryllium-palladium alloys, wetting of Be, 75
Beryllium powder, forging, 232
Beryllium powder (irradiated), He-bubble formation in hot-extruded, 41
Beryllium sandwich structure, performance, 109
Beryllium sheet, mechanical properties, 111-12
oxidation, 112
performance, 109
pressure bonding, 141
Beryllium single crystals, 38-9
solid-solution strengthening, 232
Beryllium-thorium alloys, phase studies, 154
Beryllium–thorium beryllide–uranium beryllide dispersions (irradiated), swelling, 233-4
Beryllium-titanium alloys, corrosion, 232
ductility, 232
preparation, 232
solubility of Ni, Ti, Y, and Zr in, 39
wetting of Be, 75
Beryllium-titanium-zirconium alloys, brazing applications, 144, 263
Beryllium tubing, burst strength and extrusion, 108
Beryllium-tungsten alloys, phase studies, 126, 194
Beryllium weldments, strength, 109
Beryllium wire, fabrication, 37, 108, 232
properties, 37
tensile strength, 108
Beryllium-yttrium alloys, solubility of Ni, Ti, Y, and Zr in, 39
Beryllium-zirconium alloys, corrosion, 232
ductility, 232
preparation, 232

Beryllium-zirconium alloys (Continued)
solubility of Ni, Ti, Y, and Zr in, 39
wetting of Be, 75
Beryllium-zirconium intermetallic compounds, oxidation, 233
Bismuth-thorium alloys, phase studies, 154
Boiling Reactor Experiments V, control-rod poison material, 47
Bonding, nondestructive testing, 265
review of diffusion and hot-pressure, 203
Boride compounds, refractory, 177
Borides (metallic)(irradiated), crystallography, 45
Boron, preparation, 204
properties of stainless steel containing ferro-, 177
Boron carbide, addition to UO_2, 45
compatibility with cladding materials, 237
corrosion, 177-8
fabrication, 177-8
pyrolytic synthesis, 142
Boron carbide (Zircaloy-clad)(irradiated), properties, 118
Boron carbide fibers, formation, 204
Boron carbide–glass mixtures, formation, 47
Boron carbide powder, oxidation, 118
Boron carbide–silicon carbide mixtures, corrosion and fabrication, 177-8
Boron carbide–silicon carbide systems (Zircaloy-clad)(irradiated), properties, 118
Boron carbide–uranium dioxide system, B distribution in and fabrication, 178
Boron-chromium-nickel-silicon system, brazing applications, 263
Boron compounds (irradiated), He release, swelling and/or fragmentation, 45
Boron fibers, formation, 204
Boron filaments, vapor deposition, 261
Boron films, preparation, 177
Boron-hydrogen-zirconium system, compound in, 234
Boron-iron system (S.S.-clad)(irradiated), bond failure, 237
Boron Pyralloy, chemical vapor deposition and properties, 73
Boron–stainless-steel control rods (irradiated), properties, 177
Boron-tungsten system, phase studies, 126, 194
Brass, corrosion, 124-5
ultrasonic detection of surface strain, 264
Braze alloys, corrosion, 50, 52
oxidation, 51
Brazed joints, corrosion, 52-3
Brazing, 75, 205-6
Bromine-carbon system, Br_2 exchange, 106
Bronze, corrosion, 124-5
Bronze (Be), aging, tensile-force effects on, 246
Bronze [silicon (A)], corrosion, 121

C

C-129Y (Al-Si-Ag system-coated), oxidation, 240-1
Cadmium, nuclear poison applications, 118
Cadmium-indium-silver alloys (plated)(irradiated), mechanical properties, 45
Cadmium–tantalum oxide, neutron absorption, 45
Cadmium-uranium intermetallic compounds, 81
Calcium, phase diagram at high pressures, 195
Calcium (irradiated), monovacancy-formation energy relation to melting point, 187
Calcium hydride, dissociation pressure and free energy of formation, 42-3
Calcium oxide–silicon dioxide–sodium oxide glass (UO_2-fueled), density and UO_2 solubility, 97
Calcium-zirconium alloys, oxidation, 238
Carbide fuel particles (coated)(irradiated), properties, 23-7
Carbide fuel particles (PyC-coated), research review, 91
Carbide fuel particles (PyC-coated)(irradiated), fission-gas release, 23
Carbides, 196
preparation of high-compressive-strength, 249
Carbon
See also Graphite and Soot
oxidation, 36-7
Carbon (irradiated), stresses, 23
Carbon (pyrolytic)
See also Boron Pyralloy
deposition, 73, 142
diffusion in, 94, 221-2
Carbon-chromium-uranium system, phase studies, 98
Carbon (pyrolytic) coatings, crushing strength, 20
deposition, 19, 142
development, 158
hardness, 20
preparation, 91, 219
strain, 219
stress, 219
U migration into, 19, 158
Carbon-hafnium-tantalum system, phase studies, 177
Carbon-hafnium-tantalum-tungsten systems, stress-rupture properties, 244
Carbon-iron-plutonium system, eutectic temperatures, 98
Carbon-iron systems (irradiated), properties, 250
Carbon-iron-uranium system, eutectic temperatures, 98
Carbon-molybdenum-niobium-titanium system, engineering properties, 125
Carbon-molybdenum-niobium-tungsten-zirconium system, creep, 125-6
Carbon-molybdenum-thorium system, phase studies, 98
Carbon-molybdenum-titanium-zirconium system, engineering properties, 125
Carbon-molybdenum-tungsten-zirconium system, engineering properties, 125
Carbon-molybdenum-uranium system, corrosion, 52
phase studies, 98
Carbon-niobium-tungsten-yttrium-zirconium system, creep, 125-6
Carbon-niobium-tungsten-zirconium system, engineering properties, 125
Carbon-niobium-tungsten-zirconium system tubing, fabrication, 71, 139
Carbon-niobium-uranium system, phase studies, 98
Carbon-oxygen-uranium system, phase studies, 15
Carbon-plutonium system, phase studies, 16-18, 153
Carbon-plutonium-thorium system, phase studies, 88
Carbon-plutonium-uranium system, phase studies, 88, 98, 153
Carbon-rhenium-uranium system, phase studies, 98
Carbon-tantalum system, phase studies, 66
Carbon-thorium system, phase studies, 154
Carbon-thorium-uranium system, phase studies and properties, 30
Carbon-tungsten system, phase studies, 126
Carbon-tungsten-uranium system, phase studies, 98
Carbon-uranium-yttrium system, phase studies, 98
Carbon-zirconium system, phase studies, 66
Cb-752, ingot preparation, 201-2
welding, 204-5
Cb-752 (irradiated), elongation and yield strength, 189
Ceramic coatings, development, 74
nondestructive testing, 78
Ceramic-powder–metal-powder mixtures, pressure bonding, 141
Ceramic powders, compaction, 72, 141
Ceramics, sealing to metals, 144
self-healing reactions with K, 182-3
technology, 66, 128, 196-7, 247-9
Ceramics (irradiated), damage in nonfissile, 132
properties, 32-3
Ceramics (refractory), properties, 128
thermal stability, 196
Cerium-cobalt-plutonium alloys, heat capacity, 214
Cerium-copper-plutonium alloys, phase studies, 85
Cerium dioxide–glass coatings, oxidation resistance, 204
Cerium dioxide–zirconium dioxide system, solid solutions, 128
Cerium-gadolinium alloys, phase studies, 236
Cerium-nickel-plutonium alloys, melting points, 85
Cerium-thorium alloys, phase studies, 154
Cermets, self-healing reactions with K, 182-3
Cesium (molten), corrosive effects, 52-3, 241
Cesium (vaporized), corrosive effects, 52-3, 124-5
Cesium-cobalt-plutonium alloys (molten), compatibility with Nb, Ta, and Ta-W alloys, 16
Cesium-graphite compounds, decomposition, 171-2
Chance Vought IV coating, emittance, 74
Chemical vapor deposition, development, 73
Chromium, corrosion, 52
crystallography, 16-17
diffusion in, 246
diffusion in U, 81, 127
solubility in Hg, 183
Chromium carbide, properties, 66
Chromium-copper-germanium-nickel-palladium alloys, brazing applications, 263
Chromium-copper-iron-zirconium alloys, corrosion and H pickup, 119
Chromium dioxide, corrosion, 183
Chromium-iron alloys, diffusion in, 195-6, 246
^{133}Xe release, 195
Chromium-iron-nickel alloys, brazing, 263
stress corrosion, 121
Chromium-iron–uranium monocarbide system, phase studies, 98
Chromium lamella, vapor deposition, 260
Chromium-manganese-nickel-silicon system, use in brazing René 41, 144
Chromium-molybdenum-nickel alloys, corrosion, 121
Chromium-molybdenum-uranium alloys, properties and structure, 150
Chromium-nickel alloy-uranium dispersions (irradiated), volume change, 219
Chromium-nickel alloys, corrosion, 121
Chromium-nickel alloys (irradiated), electrical resistivity, 134
structural transformation, 129
Chromium-nickel-niobium alloys, phase studies, 62
structural transformation, 194
Chromium-nickel-silicon system, brazing applications, 263
Chromium-niobium alloy tubing, fabrication, 71
Chromium-niobium alloys, corrosion, 51-2
hardness, 62
phase studies, 62
Chromium-niobium-titanium alloys, corrosion, 51-2
phase studies, 61-2
scale formation, 62

Chromium-niobium-titanium-vanadium alloys, oxidation, 50
Chromium-niobium-uranium alloys, phase studies and structure, 213
Chromium-niobium-zirconium alloy tubing, fabrication, 71
Chromium oxide–Inconel–magnesium oxide coatings, heat resistance, 74
Chromium-silicon-titanium system coatings, development, 74
oxidation of, on Nb alloys, 181
Chromium-tellurium-zirconium alloys, corrosion, 48
Chromium-titanium alloys, brazing using, and foil production, 206
Chromium-titanium-vanadium alloys, brazing using, 206
Chromium-uranium alloys, properties and structure, 150
Chromium-uranium alloys (irradiated), damage annealing and swelling, 101
Chromium-zirconium intermetallic compound–zirconium cells, electrochemical potentials, 49
Chromizing Durak B coatings, emittance, 74
Cladding
See Fuel cladding
Coatings, high-temperature inorganic, 241
multilayer diffusion, 204
Cobalt, corrosion, 24-5, 47
crystallography, 16-17
diffusion in U, 81, 127
solubility in Hg, 183
Cobalt-dysprosium oxide dispersions, 47
Cobalt-dysprosium oxide dispersions (irradiated), economics and strength, 236
Cobalt-manganese alloys, diffusion, 127
Cobalt-palladium alloys, use in brazing W-metallized Al_2O_3 to Nb-Zr alloy, 144
Cold working, 71-2
Compaction (vibratory), densities of spherical shapes produced by, 259-60
Composites (fibrous), joining and seaming, 260
Compounds (irradiated), phase transformations, 253
Containment materials, compatibility with molten Cs, 241
Control rods (Al-B_4C dispersion)(S.S. 304L-clad), fabrication and assembly, 47
Control rods (B-S.S.), properties, 177
Copper, compatibility with boron carbide, 237
corrosion, 124-5
crystallography, 16-17
diffusion in, 239
diffusion in U, 81, 127
explosive forming, 75-6
H and He permeability, 126-7
oxidation, 239
Pd diffusion in, 127, 247
thermal-diffusivity testing of soft-soldered, 146
wetting of Be, 75
Copper (irradiated), annealing, 53, 185
binding energy and migration energy of divacancies, 53-4
channeling effects, 55
cluster density, 53
damage, 249, 253
defect concentration, 186
deuteron range in, 185-6
effective collision radius, 185
hardening, 54
monovacancy-formation energy relation to melting point, 187
strength, 251
Copper alloys, explosive bonding to Al alloys, 261
explosive welding, 262
H and He permeability, 126-7
Copper alloys (braze), corrosion, 50
Copper crystals (irradiated), channeling effects, 55
Frenkel pairs, 56
radioactivity, 129
Copper films (irradiated), properties, 129-30
Copper-molybdenum-zirconium alloys, oxidation, 238
Copper-nickel alloys, corrosion, 121
Copper-nickel alloys (irradiated), recovery, 250
Copper-niobium-zirconium alloys, delayed failure H embrittlement, 195
Copper-phosphorus-zirconium system, oxidation, 238
Copper single crystals, microstructure of explosively formed, 77-8
Copper-uranium alloys (splat-cooled), preparation and properties, 72
Copper-uranium dispersions, production, 82
Copper-zinc alloys, diffusion, 127
Copper-zirconium alloys, oxidation, 238
Copper-zirconium intermetallic compound–zirconium cells, electrochemical potentials, 49
Copper-zirconium intermetallic compounds, H overvoltage, 49
Coumarin, Ni plating using, 143
Croloy-9M, corrosion-product removal, 183
Crystals (irradiated), cascades, lattice effects on, 132
Cu-atom slowing, 131
damage, 186
particle tracks, 186
Crystals (single)(irradiated), fission tracks in heat-sensitive, 55
Cuprous oxide (irradiated), exciton spectrum, 186

D

D-31, hot rolling, 71
welding, 204-5
D-36, brazing, 206
diffusion bonding, 144
welding, 144-5, 204-5
D-43, diffusion bonding, 144
ingot preparation, 201-2
welding, 262-3
D-43 (coated), oxidation, 240-1
D-43 tubing, fabrication, 71
Deuterium-zirconium system, properties, 175
Diffusion coatings, multilayer, advantages of, 204
Diffusion bonding, reviews, 203
Dresden reactor, S.S. (17-4 PH), stress corrosion, 4
Dysprosium oxide, corrosion, 47
solubility in glasses, 47
stabilization, 248-9

E

Eddy-current testing, parameter separation, 207
Erbium sheet, fabrication, 139
Europium oxide, solubility in glasses, 47
stabilization, 248-9
Europium oxide (PyC-coated), preparation and properties, 19
Europium oxide–plutonium dioxide system, phase studies, 87-8
Europium oxide–plutonium oxide system, lattice parameters and phase studies, 177
Europium oxide–stainless-steel–titanium dioxide dispersions (S.S.-clad), development, 237
Europium oxide–uranium dioxide system, phase structure, 96
Europium oxide–uranium oxide system, lattice parameters and phase studies, 177
Experimental Beryllium Oxide Reactor, ^{131}I plateout, 51
Experimental Boiling-Water Reactor, impaction of canned PuO_2-UO_2 system fuel, 141
Experimental Breeder Reactor II, Al-Pu alloy core development and manufacture, 85
Na bonding of S.S.-canned fuel, 141
Experimental Breeder Reactor II core 2, alloy development, 71
Extrusion presses, temperature-sensing instruments, 201

F

F-48, extrusion, 72
hot rolling, 71
properties, 60
upset forging, 72
vacuum arc melting, 71
welding, 204-5
F-48 electrodes, preparation, 71-2
Fabrication, techniques, special, 71-8
Fast reactors, alloy development for fuel jackets, 71
Ferroboron, properties of stainless steel containing, 177
Ferrous metals
See Metals (ferrous)
Fertile materials, 149-66
Fibrous materials, joining and seaming, 260
Fissium-uranium alloys, heat capacity, 82
transformation, 213
Fizzium-plutonium-uranium alloys, casting, 258
compatibility with metals and alloys, 153, 214-15
heat content, 214
heat of fusion, 214
melting, 214
solid transformation, 214
tensile properties, 16
Foils (irradiated), damage, 186
FS-82, welding, 204-5
FS-85, fabrication, 257
welding, 144-5, 204-5, 262
Fuel cladding, alloy development for fast reactor, 71
fabrication, 202-4
fission-product diffusion and release, 195-6
Fuel-cladding materials, 48-66, 119-34, 179-97
diffusion, 126-8
mechanical properties, 60-1, 125-6, 191-4
metallurgy, 61-6, 126, 194-5
Fuel materials, diffusion in PyC, 221-2
Fuel materials (irradiated), properties, 32-3, 226
Fuel materials (U-based)(irradiated), properties, 32, 165
Fuel-particle (coated)–graphite dispersions, development, 27-8
Fuel particles (Al_2O_3-coated), compatibility with graphite, 94-5
Fuel particles (BeO-coated), compatibility with graphite, 94-5
Fuel particles (C-coated), reactions with steam, 94
Fuel particles (coated)(irradiated), fission-gas release, 20
properties, 20-7
Fuel particles (graphite-coated), reactions with steam, 94
Fuel particles (MgO-coated), compatibility with graphite, 94-5
Fuel particles (PyC-coated), development, 19-20
surface area, 19

Fuel particles (PyC-coated)(irradiated), properties, 221
Fuel particles (ZrO_2-coated), compatibility with graphite, 94-5
Fuel slugs, boring, 201
Fuels, canning, 203
pressure bonding of PWR, 140
reactions with water, 31-2
Fuels (AlSi-canned), ultrasonic testing, 78
Fuels (canned), impact bonding, 141
Fuels (Cd-bearing), nuclear poison properties, 118
Fuels (clad), fabrication, patents for, 260
ultrasonic inspection, 264
Fuels (coated-particle), reviews, 158
Fuels (irradiated), fission-gas bubble diffusion, 164
fission-gas release, 32, 100
properties, 101
swelling, 100-1
ultrasonic testing, 206
Fuels (S.S.-canned), Na bonding of EBR-II, 141
Fuels (S.S. 406-clad), swaging, 140
Fuels (U-based)(irradiated), properties, 152
Furnaces, high-temperature-sensing devices in remelt, 201

G

Gadolinum oxide, fabrication, 45, 47
solubility in glasses, 47
Gadolinium oxide–samarium oxide mixtures, solubility in glasses, 47
Gadolinium oxide–uranium dioxide system, phase studies, 236
Gadolinium trialuminide, decomposition temperature, 177
Gallium-plutonium alloys, homogenization behavior, 152-3
Generators (steam), S.S. 304 stress corrosion in PWR, 3, 5-6
S.S.(austenitic) stress corrosion in HRE-2, 11
Germanium, wetting of Be, 75
Germanium (irradiated), damage, 253
displacement-spike crystallization, 251
Germanium films (irradiated), displacement-spike crystallization, 130
Glass–rare-earth oxide mixtures, preparation and properties, 47
Glasses, lubricant for Y-tubing production, 139
solubility of rare-earth oxides in, 47
Glasses (Cd-bearing), nuclear poison applications, 118
Glasses (irradiated), fission tracks, 55
Glasses (poison), development, 47
Glasses (UO_2-fueled), 97
Gold, corrosion, 52, 124-5
H and He permeability, 126-7
self-diffusion, activation energy for, 246
wetting of Be, 75
Gold (irradiated), annealing, 185
deuteron range in, 185-6
focused-collision sequences, 129
monovacancy-formation energy relation to melting point, 187
Gold alloys, H and He permeability, 126-7
Gold-197 crystals (irradiated), transmutation effects, 250
Gold films (irradiated), properties, 129-30
Gold films (single-crystal)(irradiated), damage, 53
Gold-nickel alloys, brazing applications, 263
Graphite
See also Carbon and Soot
compatibility with fuel particles (oxide-coated), 94-5
creep, 230
deposition by sublimation, 230
oxidation, 36-7, 106
radial microcracking, 160
reaction, with CO_2-He mixtures, 169
with He-H_2O mixtures, 169-70
with steam, 169-70
research and development in Japan, 230
Graphite (AGXP)(irradiated), neutron scattering, 251
Graphite (ATJ), stress-strain properties at high temperatures, 196
Graphite (carbonyl Ni-coated), preparation, 73
Graphite (colloidal), lubricant for Y-tubing production, 139
Graphite (Hf-coated), preparation by vapor deposition, 143
Graphite (irradiated), contraction, tensile load effects on, 170
creep, 106
damage, 36, 54-5, 131, 186, 253
dimensional changes, 130-1, 170
elasticity, 36
energy release, 186
oxidation, 106
properties, 132
thermal resistivity, 56, 130
Young's modulus, 36
Graphite (polycrystalline)(irradiated), damage retention and dimensional changes, 171
Graphite (porous), diffusion of Pa, Th, and U in, 94
Graphite (pyrolytic), properties, 37
thermal conductivity, 260
U diffusion in, 159-60
Graphite (pyrolytic)(irradiated), dimensional changes, 55
electrical conductivity, 260-1
properties, 170-1
Graphite (W-coated), preparation, 261
Graphite (ZrO_2-coated), preparation by vapor deposition, 143
Graphite cloth (irradiated), properties, 230
Graphite compounds, Br_2 exchange in, 106
Graphite crystals (irradiated), annealing, 131
spin resonance, 131
vacancy-formation energy, 56
Graphite–hafnium monocarbide–uranium dicarbide system, phase studies, 98
Graphite-matrix compacts, research review, 91
Graphite–niobium monocarbide mixtures, addition of UC, 29
Graphite–niobium monocarbide–uranium dicarbide system, phase studies, 98
Graphite spheres (fueled), eddy-current inspection, 146
Graphite–tantalum monocarbide–uranium dicarbide system, phase studies, 98
Graphite–uranium carbide particle (PyC-coated) dispersions, fabrication effects, 27-8
Graphite–uranium dicarbide–zirconium monocarbide system, phase studies, 98
Graphite–uranium dioxide particle (PyC-coated), dispersions, fabrication effects, 28
Graphite–uranium monocarbide–zirconium monocarbide particle (pyrolytic graphite-coated) dispersions, hot-working effects, 28
Graphite–zirconium monocarbide mixtures, addition of UC, 29
Graphite (pyro-)-zirconium system, flexural strength and microstructure, 66

H

Hafnium, atomic force constant, 65
Debye temperature, 65
electrodeposition, 260
electron term, 65
heat content, 177
fracture, 45
O diffusion in, 118
purification, 45
specific heat, low-temperature, 65
temperature effects on, 244
vapor plating using metal-organic compounds, 204
Hafnium boride, kinetics and thermodynamics, 128
Hafnium carbide, casting, 118, 236
fabrication, 177
kinetics, 128
oxidation, 236
properties, 66, 177
thermodynamics, 66, 128, 197
Hafnium diboride, properties, 237
thermodynamics, 197
Hafnium dioxide coatings, plasma spraying, 74
vapor deposition on graphite, 143
Hafnium monocarbide powder, nitriding, 248
Hafnium mononitride powder, carburization, 248
Hafnium monoxide, thermodynamics, 197
Hafnium-niobium-titanium-zirconium alloys, engineering properties, 125
Hafnium-niobium-tungsten alloys, creep, 125-6
engineering properties, 125
Hafnium-niobium-tungsten alloys (Al-Si-Ag system-coated), oxidation, 240-1
Hafnium nitride coatings, protection of W from C diffusion, 74
Hafnium oxide, thermodynamics, 197
Hafnium sheet, mechanical properties, 118
Hafnium-tantalum-tungsten alloy tubing, fabrication, 139
Hafnium-tantalum-tungsten alloys, engineering properties, 125
ingot preparation, 201-2
Hafnium-thorium alloys, phase studies, 154
Hafnium-zirconium alloys, corrosion, 48
thermal expansion, 65
Hanford Production Reactor (N), S.S. heat-exchanger stress-corrosion cracking and pitting, 49
Hastelloy B, oxidation, 122
Hastelloy C, corrosion, 121
welding, 75
Hastelloy F, compatibility with UC, 163
Hastelloy N, corrosion, pressure effects on, 120-1
Hastelloy N (irradiated), tensile properties, 189
Hastelloy R-235 (irradiated), tensile properties, 189
Hastelloy W, filler-metal applications in welding, 204
Hastelloy X, compatibility with Fz-Pu-U alloys, 214-15
corrosion, 50, 120-1, 180-1
oxidation, 51, 181, 239
steam effects on, 180-1
stress corrosion, 121
welding, 75
Hastelloy X (irradiated), tensile properties, 134, 189
Hastelloy X-280, oxidation, 122
Hastelloys, welding, 204
Haynes 25, corrosion-product removal, 183
diffusion bonding to Nb-752, 144
oxidation, 51, 181
pretreatment with Hg, 184
solubility in molten Cs, 241
welding, 75
Haynes 26–niobium-zirconium combinations, mass transfer of metallic constituents, 241
Haynes alloys, welding, 75, 204
Heat exchangers, S.S. stress-corrosion cracking and pitting in Hanford Production Reactor (N), 49
S.S.(austenitic) stress corrosion, 3
High-Temperature Lattice Test Reactor, oxidation of cladding and structural components, 122
Holmium-thorium alloys, phase studies, 89

Homogeneous Reactor Test, S.S.(304) stress corrosion, 2
S.S.(347) stress corrosion, 2
S.S.(austenitic) stress corrosion in steam generators, 11
Honeycomb panels, explosive forming, 261
Hot-pressure bonding, review, 203
Human beings, neutron dosage from irradiated Be, 41
Hydrides, formation of metallic, 43
Hydrogen-nitrogen-zirconium systems, compound in, 234
Hydrogen-strontium system, phase studies, 115-16

I

INCO-270, oxidation, 51
Incoloy, corrosion, 50, 120-1, 180
steam effects on, 180-1
stress corrosion, 121
Incoloy (irradiated), corrosion, 49
Inconel, compatibility with UC, 163
corrosion, 50, 180-1
corrosion-product solubility in water, 239
reaction with PuN, 218
steam effects on, 180-1
stress corrosion, 6
welding, 145
Inconel (irradiated), corrosion, 49
Inconel 600, corrosion-film removal, 239-40
oxidation, 122, 181
stress corrosion, 121
Inconel 625, oxidation, 122
stress corrosion, 121
Inconel 625 (irradiated), tensile properties, 189
Inconel 700, brazing effects on, 263
Inconel 702, brazing to Mo, 144
oxidation, 181
Inconel 718 (irradiated), tensile properties, 189
Inconel C, stress corrosion, 121
Inconel X, corrosion, 50, 120-1
explosive forming, 261
stress corrosion, 121
welding, 145
Inconel X (irradiated), corrosion, 49
Indium-115 crystals (irradiated), transmutation effects, 250
Indium-115 oxide powder (irradiated), transmutation effects, 250-1
Indium-oxygen-tantalum compounds ($In_2Ta_2O_8$), neutron absorption, 45
INOR-8 (irradiated), tensile properties, 189
Intermetallic compounds, hydriding of binary, 43
Iridium, reaction with UC, 29-30
Iridium (irradiated), monovacancy-formation energy relation to melting point, 187
Iridium-193 powder (irradiated), transmutation effects, 250
Iron, corrosion, 124-5
crystallography, 16-17
diffusion in U, 81, 127
mechanical properties, temperature effects on, 132
recovery of cold-worked, 249
self-diffusion, activation energy for, 246
solubility, in Be, 40
in Hg, 183
Iron (irradiated), annealing, impurity effects on, 53
channeling effects, 55
damage, 131, 249-50, 252
defect production, impurity effects on, 53
displacement spikes, saturation effects on, 252-3
impurity separation in, 249
interstitials, 252
mechanical properties, 132
N precipitation, 56, 60
neutron production, 41
recovery, 249
vacancies, 252
Iron alloys, corrosion, pressure effects on, 120-1
reaction with PuN, 218
Iron-molybdenum-titanium alloys, use in brazing Nb-Zr alloy, 144
Iron-nickel alloys, deposition from mixed Fe and Ni carbonyls, 203
^{133}Xe release, 195
Iron-nickel alloys (irradiated), 186
Iron-plutonium alloys, liquidus temperatures, 153
Iron-plutonium alloys (molten), viscosity, 85-96
Iron-uranium alloy–uranium monocarbide pellets (S.S.-clad)(irradiated), 30
Iron-uranium alloys, transformation, 213
Iron-zirconium alloys, phase studies, 126
Iron-zirconium intermetallic compound–zirconium cells, electrochemical potentials, 49

J

J-8900, brazing applications, 263
Joints (brazed), corrosion, 52-3

K

K-Monel, explosive bonding to S.S. 321, 261

L

L-605, brazing effects on, 263
corrosion, 51
L-605–molybdenum brazed joints, corrosion, 51
L-605–molybdenum-titanium alloy brazed joints, corrosion, 51
Lanthanum, Pu solubility in, 16
Lanthanum oxide–zirconium dioxide system, solid solutions, 128
Lava, corrosion, 124-5
Lead (irradiated), monovacancy-formation energy relation to melting point, 187
Lead alloys (irradiated), damage, 253
Lead oxide–rare-earth oxide ceramics, neutron-capture cross sections and specific gravities, 248
Lead oxide–zirconium oxide ceramics, gamma-radiation attenuation, 248
Lead-thorium alloys, phase studies, 154
Liquids, diffusion in, 195
Lithium (molten), alloy creep in, 241
corrosive effects, 52, 124, 184, 241
Lithium fluoride (irradiated), fission tracks, 55
Lutetium-176 oxide powder (irradiated), transmutation effects, 250-1

M

Magnesium, compatibility with Pu, Th, and U, 14
corrosion, 124-5
diffusion of Pu and U in, 127-8
self-diffusion, activation energy for, 246
solubility of Pu and U in, 127-8
Magnesium (irradiated), neutron production, 41
Magnesium nitride, thermodynamics, 197
Magnesium oxide, corrosion, 52, 183
fracture, 128
mechanical behavior, 196
sintering, water vapor effects on, 196
use for ceramic-to-metal seals, 144
Magnesium oxide (irradiated), annealing, 114
damage, 132
growth, 113-14
stresses, 23
Magnesium oxide crystals (irradiated), properties, 130
Magnesium oxide–plutonium dioxide system, eutectic, 86
Magnesium oxide single crystals, mechanical behavior, 247-8
Magnesium oxide single crystals (irradiated), annealing and mechanical properties, 55
Magnesium-thorium alloys, phase studies, 154
Magnesium-zirconium alloys, boundary cracking, 246
directional diffusion in, 247
Magnetic materials (irradiated), damage, 249-50
Manganese, diffusion in U, 81, 127
solubility in Hg, 183
Manganese-nickel alloys, corrosion, 52
Melting, 71-2
high-temperature sensing devices, 201
thermodynamics of cold-mold arc, 201
vacuum induction, 201
Mercury, carbon-steel pretreatment with, 184
corrosive effects, 53, 183-84
Haynes 25 pretreatment with, 184
Ti and Zr addition to boiling, 183-4
Mercury (vaporized), corrosive effects, 53
Metal borides (irradiated), crystallography, 45
Metal (refractory) carbide–uranium carbide systems, phase studies, 98
Metal (refractory) coatings, preparation, 261
Metal hydrides, formation, 43
Metal-organic compounds, vapor plating applications, 204
Metal oxides, melting points, 247
preparation by vapor deposition, 261
Metal (refractory) powders, pressure bonding, 141
Metal (refractory) tubing, production techniques, 71
Metallic coatings, development, 74
Metals, brazing, 205-6
diffusion in, 195, 247
explosive forming, 75-8, 144, 261
joining, 204-6
sealing to ceramics, 144
self-diffusion, activation energies for, 246
thermal-diffusivity testing of bonds, 146
Metals (Admiralty), corrosion, 121
Metals (bcc), channeling effects, 55
diffusion in, 246
lattice-friction stress, 126
microstructure of explosively formed, 77
Metals (ceramic-coated), nondestructive testing, 78
Metals (fcc), microstructure of explosively formed, 77
Metals (fcc)(irradiated), channeling effects, 55-6
Metals (ferrous), compatibility with Pu, Th, and U, 14
Metals (irradiated), damage, 131, 253
defects, 187
heavy-ion stopping power, 132
mechanical properties, 252
phase transformations, 253
point defects, 253
range-energy relations, 132
Metals (molten), corrosive effects, 51-3, 184
Metals (refractory), brazing, 205-6
coatings for, 124
compatibility with Pu, Th, and U, 14
corrosion, 50, 52, 122-4
creep, 125
diffusion bonding, 203
electroforming, 260
electroplating, 260
engineering properties, 125

Metals (refractory) (Continued)
joining using vapor-deposited W, 142
mechanical properties, 60-1
metallurgical aspects, 61-4
oxidation, protection from, 50
reactions with PuN, 218
vapor plating using metal-organic compounds, 204
welding, 145
Metals (refractory)(coated), preparation, 261
Metals (refractory)(Hastelloy X-clad), fabrication, 259
Metals (refractory)(irradiated), test results, 191
Metals (refractory)(S.S.-clad), fabrication, 259
Moderator materials, 36-43, 169-75
Molybdenite (irradiated), fission tracks, 55
Molybdenum, brazing, 144-5
coatings for, 124
compatibility, with Fz-Pu-U alloys, 214-15
with PuN, 88
with PuO_2, 87
with Pu_2O_3, 153, 218
with UC, 163
corrosion, 124-6
creep, 125
diffusion in Ti, 127
ductility, 126
electrodeposition, 260
engineering properties, 125
fabrication, 126
fracture, 126
mechanical properties, effects of fabrication and microstructure on, 125
metallurgy, 126
necking, 126
oxidation, 122
physical properties, 126
purification, 126
reaction with steam, 243
refining, 126
self-diffusion, 62
solubility in molten Cs, 241
spot welding, 263
vapor deposition, 142
vapor plating using metal-organic compounds, 204
welding, 145
Molybdenum (arc-cast), creep properties, 63
stress-rupture properties, 63
Molybdenum (Chance Vought IV-coated), emittance, 74
Molybdenum (Chromizing Durak B-coated), emittance, 74
Molybdenum (irradiated), corrosion, 189
damage, 129, 185
hardening, 54
test results, 191
Molybdenum (Pfaudler-coated), emittance, 74
Molybdenum (Pt-clad), oxidation, 239
Molybdenum (Pt-Rh alloy-clad), oxidation, 239
Molybdenum (Re-coated), preparation, 73
Molybdenum (silicide-coated), failure, 261
oxidation, 181
preparation by vapor deposition, 143
Molybdenum (sintered), creep and stress-rupture properties, 63
Molybdenum alloy tubes, extrusion, 257
Molybdenum alloys, phase diagrams of binary and ternary, 63
properties, 125
Molybdenum boride, phase studies, 128
Molybdenum carbide, phase studies, 128
properties, 66
Molybdenum coatings, vapor deposition, 73, 142
Molybdenum dioxide, corrosion, 183
Molybdenum disilicide coatings, oxidation, 181
Molybdenum disulfide, lubricant for Y-tubing production, 139
Molybdenum-nickel alloys, corrosion, 121
Molybdenum-niobium alloys, corrosion, 51-2, 126
engineering properties, 125
fabrication, 126
metallurgy, 126
physical properties, 126
Molybdenum-niobium-tantalum-tungsten alloys, mechanical properties, 60
Molybdenum-niobium-titanium alloys, creep, 125-6
Molybdenum-niobium-titanium-tungsten alloys, engineering properties, 125
Molybdenum-niobium-titanium-tungsten-zirconium alloys, engineering properties, 125
Molybdenum-niobium-titanium-uranium-zirconium alloys, transformation, 14
Molybdenum-niobium-tungsten-zirconium alloys
See also F-48
engineering properties, 125
Molybdenum-niobium-uranium alloys, properties and structure, 150
Molybdenum-niobium-uranium-zirconium alloys, properties and structure, 150
Molybdenum-niobium-vanadium-zirconium alloys, creep, 125-6
engineering properties, 125
fabrication, 71, 257
welding, 262-3
Molybdenum-niobium-vanadium-zirconium alloys (coated), oxidation, 240
Molybdenum-niobium-zirconium alloys, corrosion, 48
phase studies, 194
Molybdenum-nitrogen-rhenium-tantalum-zirconium system, development, 257-8
Molybdenum-palladium alloys, phase studies, 246
Molybdenum-rhenium alloys, creep, 125
use in welding W, 145
Molybdenum rods (single-crystal)(irradiated), length increase, impurity effects on, 53
Molybdenum silicide, oxidation, 181
phase studies, 128
Molybdenum-silicon-uranium system (irradiated), annealing, 151
swelling, 151, 164
Molybdenum-tantalum-tungsten alloys, engineering properties, 125
strength, Hf and Zr effects on, 193
Molybdenum-tin-uranium alloys (irradiated), annealing, 151
swelling, 151, 164
Molybdenum-titanium alloys, creep properties, nitriding effects on, 193
engineering properties, 125
hot rolling, 71
use in welding W, 145
Molybdenum-titanium-uranium alloys, transformation, 14
Molybdenum-titanium-zirconium alloys, corrosion, 124
Molybdenum trioxide, corrosion, 183
Molybdenum-tungsten alloys, corrosion, 124
engineering properties, 125
reaction with UC, 224
Molybdenum-uranium alloy rods (Al-clad), fabrication, 82
Molybdenum-uranium alloy rods (APM-clad), fabrication, 82
Molybdenum-uranium alloys, creep, 15
deformation, 82, 212-13
extrusion, 140
fabrication, 258
isothermal decomposition, kinetics of, 151
mechanical properties, 212
oxidation, 152
properties, 150
rolling, 140
structure, 150
transformation, 14, 151, 213
Molybdenum-uranium alloys (irradiated), annealing, 151
properties, 82
swelling, 151-2
Molybdenum–uranium dioxide cermets, mechanical properties and preparation, 19
Molybdenum–uranium dioxide dispersions, production, 219
Molybdenum–uranium mononitride cermets, impaction, 90
Molybdenum-uranium ternary alloys (irradiated), swelling, 100-1
Molybdenum-uranium-zirconium alloys, properties and structure, 150
Molybdenum–uranium-zirconium monocarbide solid-solution brazed joints, corrosion, 52-3
Molybdenum-vanadium alloys, preparation of arc-melted buttons, 139
Molybdenum-vanadium-zirconium alloys, corrosion, 48
Molybdenum-zirconium alloys, creep properties, nitriding effects on, 193
engineering properties, 125
Morganite, corrosion, 124-5
Mycolex, corrosion, 124-5
Mykroy, corrosion, 124-5

N

NaK, corrosive effects on valves, 241
Nb-752, diffusion bonding to Haynes 25, 144
welding, 144-5
Neodymium dioxide–uranium dioxide system, 47
Neodymium sheet, fabrication, 139
Neodymium-thorium alloys, phase studies, 89
Neptunium monocarbide–thorium monocarbide solid solutions, formation, 225
Neutrons, dosage from irradiated Be and production in irradiated materials, 41
Nichrome V, corrosion, pressure effects on, 120-1
oxidation, 181
Nickel, corrosion, 124-5
crystallography, 16-17
diffusion bonding to Al and U, 202-3
diffusion in U, 81, 127
H and He permeability, 126-7
plating, on Al-U composites, 143
from Ni carbonyl vapor, 203
on Oralloy, 143
on U, 143, 260
self-diffusion, activation energy for, 246
solubility, in Be, 39-40
in Be binary alloys, 39
in Be foils, 39
in Hg, 183
stripping from U, 260
use for ceramic-to-metal seals, 144
Nickel (irradiated), damage, 249-50
mechanical properties, 133
monovacancy-formation energy relation to melting point, 187
recovery of deformed, 249
Nickel (wrought), corrosion film, 50
Nickel alloy (TD)-molybdenum-titanium combinations, mass transfer of metallic constituents, 241
Nickel alloy (TD)-niobium-zirconium combinations, mass transfer of metallic constituents, 241
Nickel alloys, corrosion, 120-1
H and He permeability, 126-7
stress corrosion, 6
Nickel alloys (330)(irradiated), mechanical properties, 133-4
Nickel alloys (A), oxidation, 122
Nickel alloys (braze), corrosion, 50, 52
oxidation, 51

Nickel alloys (irradiated), tensile properties, 189
Nickel alloys (TD), corrosion, 239
  corrosion film, electrical resistance of, 50
  diffusion bonding, 205
  oxidation, 50-1, 121-2, 181
  welding, 205
Nickel alloys (TD)(irradiated), tensile properties, 189
Nickel (carbonyl) coatings, chemical vapor deposition, 73
Nickel films (irradiated), properties, 129-30
Nickel-niobium solid solutions, lattice parameters and paramagnetic susceptibility, 246
Nickel-silicon-titanium system, corrosion, 239
Nickel–thorium dioxide dispersions, oxidation, 121-2
Nickel–thorium dioxide system, oxidation, 239
Nickel-uranium alloys, diffusion in, 196
  transformation, 213
Nickel-zirconium intermetallic compound–zirconium cells, electrochemical potentials, 49
Nickel-zirconium intermetallic compounds, H overvoltage, 49
Nimonic 75, explosive forming, 76
Nimonic 90, explosive forming, 76
  microstructure of explosively formed, 77
Nimonic alloys, explosive forming, 75
Niobium, Be diffusion in, 110
  brazing, 144-5
  coatings for, 124
  compatibility, with Fz-Pu-U alloys, 214-15
    with molten Cs-Co-Pu alloys, 16
    with PuN, 88
    with Pu_2O_3, 153, 218
    with Pu-U alloys, 214-15
  corrosion, 126, 182
  creep, 125-6
  diffusion in U, 81, 127
  electroforming, 260
  engineering properties, 125
  fabrication, 126
  mechanical properties, effects of fabrication and microstructure on, 125
  metallurgy, 126
  physical properties, 126
  purification, 126
  reaction with steam, 243
  refining, 126
  solubility in molten Cs, 241
  tensile properties, 245
  thermodynamic stability of dissolved O in, 50
  vapor plating using metal-organic compounds, 204
  W diffusion in, 246-7
  welding, 145
  yield stress of flash-annealed, strain-rate effects on, 191, 193
Niobium-95, diffusion in UO_2, 127
Niobium (Pt-clad), oxidation, 239
Niobium (Pt-Rh alloy-clad), oxidation, 239
Niobium alloy tubing, fabrication, 71
Niobium alloys, brazing, 206
  creep, 125-6
  engineering properties, 125
  fabrication, 201-2
  mechanical properties, effects of fabrication and microstructure on, 125
  phase diagrams of binary and ternary, 63
  welding, 204-5
Niobium alloys (B-66), diffusion bonding, 144
  mechanical properties, 181
  oxidation, 181
  welding, 144-5
Niobium alloys (canned), extrusion, 139
Niobium alloys (Cr-Si-Ti system-coated), preparation, 74
Niobium alloys (D-36), diffusion bonding, 144
  welding, 144-5
Niobium alloys (D-43), diffusion bonding, 144
Niobium alloys (D-43)(coated), mechanical properties and oxidation, 181
Niobium alloys (F-48)(ceramic-coated), oxidation, 50
Niobium alloys (FS-85), welding, 144-5
Niobium alloys (irradiated), corrosion, 189
Niobium alloys (Nb-752), diffusion bonding to Haynes 25, 144
  welding, 144-5
Niobium beryllides, evaporation, 115
  oxidation, 233
  Seebeck coefficient, 115
Niobium boride, phase studies, 128
  properties, 237
Niobium carbide, phase studies, 128
  properties, 66
  thermodynamics, 197
Niobium carbide powder, nitriding, 248
Niobium carbide single crystals, plasticity, 248
Niobium nitride powder, carburization, 248
Niobium oxide, corrosion, 183
Niobium oxide–tantalum oxide system, phase studies, 66
Niobium oxide–tungsten oxide system, phase studies, 66
Niobium quasibinary ($NbCr_2$-Ni_3Nb) alloy, phase studies, 62
Niobium-ruthenium alloys, phase studies, 62
Niobium silicide, phase studies, 128
Niobium single crystals, glide systems and work-hardening, 194
Niobium-tantalum-tungsten alloy tubing, fabrication, 139
Niobium-tantalum-tungsten alloys, creep, 125-6
  engineering properties, 125
Niobium-tantalum-tungsten-zirconium alloys, creep, 125-6
  engineering properties, 125
  fabrication of sheet, 257
  welding, 262
Niobium-tantalum-vanadium alloys, engineering properties, 125
  fabrication, 257
  melting, 257
Niobium-tantalum-zirconium alloys, compatibility with UC, 163
  creep, 125-6
  engineering properties, 125
Niobium-tellurium-zirconium alloys, corrosion, 48
Niobium-thorium alloys, phase studies, 154
Niobium-tin intermetallic compound wire (Nb-Zr alloy-clad), preparation, 72
Niobium-titanium alloys, corrosion, 182
  preparation of arc-melted buttons, 139
Niobium-titanium-uranium alloys, properties and structure, 150
Niobium-titanium-vanadium alloy cladding, corrosion, 51-2
  development, 71
  preparation of arc-melted buttons, 139
Niobium-titanium-vanadium alloys (silicide-coated), oxidation, 74
Niobium-titanium-zirconium alloys, creep, 125-6
  engineering properties, 125
Niobium-tungsten alloys, chemical vapor deposition and properties, 73
  corrosion, 124
  engineering alloys, 125
  tensile strength, 60-1
Niobium-tungsten-vanadium-zirconium alloys, mechanical properties, effects of C on, 125
Niobium-tungsten-zirconium alloys, creep, 125-6
  engineering properties, 125
  phase studies, 194
  welding, 262-3
Niobium-tungsten-zirconium alloys (coated), oxidation, 240-1
Niobium-uranium alloys, phase studies, 211-12
  properties, 150
  structure, 150
Niobium-uranium alloys (irradiated), properties, 82
Niobium-uranium-zirconium alloys, properties, 150
  reaction with water, 184
  structure, 150
Niobium–uranium-zirconium carbide solid-solution brazed joints, corrosion, 52-3
Niobium-vanadium alloy cladding, development, 71
Niobium-vanadium alloy tubing, fabrication, 71
Niobium-vanadium alloys, corrosion, 51-2
  creep, 125-6
  dispersion strengthening, 193-4
  engineering properties, 125
  preparation of arc-melted buttons, 139
Niobium-zirconium alloy tubing, fabrication, 71
Niobium-zirconium alloy–zirconium cells, electrochemical potentials, 49
Niobium-zirconium alloys, brazing, 144
  compatibility, with Fz-Pu-U alloys, 214-15
    with UC, 163
  corrosion, 51-3, 119, 183
  creep, 125-6, 243-4
  engineering properties, 125
  H embrittlement, 195, 245
  H overvoltage, 49
  H pickup, 119
  impedance of oxide film on, 120
  metastable omega phase, 244-5
  pressure bonding to Be, 259
Niobium-zirconium alloys (irradiated), elongation, 189
  impact properties, 134
  mechanical properties, 188
  yield strength, 189
Nionel, corrosion, 180-1
  steam effects on, 180-1
  stress corrosion, 121
Nitroguanidine, use in explosive forming of metals, 144
Nondestructive testing, 78, 206-7
  defect size determination in ultrasonic inspection, 145-6
Nonfuel materials, radiation effects, 53-60
Nonmetallic coatings, development, 74
Nonmetals, diffusion in, 195
Nuclear detectors, track registration in solid-state, 186
Nuclear poisons, metallic, 45
  nonmetallic, 45-7

O

Oralloy (Ni-plated), preparation, 143
Osmium-uranium alloys, phase studies, 150
Oxide ceramics, brittle behavior, 247
  development, 20
  pressure bonding, 141
  vapor depositions, 142-3
Oxide fuel particles (coated)(irradiated), properties, 20-3
Oxide powders, compaction, vibratory, 142
Oxides, neutron absorption, 45
  preparation of high-compressive-strength, 249
Oxygen-plutonium system, 216
  phase studies, 17
Oxygen–Zircaloy-2 system, oxidation, 179
Oxygen-zirconium system, H solubility in, 174-5

P

Palladium, diffusion, in Ag, 127, 247
in Cu, 127, 247
self-diffusion, 127, 247
use, in brazing Nb to Al_2O_3, 144
in brazing W-metallized Al_2O_3 to Nb-Zr alloy, 144
Panels, explosive forming of honeycomb, 261
Particles, compaction, vibratory, 142
Particles (coated)(irradiated), properties of U-based, 32
Peach Bottom Power Reactor, coated particle fuel, 91
Pfaudler coating, emittance, 74
Platinum, corrosion, 124-5
H and He permeability, 126-7
oxidation, 239
self-diffusion, activation energy for, 246
Platinum (irradiated), monovacancy-formation energy relation to melting point, 187
Platinum alloys, He and H permeability, 126-7
Platinum-rhodium alloys, oxidation, 239
Plutonium, compatibility with metals, 14
cracking, 15
creep, 152
crystallography, 15-16
diffusion in Mg, 127-8
electrorefining, 143
flat rolling, 83
ignition temperature, 215-16
neutron diffraction analysis, 16
oxidation, moisture effects on, 85
phase transformation, 15, 83, 85, 152
reaction with Pr, 16
solubility, in La, 16
in Mg, 127-8
in Pr, 16
thermal expansion, 15-16
veining, 15
Plutonium (molten), Ta solubility in, 213
Plutonium (self-irradiated), annealing and electrical resistivity, 101
Plutonium-239, diffusion in sintered UO_2, 96
thermal expansion, 15-16
Plutonium alloys (irradiated), properties, 101
Plutonium aluminide single crystals, transformation, 85
Plutonium arsenide, preparation, 88
Plutonium carbide, properties, 17
Plutonium carbide–uranium carbide powder, vibratory compaction, 259
Plutonium carbide–uranium carbide system, hardness, 88
properties, 153
Plutonium dioxide, activation energy, 216
compatibility with austenitic S.S., Mo, and W, 87
corrosion, 124
diffusion in PuO_2-UO_2 system, 87
dissolution, in HNO_3, 216, 218
in SiO_2, 216
in sulfamic acid, 216, 218
halogen removal, 86
melting, 86
oxidation, 17
preparation, 17
reduction, 17
thermal expansivity, 216
volatility, 17
Plutonium dioxide (self-irradiated), damage, 218
Plutonium dioxide (sintered), density, 87
Plutonium dioxide particles, voids, 216
Plutonium dioxide powder, densification, 17
sintering, 153, 216
Plutonium dioxide–stainless-steel(302B) cermets, preparation, 90
Plutonium dioxide–stainless-steel(304) dispersions, preparation, 89
Plutonium dioxide–thorium dioxide system, lattice parameters, 86
Plutonium dioxide–uranium dioxide mixtures (irradiated), properties, 17
Plutonium dioxide–uranium dioxide powder, densification, 17, 260
fabrication into fuel, 258-9
sintering, 153
Plutonium dioxide–uranium dioxide system, corrosion, 87, 124
decontamination in codeposition, 143
density, 224
electrical resistivity, 153
PuO_2 diffusion in, 87
segregation, 86-7
swaging, 72
thermodynamics, 87
Plutonium dioxide–uranium dioxide system (canned), impaction, 141
Plutonium dioxide–uranium dioxide system, (irradiated), fission-gas release, 87
properties, 154
thermal conductivity, 154
Plutonium dioxide–uranium dioxide system (Zircaloy-clad), corrosion, 119
failure, 119
swage compacting, 202
Plutonium dioxide–zirconium dioxide system, structure, 86
Plutonium monocarbide, evaluation, 17
preparation, 17
sintering, 153
thermal coefficient of linear expansion, 153
volatility, 218
Plutonium monocarbide (irradiated), fission-gas release, 153
fracture, 153
properties, 17
Plutonium monocarbide (self-irradiated), lattice-parameter increase, 218
Plutonium monocarbide–tantalum monocarbide system, melting, 18
Plutonium monocarbide–tantalum compacts, reactions, 88
Plutonium monocarbide–tantalum system, maximum temperature limit, 218
Plutonium monocarbide–thorium monocarbide solid solutions, formation, 225
Plutonium monocarbide–uranium monocarbide mixtures, properties, 17
Plutonium monocarbide–uranium monocarbide pins (S.S.-clad)(irradiated), 30
Plutonium monocarbide–uranium monocarbide solid solutions, preparation, 218
Plutonium monocarbide–uranium monocarbide solid solutions (irradiated), properties, 17
Plutonium monocarbide–uranium monocarbide system, evaluation, 17
O solubility in, 88
phase studies, 88
preparation, 17
Plutonium monocarbide–uranium monocarbide system (irradiated), diametral change, 88
Plutonium monocarbide–zirconium monocarbide system, phase studies, 88
Plutonium mononitride, compatibility with metals, 88
heat effects, 88
heat of reaction, 218
oxidation, 18
stability, 18
Plutonium mononitride (self-irradiated), damage, 218
Plutonium mononitride–plutonium dioxide system, sintering, 154
Plutonium mononitride–tungsten cermets, heat-transfer effects, 88
Plutonium mononitride–uranium mononitride solid solutions, 218
Plutonium mononitride–uranium mononitride system, phase studies, 88
solid-solution formation, 154
Plutonium monophosphide, preparation, 88
Plutonium monosilicide, 16
Plutonium monosulfide, preparation, 88
Plutonium monoxide, melting point, 17
Plutonium nitride, properties, 30
reactions with metals and alloys, 218
Plutonium nitride–uranium nitride system, compatibility with S.S. 304 and hardness, 88
Plutonium oxide, activation energy, 216
microstructure, 17
thermodynamics of PuO_{2-x}, 87
Plutonium–plutonium mononitride cermets, compatibility with Al_2O_3, 88
heat effects, 90
Plutonium-scandium alloys, density and phase studies, 153
Plutonium sesquicarbide, volatility, 218
Plutonium sesquicarbide (self-irradiated), damage, 218
Plutonium sesquicarbide–uranium sesquicarbide system, evaluation, 17
phase studies, 88
preparation, 17
Plutonium sesquioxide, compatibility with metals, 153, 218
preparation, 17
volatility, 17
Plutonium silicide, 16
Plutonium-silicon system, eutectic reactions, 16
Plutonium solid solutions (irradiated), properties, 87
Plutonium sulfide, properties, 30
Plutonium-thorium-uranium alloys, phase studies, 154
Plutonium-uranium alloys, compatibility, with Nb, 214-15
with V, 215
corrosion, 215
heat content, 214
heat of fusion, 214
heat of transformation, 214
melting, 214
solid transformation, 214
Plutonium-yttrium alloys, phase studies, 213-14
Plutonium-zirconium alloys (irradiated), dissolution in irradiated UO_2 and oxidation, 153-4
Plutonium-zirconium alloys, (Zircaloy-clad), rolling, 72
Poisons, 118, 177-8
development of glasses, 47
metallic, 45
nonmetallic, 45-7
Polymers (irradiated), fission tracks, 55
Potassium (molten), corrosive effects, 51, 182-3
Potassium aluminate, formation, 183
Potassium oxide–silicon dioxide–sodium oxide glass (UO_3-fueled), density, thermal expansion, and UO_2 solubility, 97
Powders, pressure bonding, 141
vibratory compaction of oxide, 142
Praseodymium, Pu solubility in and reaction with Pu, 16
Praseodymium sheet, fabrication, 139
Praseodymium-thorium alloys, hardness, 89
phase studies, 89, 154
Premabraz, 130
brazing applications, 263
Presses, temperature-sensing instruments for extrusion, 201
Protactinium, diffusion in porous graphite and PyC, 94
Pyrolytic carbon
See Carbon (pyrolytic)
Pyrolytic graphite
See Graphite (pyrolytic)

R

R-27, corrosion, pressure effects on, 120-1
Radiation effects, cascade theory, 56, 186
  displacement processes, 56
  dynamics, 187
  integral equations, 186-7
  mechanical properties, 56-60
  nonfuel materials, 53-60
  symposium, 132
  theory, 55-6, 131-2, 252-3
  thermal distribution around damage spike, 187
Reactors, temperature measurement using ultrasonic techniques, 264
Refractories
  See also Alloys (refractory), Ceramics (refractory), Metals (refractory)
  boride compounds, 177
  fiber formation by chemical vapor deposition, 204
  mechanical properties of coated alloys, 181
  thermal stability of ceramic, 196
  thermodynamics, 197
René 41, brazing, 144
Rhenium, containment properties, 128
  creep, 125
  reaction, with steam, 243
    with UC, 29-30
Rhenium coatings, chemical deposition, 73
  vapor deposition, 142
Rhenium oxide, thermodynamics, 197
Rhenium-tungsten alloy tubing, production, 71, 202
Rhenium-tungsten alloys, containment properties, 128
  corrosion, 124
  creep, 125
  engineering properties, 125
  extrusion, 257
  fabrication, 202
  reaction with UC, 30
Rhenium-tungsten alloys (irradiated), corrosion, 189
  creep-rupture properties, 253
  test results, 191
Rhodium-thorium alloys, phase studies, 218
Ruthenium-thorium alloys, phase studies, 218

S

Salts (fused), lubricant for Y-tubing production, 139
Sapphire, corrosion, 124-5
  mechanical behavior, 248
Savannah River Plant, S.S. 304 stress corrosion, 2-3
Scandium sheet, fabrication, 139
Scandium-yttrium alloys, phase studies, 61
Scandium-zirconium alloys, phase studies, 61
Selenium-thorium systems, phase studies, 154
Semiconductors (irradiated), annealing, impurity effects on, 53
  damage, 253
Shippingport Pressurized-Water Reactor, pressure bonding of fuel, 140
  S.S. 304 stress corrosion in steam generator, 3, 5-6
  UO_2-ZrO_2 fuel wafer fabrication, 97-8
Silicide coatings, effects on mechanical properties of Nb alloys, 181
  formation using fluidized-bed method, 204
  oxidation, 181
Silicide (pack) coatings, oxidation protection properties, 74
Silicide (refractory metal) coatings, vapor deposition on refractory metals, 143
Silicon, corrosion, 52
  vapor plating using metal-organic compounds, 204
Silicon (irradiated), fission tracks, 55
Silicon bronze (A), corrosion, 121
Silicon carbide, pyrolytic synthesis, 142
  vapor deposition of filaments, 261
Silicon dioxide, corrosion, 183
  preparation by vapor deposition, 261
  PuO_2 dissolution in, 216
Silicon dioxide (irradiated), stresses, 23
Silicon monocarbide, barrier to U migration into PyC, 19
Silicon monocarbide (irradiated), stresses, 23
Silicon monoxide, thermodynamics, 197
Silicon oxide (sintered), strength, 66
Silicon oxide (slip-cast fused), sintering, 66
Silicon-uranium system, transformation, 213
Silicon-uranium system (irradiated), properties, 82
Silver, corrosion, 124-5
  Pd diffusion in, 127, 247
  plating on U, 143
  wetting of Be, 75
Silver (irradiated), annealing, 185
  monovacancy-formation energy relation to melting point, 187
Silver-107 crystals (irradiated), transmutation effects, 250
Silver films (irradiated), properties, 129-30
SI-1, reaction with steam, 242
SNAP-10A/2/8 reactor, liquid-metal technology, 184
Sodium (molten), corrosive effects, 51-2, 124, 181-2, 184
Solids, diffusion in, 195-6
  shock waves in, 262
Solids (irradiated), damage, 56
  properties, 132
  transmutation effects in crystalline, 250-1
  vacancies, 187
Soot
  See also Carbon and Graphite
  accumulation on particles, 220-1
Special Power Excursion Reactor Tests-I, excursion, 184-5
Special Power Excursion Reactor Tests-ID, fuel-water reaction, 31
Spinel, corrosion, 52
Stainless steel, chloride deposition on, 122
  Cl deposition on, 180
  compatibility with UC, 163
  corrosion, 120-1, 180
  Cs deposition on, 180
  explosive forming, 75-7
  reaction, with UN, 100
    with water, 226
  stress corrosion, 49
  stress-corrosion prevention, 4-6
  tensile properties, 58-60
  ultrasonic detection of surface strain, 264
  welding, 204
Stainless steel (17-4 PH), corrosion, pressure effects on, 120-1
  stress corrosion in Dresden reactor, 4
Stainless steel (18-8), microstructure of explosively formed, 77
Stainless steel (302), oxidation, 50
Stainless steel (304), compatibility, with B carbide, 237
    with Fz-Pu-U alloys, 214-15
    with $Pu_{0.2}N$-$U_{0.8}N$ system, 88
  corrosion, 121-2
  diffusion bonding to W, 247
  failure, carburization-induced, 241
  oxidation, 49
  pressure bonding, 140-1
  reaction, with PuN-UN solid solutions, 218
    with UO_2, 29
  stress corrosion, 121-2
    in HRT, 2
    in PWR steam generator, 3, 5-6
    in Savannah River Plant, 2-3
    in VBWR, 3
  stress-corrosion cracking, 50, 180
    $KMnO_4$-NaOH solution effects on, 49
Stainless steel (304)(irradiated), corrosion, 189
  cracking, 180
  tensile properties, 188
Stainless steel (304)(vacuum melt), stress corrosion, 121
Stainless steel (304L), corrosion, 120-2, 180
  cracking, 182
  pressure bonding, 140-1
Stainless steel (308), stress corrosion, 121
Stainless steel,(310), corrosion, 180-1
  steam effects on, 180-1
  stress corrosion, 121
Stainless steel (316), corrosion, 122, 181-2
  pressure bonding to Be, 259
  stress corrosion, 121
  stress-corrosion cracking, $KMnO_4$-NaOH solution effects on, 49
  welding, 75
Stainless steel (316L), corrosion, 120-2
  filler-metal applications in welding, 204
Stainless steel (321), corrosion, 52
  explosive bonding to K-Monel, 261
  explosive forming, 261
Stainless steel (347), corrosion, 50, 52
  pressure bonding, 140-1
  stress corrosion, 2-3, 121
  welding, 75
Stainless steel (347)(irradiated), fatigue, 133
Stainless-steel (347) cladding properties, 73
Stainless steel (348)(irradiated), tensile properties, 188
Stainless steel (406), corrosion, 120-1, 180-1
  steam effects on, 180-1
Stainless steel (410)(irradiated), tensile properties, 188
Stainless steel (430), compatibility with B carbide, 237
  corrosion, pressure effects on, 120-1
Stainless steel (430 boron), properties, 177
Stainless steel (446), corrosion, 120-1, 180
Stainless steel (A-286)(irradiated), creep, 133
  stress-rupture properties, 253-4
Stainless steel (AM-350SS)(irradiated), tensile properties, 188
Stainless steel (austenitic), compatibility with PuO_2, 87
  corrosion, 122
  stress corrosion, 1-11
Stainless steel (austenitic)(irradiated), mechanical properties, 187-8, 253
  tensile properties, 132-3
Stainless steel (boron)(irradiated), properties, 177
Stainless steel (irradiated), mechanical properties, 132
  stress-corrosion cracking, 49
  structure, 132
  tensile properties, 58, 60
Stainless-steel foil, production, 72
Stainless-steel tubing (irradiated), stress-rupture properties, 60
Stainless-steel–uranium dioxide cermets, preparation, 90
Stainless-steel–uranium dioxide dispersions, defects in structure and mechanical testing, 18
Stainless-steel (347)–uranium dioxide dispersions, (S.S. 347-clad)(irradiated), stability, 89-90
Stainless-steel (304)–uranium dispersions (irradiated), volume change, 219
Stainless-steel–Zircaloy-2 joints (irradiated), damage, 188-9
Stationary Low Power Plant No. 1, core-water reaction, 31
  excursion, 184-5
Steam generators, S.S. 304 stress corrosion in PWR, 3, 5-6
  S.S.(austenitic) stress corrosion in HRE-2, 11

Steel, corrosion, 181-2
embrittlement, 143
explosive welding, 262
H and He permeability, 126-7
radiation resistance, 253
welding, 74-5
Steel (4S4), corrosion, 124
Steel (4S8), corrosion, 124
Steel (4130), compatibility with B carbide, 237
embrittlement, 143
explosive forming, 261
Steel (4330), explosive bonding to Ta-W alloys, 262
Steel (A-212 carbon), corrosion, 121
Steel (A-212B)(irradiated), embrittlement, annealing effects on, 253
impact properties, 132
Steel (A-302B)(irradiated), embrittlement, annealing effects on, 253
impact properties, 132
Steel (A-350-LFI (modified)(irradiated), embrittlement, annealing effects on, 253
Steel (alloy), explosive forming, 75
Steel (austenitic)(irradiated), lattice constant increase, 54
Steel (carbon), corrosion, 180
pretreatment with Hg, 184
stress corrosion, 6
Steel (carbon)(Hastelloy-clad), explosive bonding, 262
Steel (carbon)(Stellite-clad), explosive bonding, 262
Steel (carbon, Zr pretreated), corrosion, 53
Steel (Cr-Mo), corrosion, 181-2
Steel (Cr-Mo-Ti), corrosion, 181-2
Steel (CrNi-189)(irradiated), damage, 253
Steel (ferritic), corrosion, 124
Steel (ferritic)(irradiated), lattice constant increase, 54
Steel (HY-150), toughness and weldability, 74
Steel (irradiated), mechanical properties, 188
Steel (low-alloy), corrosion, 180, 183
stress corrosion, 6
Steel (low-alloy)(irradiated), properties, 132, 253
Steel (low-carbon), explosive forming, 144
Steel (low-carbon)(irradiated), mechanical properties, 253
Steel (maraging), welding, 74-5
Steel (martensitic), corrosion, 183
Steel (mild), Cs and Cl deposition on, 180
explosive forming, 75-7
Steel (mild)(irradiated), hardening, 132
mechanical properties, 187
Steel (MnSi)(irradiated), damage, 253
Steel (carbon) foils (irradiated), defects, 54
Stellites, corrosion, 51
Strontium, phase diagram at high pressures, 195
Strontium (irradiated), monovacancy-formation energy relation to melting point, 187
Strontium hydride, phase studies, 115-16
Strontium titanate (irradiated), split interstitial configuration, 251
Structural materials, diffusion, 126-8
mechanical properties, 60-1, 125-6, 191-4
metallurgy, 61-6, 126, 194-5
Submarine Thermal Reactor (Mark I), S.S. 347
stress corrosion in, 3
Superalloys, coatings for, 74
Superheat fuels, corrosion, 49-50

T

T-111, brazing, 206
ingot preparation, 201-2
T-222, stress-rupture properties, 244
Tantalum, binding energy, 126
brazing, 145
compatibility, with molten Cs-Co-Pu alloys, 16
with PuN, 88
with Pu_2O_3, 153, 218
with UC, 163
corrosion, 53, 124-5, 183
creep, 125
electroforming, 260
engineering properties, 125
hardness, 64
mechanical properties, effects of fabrication and microstructure on, 125
reaction with steam, 243
solubility in molten Pu, 213
strength, C addition effects on, 245
stress-rupture properties, 63-4
vapor plating using metal-organic compounds, 204
welding, 145
Tantalum alloys, coatings for, 124
development, 193
engineering properties, 125
mechanical properties, effects of fabrication and microstructure on, 125
phase diagrams of binary and ternary, 63
strength, C addition effects on, 245
Tantalum alloys (canned), extrusion, 139
Tantalum alloys (irradiated), corrosion, 189
Tantalum alloys (silicide-coated), development, 261
preparation by vapor deposition, 143
Tantalum carbide, properties, 66
Tantalum coatings, vapor deposition, 142
Tantalum crystals, discontinuous yielding, 126
Tantalum diboride, properties, 237
Tantalum monocarbide powder, nitriding, 248
Tantalum monocarbide–tungsten system, engineering properties, 125
Tantalum mononitride powder, carburization, 248
Tantalum pentoxide, corrosion, 183
Tantalum tungsten alloys, compatibility with molten Cs-Co-Pu alloys, 16
corrosion, 124
creep, 125
engineering properties, 125
explosive bonding to steel (4330), 262
hot rolling, 71
ingot preparation, 201-2
Tantalum-tungsten-zirconium alloys, phase studies, 245-6
Tetryl, use in explosive forming of metals, 144
Thorium, compatibility, with metals, 14
with Pu_2O_3, 218
diffusion, in porous graphite, 94
in PyC, 94, 222
dispersion hardening, 88
electropolishing, 154
grain size, mechanical work effects on, 218
oxide removal from, 218
reduction, 139
transformation lowering, Pu effects on, 154
twinning, 154
work hardening, 18
Thorium (irradiated), monovacancy-formation energy relation to melting point, 187
properties, 101
Thorium alloys, properties and structure, 150, 213
Thorium beryllide, reaction pressing, 42
Thorium beryllide–uranium beryllide system, reaction pressing, 42
Thorium beryllide–uranium beryllide system (irradiated), stability, 233
Thorium dicarbide, 30
free energy of formation, 163
melting point, 224
transformation, 224
Thorium dicarbide–uranium dicarbide particles (PyC-coated), fuel preparation for Peach Bottom Power Reactor, 91
reaction with steam, 170
U migration, 160, 162
Thorium dicarbide–uranium dicarbide particles (PyC-coated)(irradiated), coating cracking, 159
fission-gas release, 20-1
properties, 92-3
Thorium dicarbide–uranium dicarbide solid solutions, melting point, 224
Thorium dioxide, corrosion, 183
electrodeposition on Al, 260
Thorium dioxide compacts (reinforced), oxidation, 19
preparation, 18-19
properties, 19
thermal conductivity, 19
Thorium dioxide crystals (irradiated), activation energy and Xe diffusion, 227
Thorium dioxide particles, attrition, 90
density of compacted, 260
Thorium dioxide particles (Al_2O_3-coated), attrition, 90
Thorium dioxide–tungsten system, engineering properties, 125
Thorium dioxide–uranium dioxide ceramics (irradiated), ^{133}Xe release, 102
Thorium dioxide–uranium dioxide compacts (reinforced), brazing, 19
preparation, 18-19
Thorium dioxide–uranium dioxide compacts (reinforced)(irradiated), heat transfer, 19
Thorium dioxide–uranium dioxide system, 47
Thorium monocarbide, free energy of formation, 163
homogeneity, 163
thermal conductivity, 30
Thorium monocarbide–uranium monocarbide particles (C-coated), coating failure, 93
Thorium monocarbide–uranium monocarbide solid solutions, formation, 225
Thorium monosulfide, thermal conductivity, 224
Thorium nitride, properties, 30
Thorium oxide, removal from Th, 218
Thorium oxide–uranium oxide system, density of compacted, 141-2
Thorium oxide–yttrium oxide solid solutions (irradiated), ^{133}Xe release, 227
Thorium sesquicarbide, phase studies, 30
Thorium sulfide, properties, 30
Thorium–thorium dioxide system, hardness, 154
Thorium–thorium monocarbide–uranium system, phase studies, 99
Thorium-titanium alloys, phase studies, 154
Thorium trialuminide, transformation, 89
Thorium-uranium alloys, mechanical properties, 18
phase studies, 154
Thorium-uranium alloys (irradiated), properties, 101
Thorium-uranium-zirconium alloys, extrusion, 218
hardness, 155, 218
phase studies, 154
strength, Al and Be effects on, 88-9
stress-rupture properties, 88
Thorium-uranium-zirconium alloys (Zircaloy-2-clad)(irradiated), volume change, 154-5
Thorium-vanadium alloys, phase studies, 154
Thorium-zirconium alloys, phase studies, 154
Titanium, addition to boiling Hg, 183-4
atomic force constant, 65
C addition distribution, 65-6
crystallography, 16-17
Debye temperature, 65
electronic term, 65
explosive bonding to Al alloys (6061), 261-2
explosive forming, 75-7
melting, 201
Mo diffusion in, 127
O diffusion in, 127

Titanium (Continued)
phase transformation, 65
self-diffusion, 127
solubility in Be, Be binary alloys, and Be foils, 39
specific heat, low-temperature, 65
temperature effects on, 244
^{44}Ti diffusion in, 127
use in diffusion bonding Nb-752 to Haynes 25, 144
V diffusion in, 127
^{48}V diffusion in, 127
vapor plating using metal-organic compounds, 204
Zr diffusion in, 127
Titanium (I.C.I. 130), explosive forming, 76
Titanium (irradiated), neutron production, 41
Titanium-44, diffusion in Ti, 127
Titanium alloys, C addition distribution, 65-6
explosive forming, 75, 77
explosive welding, 262
mechanical properties, Zr addition effects on, 245
metastable constitution, 244
Titanium carbide, fiber formation by vapor deposition, 204
filament formation by vapor deposition, 261
properties, 66
thermal conductivity, 248
Titanium diboride, properties, 237
pyrolytic synthesis, 142
Titanium dioxide, corrosion, 183
preparation by vapor deposition, 261
Titanium monocarbide powder, nitriding, 248
Titanium monocarbide single crystals, plasticity, 248
Titanium mononitride powder, carburization, 248
Titanium monoxide, thermodynamics, 197
Thorium nitride, thermal conductivity, 248
Titanium-uranium-zirconium alloys, properties and structure, 150
Titanium-vanadium alloys, compatibility with Fz-Pu-U alloys, 153, 214-15
corrosion, 182
preparation of arc-melted buttons, 139
Tin-yttrium alloys, phase studies, 195
Transient Reactor Test Facility, metal-water reactions, 31
Triplex coatings, development, 158
Tubing, electromagnetic inspection, 264-5
Tungsten, brazing, 145
coatings for, 126
compatibility, with PuN, 88
with PuO_2, 87
with Pu_2O_3, 153
with UC, 163
consolidation, 126
corrosion, 124-5
creep, 125
deformation of sintered, 38
deposition of, 260
diffusion in Nb, 246-7
diffusion bonding to S.S. 304, 247
electrodeposition, 260
engineering properties, 125
extrusion, 257
fabrication, 257
fibering, 126
joining, 126
mechanical properties, effects of fabrication and microstructure on, 125
oxidation, 126
physical metallurgy, 126
preparation, 126
properties, 126
reaction with steam, 243
reactions, 126
refractory metal joining using vapor-deposited, 142
self-diffusion, activation energy for, 246
solubility in Hg, 183
vapor deposition, 142, 203-4
vapor plating using metal-organic compounds, 204
welding, 75, 145
working, 126
Tungsten (doped), engineering properties, 125
Tungsten (HfN-coated), C diffusion in, 74
Tungsten (HfO_2-coated), preparation, 74
Tungsten (irradiated, ^{41}Ar range in, 128
channeling effects, 55
creep, 134
creep-rupture properties, 59-60, 253
damage, 249
stress rupture, 134
test results, 191
^{133}Xe range in, 128
Tungsten (Mo-coated), preparation and properties, 73
Tungsten (pyrolytic), tensile properties, 260
Tungsten (re-coated), preparation, 73
Tungsten (silicide-coated), development, 261
preparation by vapor deposition, 143
Tungsten (sintered), creep and stress-rupture properties, 63
Tungsten (W-coated), preparation and properties, 73
Tungsten (ZrO_2-coated), preparation, 74
Tungsten alloy rocket nozzles, fabrication and performance, 126
Tungsten alloys, 125-6
fabrication, 257
phase diagrams of binary and ternary, 63
Tungsten alloys (canned), extrusion, 139
Tungsten alloys (silicide-coated), development, 261
Tungsten boride, phase studies, 128
Tungsten carbide, phase studies, 128
properties, 66
thermodynamics, 197
Tungsten coatings, vapor deposition, 73, 142
Tungsten crystals, growth from vapor, 142
Tungsten dioxide, corrosion, 183
Tungsten foil, production, 72
Tungsten sheet, mechanical properties, 60
Tungsten silicide, phase studies, 128
Tungsten single crystals (irradiated), channeling of heavy ions, 186
Tungsten trioxide, corrosion, 183
Tungsten trioxide (irridiated), ^{85}Kr range in, 128-9
Tungsten tubing, extrusion, 202
formation by vapor deposition, 142
production, 71
Tungsten-tungsten joints, pressure bonding and properties, 73
Tungsten-uranium dioxide cermets, creep-rupture testing, 157
mechanical properties, 19
preparation, 19
Tungsten–uranium dioxide (W-coated) cermets, electrical resistivity and thermal conductivity, 90
Tungsten–uranium dioxide cermets (irradiated), stability, 219
Tungsten–uranium dioxide dispersions, fabrication, 157
production, 219
properties, 157
Tungsten–uranium monocarbide system, creep, 99
Tungsten–uranium mononitride cermets (irradiated), fission-gas release and reactions in, 219
Tungsten-uranium monosulfide system, corrosion, 52
TZM, brazing, 206
corrosion, 124
hot rolling, 71
reduction, 202
welding, 205
TZM (irradiated), corrosion, 189
test results, 191

U

Ultrahigh-Temperature Reactor Experiment, PyC-coated fuel, 19
Ultrasonic inspection, defect size determination, 145-6
development, 206-7
Uranium, casting of fine-grained, 211
chemistry, melting effects on, 72
Co diffusion in, 81, 127
compatibility with metals, 14
corrosion, 152
Cr diffusion in, 81, 127
creep, 14
crystallography, 14
Cu diffusion in, 81, 127
diffusion, in Be, 172
in Mg, 127-8
in porous graphite, 94
in PyC, 94
in pyrolytic graphite, 159-60
in self-bonding, 203
diffusion bonding to Al and Ni, 202-3
dislocation networks, 101
drilling, 139-40
electron-beam melting, 72
fabrication, 201, 258
Fe diffusion in, 81, 127
friction with mill rolls, 139
heat capacity, 82
heat-treatment, 81
internal friction, 149
microstructure, 149
migration into PyC, SiC barrier to, 19
Mn diffusion in, 81, 127
Nb diffusion in, 81, 127
Ni diffusion in, 81, 127
oxidation, by CO_2, 100
Cu effects on, 164
plasticity, 149-50
plating with Ni, 260
residual stresses, 149
self-diffusion, 127
solubility in Mg, 127-8
surface tension at melting point, 150
tensile fracture, 149
tensile properties, P effects on, 81-2
texture, 14
thermodynamics, 197
ultrasonic inspection, 264
^{133}Xe diffusion in, 14
Young's modulus, 149
Uranium (Ag-plated), preparation, 143
Uranium (irradiated), annealing, 101, 151, 211
density, 211
dimensional changes, 164-5
ejection by fission fragments, 32
electrical resistivity, 164-5
growth, 14
He behavior in, 101, 150
properties, 32, 82, 101
stability, 149
swelling, 101, 151, 211
swelling during annealing, 32
^{133}Xe diffusion in, 101
Uranium (molten), compatibility with V, 215
N solubility in, 100
Uranium (Ni-plated), preparation, 143
stripping of Ni from, 260
Uranium (Zn-plated), porosity and preparation, 143
Uranium-235, fission-fragment interaction with metals, 129
Uranium alloys, corrosion, 152
cracking, quenching effects on, 213
diffusion, 149
phase studies, 149

Uranium alloys (Continued)
properties, 149-50, 213
structure, 150, 213
tempering, impurity effects on, 213
Uranium alloys (irradiated), He behavior in, 101, 150
properties, 32, 82, 101
Uranium beryllide, reaction pressing, 42
Uranium carbide, creep, plastic deformation, and vapor pressure, 99
Uranium carbide (irradiated), damage in cast, 227
properties, 30, 32
Uranium carbide (Nb-Zr alloy-clad)(irradiated), properties, 99
Uranium carbide (S.S.-clad)(irradiated), dimensional changes and microstructure, 30
Uranium carbide (W-coated), diffusion-emission testing, 204
Uranium carbide (UC_{2-x}) compacts, microstructure, 72
Uranium carbide particles, metallographic examination, 90-1
Uranium carbide particles (coated), metallographic examination, 90-1
Uranium carbide particles (PyC-coated), preparation and properties, 91
Uranium carbide (UC_{2-x}) powder, 72
Uranium crystals, creep, 211
Uranium dicarbide, heat capacity, 30
heat of transformation, 30
melting point, 224
reaction with Zr, 163
reduction, 30
stability, 29
transformation, 30, 224
Uranium dicarbide particles (C-coated), coating failure, heating effects on, 93-4
Uranium dicarbide particles (irradiated), fission-product release during annealing, 30
Uranium dicarbide particles (PyC-coated), coating thickness, optimum, 159
crushing strength, 220
physical properties, 169
preparation, 91
reaction with steam, 222
surface area, 19-20
U migration, 160, 162
Uranium dicarbide particles (PyC-coated) (irradiated), coating failure, 221
damage, 159
fission-gas release, 20-3, 158-9
metallographic examination, 23-7
properties, 92-3
Uranium dicarbide particles (PyC, SiC-coated), U migration into PyC, 19
Uranium dicarbide particles (PyC, SiC-coated) (irradiated), properties, 19
Uranium dicarbide–zirconium dicarbide particles (PyC-coated)(irradiated), properties, 92-3
Uranium dioxide, absorption spectra, 96
B_4C addition, 45
canning, 203
corrosion, 124
creep formation of nonstoichiometric, 95-6
electrical conductivity, 29
enthalpy, 95
grain growth, 97, 162
He solubility in, 162
magnetic properties at low temperature, 162
N diffusion in, 162
^{95}Nb diffusion in, 127
oxidation, 97
phase identification, 157
preparation from UF_6 in fluidized bed, 204
production, by pneumatic impaction, 224
by reductive precipitation, 224
^{239}Pu diffusion in sintered, 96
reaction with S.S. 304, 29
^{220}Rn emanation and diffusion in, 96-7
swaging, 140
thermal conductivity, 95
thermal expansion, 95
thermoelectric power, 29
U-atom ejection by fission fragments, 223
Uranium dioxide (Al_2O_3-clad), interaction, 241
Uranium dioxide (APM-clad), development, 258
Uranium dioxide (Be-clad), fabrication, 231
Uranium dioxide (BeO-clad), interaction, 241
Uranium dioxide (clad), ultrasonic inspection, 264
Uranium dioxide (Inconel X-clad), pressure bonding, 73
Uranium dioxide (irradiated), annealing effects, 29
collision sequences, 129, 165
fission-fragment tracks, 32
fission-gas release, 32-3, 102, 223
fission-product behavior and effects, 165
focused-collision sequences, 129
He solubility in, 102
^{131}I release, 223
properties, Nb_2O_5 and TiO_2 effects on, 96
Pu-Zr alloy dissolution in, irradiated, 153-4
recrystallization at high temperature, 223
thermal conductivity, 29, 165-6
Xe release, 162, 227
Uranium dioxide (Mo-clad), interaction, 241
Uranium dioxide (Ni-clad)(irradiated), thermal conductivity, 223
Uranium dioxide (S.S.-clad), hot extrusion, 258
pressure bonding, 73
Uranium dioxide (S.S. 304-clad), reaction with water, 184
Uranium dioxide (ThO_2-clad), interaction, 241
Uranium dioxide (W-clad), interaction, 241
Uranium dioxide (Y_2O_3-clad), interaction, 241
Uranium dioxide (Zircaloy-clad)(irradiated), contact thermal conductance, 223
Uranium dioxide (Zircaloy-2-clad), reaction with water, 184
Uranium dioxide particles (Al_2O_3-coated), oxidation, 94
Uranium dioxide particles (Al_2O_3-coated)(irradiated), coating failure, 20
coating integrity, 92, 221
damage, 158
fission-gas release, 20-2
Uranium dioxide particles (Al_2O_3, PyC-coated), preparation, 20
Uranium dioxide particles (Al_2O_3, PyC-coated) (irradiated), coating integrity, 91-2
fission-gas release, 20-2
Uranium dioxide particles (BeO-coated), development, 91, 158
oxidation, 94
properties of coating, 20
Uranium dioxide particles (BeO-coated)(irradiated), coating failure, 92
Uranium dioxide particles (BeO, PyC-coated), preparation and properties, 91
Uranium dioxide particles (BeO, PyC-coated) (irradiated), fission-gas release, 20, 22
Uranium dioxide particles (MgO-coated), oxidation, 94
Uranium dioxide particles (Mo-coated), preparation and properties, 90
Uranium dioxide particles (PyC-coated), preparation, 91
Uranium dioxide particles (PyC-coated)(irradiated), coating integrity, 221
damage, 158
Uranium dioxide particles (S.S.-canned), compaction, 141
Uranium dioxide pellets, characterization, 97
fabrication, 97
production by sintering, 224
Uranium dioxide pellets (APM-clad), magnetic-pulse swaging, 72-3
Uranium dioxide plates, fabrication, 97
Uranium dioxide powder, characterization, 97
compaction, 29, 141-2, 162, 203
extrusion, 162
impaction, 29
sintering, 97, 224
Uranium dioxide powder (fused), impaction, 29
swaging, 72
Uranium dioxide rods, fabrication, 29
Uranium dioxide shot (BeO-coated), preparation, 221
Uranium dioxide shot (BeO-coated)(irradiated), fission-gas retention and grain-growth inhibition, 221
Uranium dioxide single crystals, infrared absorption, 29
Uranium dioxide single crystals (irradiated), damage, 55, 165
defects, 32, 102
fission-gas release, 165
fission tracks, 186
microscopy, transmission electron, 165
Uranium dioxide–yttrium oxide solid solutions (irradiated), ^{133}Xe release, 227
Uranium dioxide–zirconium dioxide solid solutions (irradiated), ^{133}Xe diffusion coefficient and release, 33
Uranium dioxide–zirconium dioxide system (Ni-clad)(irradiated), thermal conductivity, 223
Uranium dioxide–zirconium dioxide wafers, fabrication of PWR fuel, 97-8
Uranium dispersions (irradiated), properties, 32
Uranium monocarbide, addition to graphite-NbC and graphite-ZrC mixtures, 29
compatibility with metals and alloys, 163
dislocations, 163
electrical resistivity, 30
fabrication, 163-4
formation by vapor deposition, 142
microscopy, transmission electron, 163
normal spectral emittance, 30
preparation, 30
reaction, with Ir, 29-30
with Mo-W alloys, 224
with Re, 29-30
with Re-W alloy, 30
with Zr, 163
thermal conductivity, 30
total hemispherical emittance, 30
UO solubility in, 98
Uranium monocarbide (irradiated), damage, 163
properties, 224
thermal conductivity, 163
U redistribution, 163
^{133}Xe diffusion in, 102
Uranium monocarbide (Nb-clad)(irradiated), Nb-UC reaction, 30
Uranium monocarbide (S.S.-clad)(irradiated), 30
Uranium monocarbide compacts, microstructure, 72
Uranium monocarbide powder, 72
Uranium monocarbide–uranium monosulfide system, solid solutions, 99
Uranium monocarbide–zirconium monocarbide particles (PyC-coated), diffusion into coating, 160
Uranium monocarbide–zirconium monocarbide system, reactions with Nb, Ta, and W, 99
Uranium mononitride, reactions with Al, S.S., and Zr, 100
Uranium mononitride (hot-pressed), 30-1 stability, 100
Uranium monosulfide, thermal conductivity, 224
Uranium monosulfide (irradiated), properties, 224
Uranium monoxide, solubility in UC, 98
thermodynamics, 197

Uranium nitride, properties, 30
Uranium nitride (irradiated), properties, 30, 32
Uranium octoxide, magnetic properties at low temperatures, 162
Uranium oxide, magnetic properties at low temperatures, 162
thermodynamics, 197, 223
volatility, 223
Uranium oxide (irradiated), properties, 32
Uranium oxide particles (ZrC-coated), preparation, 90
Uranium oxysulfide, electrodeposition, 143
Uranium particles (PyC-coated), preparation, 91
Uranium sesquicarbide, reduction, 30
thermal expansion, 99
Uranium sheet, texture of rolled, 14
Uranium silicide (irradiated), properties, 30
Uranium single crystals, deformation, 211
Uranium sulfide, properties, 30
Uranium tetraaluminide, identification, 157
Uranium trialuminide, identification, 157
Uranium-zirconium alloys, properties and structure, 150
Uranium-zirconium alloys (hydrided), 234
Uranium-zirconium alloys (irradiated), properties, 82
U.S.S. *Nautilus*, S.S. 347 stress corrosion, 3

V

Vallecitos Boiling-Water Reactor, Inconel X fuel-cladding corrosion, 50
S.S. 304 stress corrosion, 3
S.S. 347 fuel-cladding corrosion, 50
Vallecitos Superheat Reactor, corrosion of Incoloy, Inconel, and Inconel X, 49
Valves, corrosion by Li and NaK, 241
Vanadium, compatibility, with Fz-Pu-U alloys, 153, 214-15
with molten U, 215
with Pu_2O_3, 153, 218
with Pu-U alloys, 215
corrosion, 182
diffusion, 246
in Ti, 127
electrodeposition, 260
Vanadium-48, diffusion in Ti and V, 127
Vanadium (Ni-plated)(S.S. 304-clad), extrusion, 140
Vanadium (S.S. 304-clad), extrusion, 140
fabrication, 259
Vanadium alloys, dispersion strengthening, 193-4
Vanadium alloys (silicide-coated), development, 261
Vanadium carbide, properties, 66
Vanadium crystals, ^{48}V diffusion in, 127
Vanadium pentoxide, corrosion, 183
Vanadium-zirconium alloys, oxidation, 238
Vanadium-zirconium intermetallic compound–zirconium cells, electrochemical potentials, 49
Vanadium-zirconium intermetallic compounds, H overvoltage, 49
Vapor deposition (chemical), development, 73
Vibratory compaction, densities of spherical shapes produced by, 259-60

W

Welding, review, 203

X

X-110 tubing, fabrication, 71

Y

Yttrium, plasticity, 139
pressure-temperature phase diagram, 61
solubility in Be, Be binary alloys, and Be foils, 39
Yttrium (glass-coated), oxidation, 204
Yttrium hydride, N_H and thermal stability, 43
Yttrium oxide, corrosion, 52
Yttrium oxide–zirconium dioxide systems, solid solutions, 128
Yttrium sheet, fabrication, 139
Yttrium tubing, lubricants for production of, 139

Z

Zinc, plating on U, 143
Zircaloy, cleaning for pressure bonding, 202
F pickup and release, 179
hydriding effects, 175
Zircaloy cladding, corrosion, 119
failure, 119
hydriding, 48
Zircaloy-2, Cl deposition on, 180
compatibility with UC, 163
corrosion, 48, 119, 179, 238
Cs deposition on, 180
fretting, 238
H embrittlement, 245
H pickup, 119, 238
hydriding effects, 175
impact effects, 238
impedance of oxide film on, 120
oxidation, pressure effects on, 120
stress corrosion, 121
tensile properties, 56-7
ultrasonic measurement of surface hydride, 264
Zircaloy-2 (hydrided), H in, quantitative estimation of, 234
Zircaloy-2 (irradiated), corrosion, 48, 119, 179
creep, 134
H pickup, 119
impact properties, 134
tensile properties, 188
Zircaloy-2 (O-bearing), oxidation, 120
Zircaloy-2 cladding (irradiated), tensile properties, 56-7
Zircaloy-2 sheet, creep properties, 61
Zircaloy-2 tubing, nondestructive testing, 207
Zircaloy-2 tubing (irradiated), tensile properties, 56, 189
Zircaloy-4, corrosion, 179, 238
H absorption, 179, 238
impedance of oxide film on, 120
stress corrosion, 121
Zirconium, addition to boiling Hg, 183-4
atomic force constant, 65
C-addition distribution, 65-6
Debye temperature, 65
deformation twinning, 195
diffusion in Ti, 127
dispersion strengthening, 195
electrodeposition, 260
electronic term, 65
H diffusion in, 127
H embrittlement, 245
H overvoltage, 49
He diffusion and precipitation in, 127
hydriding, 42
impedance of oxide film on, 119-20
^{95}Nb diffusion in, 127
oxidation, 238
phase transformation, 65
physical metallurgy, 195
purification, 140
reaction, with UC, 163
with UC_2, 163
with water, 226
with Zr, 100
self-diffusion, activation energy for, 246
solubility in Be, Be binary alloys, and Be foils, 39
specific heat, low-temperature, 65
temperature effects on, 244
vapor plating using metal-organic compounds, 204
^{95}Zr diffusion in, 127
Zirconium-95, diffusion in Zr, 127
Zirconium (irradiated), properties, 253
Zirconium alloys, C-addition distribution, 65-6
corrosion, 179-80, 238
D pickup, 48
H uptake, 238
metastable constitution, 244
oxidation, 179
physical metallurgy, 195
properties, 150, 213
steam effects on, 238
strengthening using carbide and oxide dispersants, 245
structure, 150, 213
Zirconium alloys (irradiated), mechanical properties, 253
Zirconium beryllide, Al solubility in, 42
evaporation, 115
mechanical properties, effects of Al, Ni, and Ti additions on, 42
oxidation, 233
Seebeck coefficient, 115
Zirconium boride, kinetics and thermodynamics, 128
Zirconium carbide, kinetics, 128
mechanical properties, 66, 196
physical properties, 66
thermal properties, 196, 248
thermodynamics, 66, 128
Zirconium coatings, vapor deposition, 142
Zirconium deuteride, free energy of formation, heat of combustion, and heat of formation, 42
Zirconium diboride, properties, 237
Zirconium dioxide, corrosion, 183
elasticity, 128, 196
preparation by vapor deposition, 261
thermal diffusivity, 196
thermal expansion, 196
thermal properties, 128
Zirconium dioxide (irradiated), damage recovery, 129
phase transformation, 129
stresses, 23
Zirconium dioxide coatings, plasma spraying, 74
properties, 74
vapor deposition on graphite, 143
Zirconium films, oxidation, 48-9
Zirconium hydride, compounds formed by, 234
free energy of formation, 42
heat of combustion, 42
heat of formation, 42
N_H, 43
thermal stability, 43
Zirconium intermetallic compounds, H overvoltage, 49
Zirconium monocarbide powder, nitriding, 248
Zirconium monocarbide single crystals, plasticity, 248
Zirconium mononitride powder, carburization, 248
Zirconium monoxide, thermodynamics, 197
Zirconium oxide films, capacitance, impedance, and resistance, 119
Zirconium-zirconium intermetallic compound cells, electrochemical potentials, 49

LEGAL NOTICE

This journal was prepared under the sponsorship of the U. S. Atomic Energy Commission. Neither the United States, nor the Commission, nor any person acting on behalf of the Commission:

A. Makes any warranty or representation, expressed or implied, with respect to the accuracy, completeness, or usefulness of the information contained in this journal, or that the use of any information, apparatus, method, or process disclosed in this journal may not infringe privately owned rights; or

B. Assumes any liabilities with respect to the use of, or for damages resulting from the use of any information, apparatus, method, or process disclosed in this journal.

As used in the above, "person acting on behalf of the Commission" includes any employee or contractor of the Commission, or employee of such contractor, to the extent that such employee or contractor of the Commission, or employee of such contractor prepares, disseminates, or provides access to, any information pursuant to his employment or contract with the Commission, or his employment with such contractor.

NUCLEAR SCIENCE ABSTRACTS

The U. S. Atomic Energy Commission, Division of Technical Information, publishes *Nuclear Science Abstracts (NSA)*, a semimonthly journal containing abstracts of the literature of nuclear science and engineering.

NSA covers (1) research reports of the U. S. Atomic Energy Commission and its contractors; (2) research reports of government agencies, universities, and industrial research organizations on a world-wide basis; and (3) translations, patents, books, and articles appearing in technical and scientific journals.

Complete indexes covering subject, author, source, and report number are included in each issue. These are cumulated quarterly, semiannually, and annually providing a detailed and convenient key to the literature.

Availability of *NSA*

SALE *NSA* is available on subscription from the Superintendent of Documents, U. S. Government Printing Office, Washington, D. C., 20402, at $30.00 per year for the semimonthly abstract issues and $22.00 per year for the four cumulated-index issues. Subscriptions are postpaid within the United States, Canada, Mexico, and all Central and South American countries, except Argentina, Brazil, British and French Guiana, Surinam, and British Honduras. Subscribers in these Central and South American countries, and in all other countries throughout the world, should remit $37.00 per year for subscriptions to semimonthly abstract issues and $25.00 per year for the four cumulated-index issues.

EXCHANGE *NSA* is also available on an exchange basis to universities, research institutions, industrial firms, and publishers of scientific information. Inquiries should be directed to the Division of Technical Information Extension, U. S. Atomic Energy Commission, P. O. Box 62, Oak Ridge, Tennessee, 37831.

TECHNICAL PROGRESS REVIEWS may be purchased from Superintendent of Documents, U. S. Government Printing Office, Washington, D. C., 20402. *Isotopes and Radiation Technology* at $2.00 per year for each subscription or $0.55 per issue; the other four journals at $2.50 per year and $0.70 per issue. The use of the coupon below will facilitate the handling of your order.

POSTAGE AND REMITTANCE: Postpaid within the United States, Canada, Mexico, and all Central and South American countries except as hereinafter noted. Add $0.50 per year, or $0.15 per single issue for the *Isotopes and Radiation Technology* journal and $0.75 per year or $0.20 per single issue for the other four journals for postage to all other countries, including Argentina, Brazil, British and French Guiana, Surinam, and British Honduras. Payment should be by check, money order, or document coupons, and MUST accompany order. Remittances from foreign countries should be made by international money order, or draft on an American bank, payable to the Superintendent of Documents, or by UNESCO book coupons.

order form

SUPERINTENDENT OF DOCUMENTS
U. S. GOVERNMENT PRINTING OFFICE
WASHINGTON , D. C., 20402

Enclosed:

document coupons ☐ check ☐ money order ☐

Charge to Superintendent of Documents No._____

Please send a one-year subscription to

☐ NUCLEAR SAFETY

☐ POWER REACTOR TECHNOLOGY

☐ REACTOR FUEL PROCESSING

☐ REACTOR MATERIALS

(Each subscription $2.50 per year; $0.70 per issue.)

☐ ISOTOPES AND RADIATION TECHNOLOGY

(Each subscription $2.00 a year; $0.55 per issue.)

SUPERINTENDENT OF DOCUMENTS
U. S. GOVERNMENT PRINTING OFFICE
WASHINGTON, D. C., 20402

(Print clearly)

Name _____

Street _____
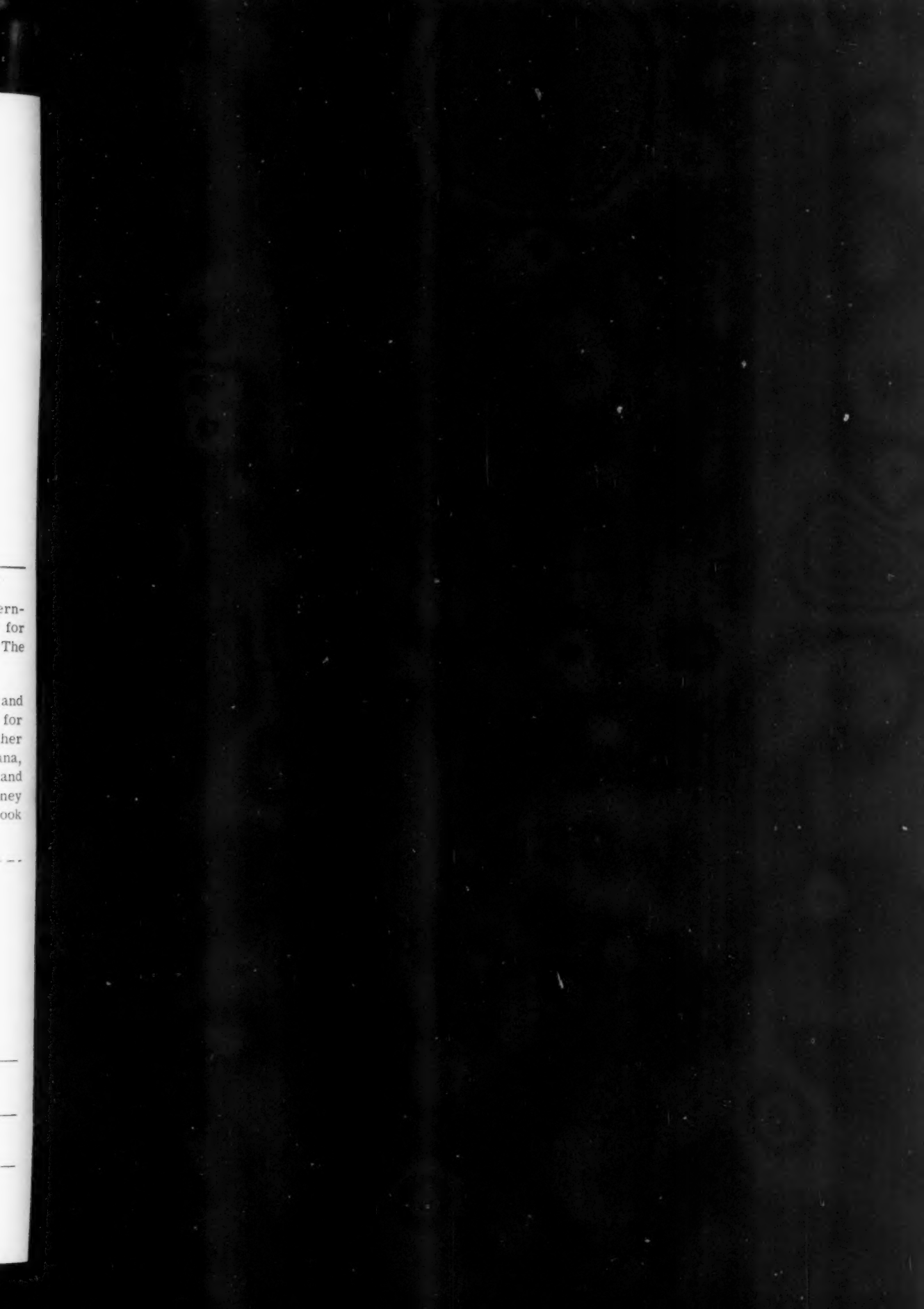
City _____ Zone ____ State _____